SISSA
Scuola
Internazionale
Superiore di
Studi Avanzati

Physics Area - PhD course in
Theory and Numerical Simulation of Condensed Matter

Electronic correlations in topological materials

Candidate:
Andrea Blason

Advisor:
Michele Fabrizio

Trieste, December 2023

ABSTRACT

The interest in topological materials has flourished in recent years due to their topological protection of remarkable physical properties under weak perturbations, which ensures the realisation of robust exotic features in realistic materials. However, many of the theoretical achievements of topology in condensed matter, such as the landmark relationship between Hall conductance and the first Chern number discovered by Thouless, Kohmoto, Nightingale and den Nijs, inherently assume a single-particle description of the many-body wave function, so that the role of interactions and correlations in topological materials is not yet fully understood. This work aims to partially fill this gap, covering a wide range of topological phenomena induced or supported by electronic interactions.

First, the topological character of spin excitons and their condensation in quantum spin Hall insulators will be investigated, with particular emphasis on their effect on the physics of electronic chiral edge states. Second, the joint effects of flat optical moiré phonons and Coulomb repulsion on the phase diagram of twisted bilayer graphene are studied, showing that their interplay can stabilise topological insulators and superconductors in agreement with experimental evidence. Third, the exact role of the Green's function zeros in the topological invariants for strongly correlated systems is elucidated, showing that the zeros contribute on an equal footing with the Green's function poles. In particular, in the case of a topological Mott insulator, it is shown that the topology is carried entirely by the Green's function zeros and not by the poles, a genuine strongly correlated effect that lacks any non-interacting counterpart. In the last part, a new explanation for the peculiar Fermi liquid properties of topological Kondo insulators is proposed, motivated by recent findings that zeros of the Green's function could directly correspond to the presence of neutral quasiparticles. In particular, a new realistic model for these strongly interacting topological insulators is introduced and then studied by means of cluster dynamical mean field calculations, confirming the presence of ingap Green's function zeros.

ACKNOWLEDGEMENTS

I want to express my deepest gratitude to Michele, my supervisor, for being an inspiring guide throughout this journey and for placing tremendous trust in my skills and intuitions. He is the primary reason I can wholeheartedly look back at my PhD as a truly fulfilling experience.

I am also thankful to Michel Ferrero for warmly hosting me in Paris and providing invaluable assistance with the cluster dynamical mean field theory calculations presented in the final chapter.

My sincere thanks go to Adriano Amaricci, Carlos Mejuto Zaera, Francesca Paoletti, and Mattia Angeli for their valuable discussions and insightful comments.

Last but certainly not least, I extend a special thanks to Elio J. König and Giorgio Sangiovanni for graciously accepting the thankless role of external reviewers.

I would also like to acknowledge the funding provided by the European Research Council (ERC) under the European Union's Horizon 2020 research and innovation program, Grant agreement No. 692670, titled "FIRSTORM."

CONTENTS

CHAPTER 1

INTRODUCTION

One of the fundamental concepts in the journey of an undergraduate student through quantum mechanics is the notion of symmetry. At the heart of this exploration lies the Schrödinger equation:

$$i\hbar\,\partial_t\,\psi(\mathbf{x},t) = -\frac{\hbar^2}{2m}\,\nabla^2\,\psi(\mathbf{x},t) + V(\mathbf{r})\,\psi(\mathbf{x},t).$$

This equation exhibits invariance under a seemingly innocuous global phase transformation of the wave function:

$$\psi(\mathbf{x},t) \to \psi(\mathbf{x},t)\,e^{-i\varphi}.$$

This symmetry lays the foundation of topology in quantum mechanics as originally envisioned by Berry. Indeed, the phase φ may depend on the Hamiltonian parameters and, as the latter are adiabatically varied along a closed loop, a non-zero phase accumulation can occur. This global phase change, quantized in multiples of 2π, forms the essence of topological non-trivial behavior in both quantum mechanics and condensed matter physics.

A striking manifestation of topology, which has fundamentally reshaped our understanding of electronic structures, is the discovery of the integer quantum Hall effect (IQHE). In 1980, von Klitzing discovered this phenomenon [1], and, two years later, Thouless, Kohmoto, Nightingale, and den Nijs (TKNN) proved its topological origin [2]. Within a thin metal slab subjected to an orthogonal magnetic field, the Hall conductance becomes quantized, with a constant offset. Intriguingly, this quantization occurs when the system is insulating, i.e., when the highest occupied Landau levels is full. Changes in the quantization integer only occur when the system transitions through a metallic state, as illustrated in Fig. 1.1.

This quantized integer is just the Barry phase accumulated by the many-body wave-function when a magnetic flux quantum is threatened into the system, and it is associated with a topological invariant known as the first Chern number that remains constants under smooth deformations of the Hamiltonian. As an illustrative example, a donut can be smoothly deformed into a mug, both possessing one hole, but not into a pair of glasses with two holes without piercing the object. In the context of condensed matter, this smooth deformation corresponds to adiabatic and symmetry-preserving transformations of the Hamiltonian. In the case of IQHE, altering the Chern number

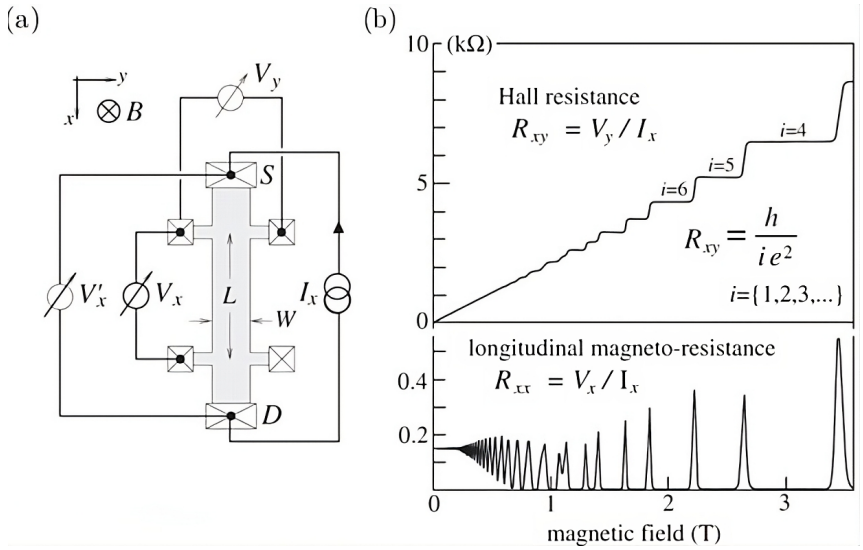

Figure 1.1: Schematic representation of the device geometry in panel (a), and the measurement results in panel (b) for an experimental realization of the integer Quantum Hall effect. Notably, in panel (b), changes in Hall resistance coincide with peaks in longitudinal resistivity, signifying a closure of the insulating gap. Figure adapted from Ref. [3].

necessitates "piercing" the ground state by closing the energy gap, thus breaking adiabaticity. Remarkably, the Hall bar also features chiral edge states that are ultimately responsible of the Hall conductance, whose quantized value is directly proportional to the number of those modes.

This remarkable property underpins the success of topological materials. It ensures that the non-trivial topological response, such as the presence of edge states, remains robust against various perturbations of the Hamiltonian, such as small interactions, disorder, impurities, and defects that are inevitable in real materials. Thus the introduction of topology into condensed matter physics has not only demonstrated that electronic properties can be elegantly described using advanced mathematical concepts but also that a deeper understanding of these abstract structures can lead to extraordinary properties in real-world materials.

However, Berry's formalism faces a significant challenge: it inherently requires working with the exact many-body wavefunction, which, apart from few cases, is almost impossible to calculate. For instance, in non-interacting systems or interacting ones that admit an independent-particle description, the calculation is easy since the many-body wavefunction is, or is well represented by, a Slater determinant of single-particle Bloch wavefunctions. Similarly, one can keep using the results of the non-interacting case when the latter is adiabatically connected to the fully interacting system. However, this simplification may no longer be feasible in strongly correlated systems. This introduces complexities to the study of these materials, but also unlocks the potential for phenomena that lack a non-interacting counterpart, most notably the fractional quantum Hall effect.

In the pursuit of exploring these new frontiers, this PhD thesis aims to investigate various facets of topological manifestations in strongly correlated systems, with particular emphasis on

the interplay between topology and electron interaction. Since it will encompass a wide array of diverse and captivating topics, to help reader comprehension this introductory chapter will provide a brief summary of each work that has been accomplished.

1.1 Exciton condensation and topology in quantum spin Hall insulators

The first part of this thesis delves into the study of excitons within a prototypical quantum spin Hall insulator (QSHI). Coulomb interaction in insulators may lead to the formation of bound states between electrons in the conduction band and holes in the valence one, so-called excitons. The excitons, which are bosonic composite particles, may also exhibit topological properties and could potentially undergo a Bose condensation, leading to excitonic insulators.

Two-dimensional materials, characterized by a finite density of states at the band edges and by an enhanced Coulomb interaction strength because of the reduced dimensionality, are ideal candidates for exciton condensation. This phenomenon has indeed been experimentally observed in bilayer graphene and transition metal dichalcogenides [4–6], with the latter that can also sustain quantum spin Hall effect [5, 6]. This raises the question whether quantum spin Hall insulators (QSHI), inherently two-dimensional, could also exhibit non-trivial excitonic properties and if those can interplay with topology. The question becomes even more intriguing when considering the role of spin excitons in purported topological insulators such as SmB_6, where they interact with chiral edge states [7, 8], playing a pivotal role in the surface physics of these materials.

In this chapter, I will conduct a comprehensive analysis of excitons, encompassing both spinful and spinless variants, within a prototypical model of a QSHI introduced by Bernevig, Hughes, and Zhang to describe topological insulators in quantum wells [9]. Unlike quantum Hall insulators or anomalous quantum Hall insulators, QSHIs exhibit a distinct feature: while their charge Hall conductivity is zero, the spin Hall conductivity is quantized. This unique behavior arises from the presence of counter-propagating edge states with opposite spin projections. Furthermore, unlike the aforementioned Hall insulators, QSHIs possesses time-reversal invariance that actually protects the topological character.
To replicate the effects of Coulomb repulsion, I will introduce a local Hubbard interaction that preserves the symmetry of the problem. Subsequently, I will address the interacting problem employing a conserving mean-field approach, wherein ground state properties are calculated using the Hartree-Fock approximation, while response functions are determined by the Bethe-Salpeter equation using as irreducible vertex the functional derivative of the Hartree-Fock self-energy with respect to the Green's function.

I will demonstrate that, starting with a non-interacting QSHI and gradually increasing the interaction strength, a branch of excitons detach from the gapped particle-hole continuum. Notably, these excitations can acquire non-trivial topological character, hinting at the existence of chiral topological surface excitons, in particular spinful in this case. It is noteworthy that these surface excitons, being spin-triplet, serve as an efficient decay channel for the topological edge modes.

Furthermore, as the interaction strength continues to increase, albeit within moderate values, an excitonic insulator sets in through the condensation of these spin-triplet excitons. While this phase is topologically trivial because of the spontaneous time reversal symmetry breaking, it exhibits an

exotic magneto-electric effect that holds significant promise for practical applications. Additionally, owing to reduced coordination at the boundary, a one-dimensional exciton condensate at the edges may appear prior to the bulk condensation, suggesting the emergence of a surface excitonic insulator. This has profound implications for the coherence of the chiral electronic surface states.

1.2 Moiré phonons and local Kekulé order in twisted bilayer graphene

The second part of this thesis is devoted to the investigation of the phase diagram of small angle twisted bilayer graphene (TBLG), with a particular emphasis on the significant influence of its distinctive phonon modes.

TBLG consists of two layers of graphene slightly twisted one with respect to the other. For particular twist angles, the system recovers periodicity but with huge supercells spanning several thousands of carbon atoms. This arrangement gives rise to a characteristic Moiré pattern. Notably, the intricate folding of the original Brillouin Zone into the much smaller Moiré Zone together with the interlayer hopping lead to the formation of remarkably flat electronic bands (few tenths of meV) around the charge neutrality point, as first predicted by Bistritzer and MacDonald [10]. This extraordinary flatness significantly diminishes the kinetic energy of the electrons, thereby amplifying the importance of electron-electron correlations.

One remarkable feature of TBLG, shared with many few-layered materials, is the ease with which its doping can be controlled using just few gate electrodes. This stands in sharp contrast to other correlated materials, such as cuprates, which often necessitate complex chemical substitutions to achieve doping control.

These compelling attributes have positioned TBLG as an ideal platform for realizing, investigating, and engineering strongly correlated electronic states, as it has been convincingly demonstrated experimentally. The flat bands in TBLG have, in fact, the capacity to accommodate up to eight electrons per Moiré cell, typically denoted by the filling $\nu = -4 + n_{el}$, and possess a non-trivial topological character. Realistic tight-binding and DFT calculations predict that TBLG is a metal with tiny Fermi velocity at any filling fraction $-4 < \nu < 4$. However, the real system undergoes transitions to insulating states at any integer fillings [11–23], with anomalous Hall effect at $\nu = 2$ [24, 25]. Additionally, superconducting domes emerge in the vicinity of the insulating states [12, 13, 15, 19, 20, 26], rendering the phase diagram reminiscent of that found in strongly correlated materials (see Fig. 1.2).

Due to the similarity of the TBLG phase diagram with that of cuprates, where superconductivity seems completely unrelated to phonons (the isotope effect is absent), considerable efforts have been invested in a TBLG description involving solely Coulomb repulsion. However, TBLG also possesses a set of extremely flat phonon modes, derived from a long wavelength modulation of the optical modes of graphene around the **K** reciprocal vector [27]. These phonons share the same emerging symmetry as the flat bands, giving rise to an effective $e \times E$ Jahn-Teller coupling, which is very effective in removing the valley degeneracy of the flat bands.

In this chapter, I will present comprehensive Hartree-Fock calculations that take into account both Coulomb repulsion and the effective attraction generated by this special set of phonons. Within this approximation, when the coupling between phonons and electrons reaches a critical

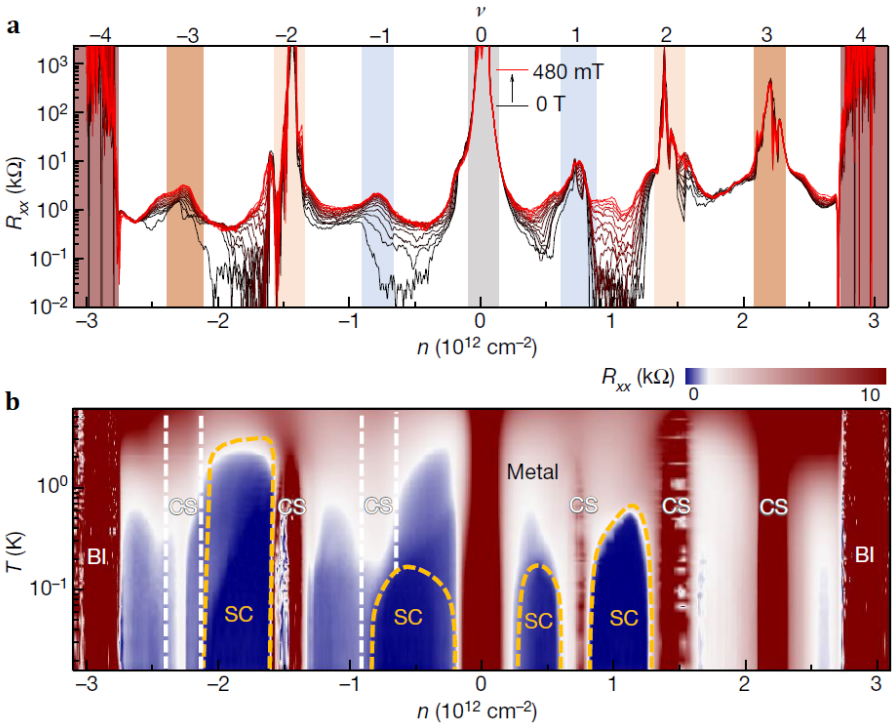

Figure 1.2: Phase diagram of TBLG depending on magnetic field (panel a) and temperature (panel b). Notably, the system displays resistance peaks at any integer fillings and drops between some of them, corresponding to insulating and superconducting states respectively. Figure adapted from Ref. [12]

threshold (though still substantially smaller than the Coulomb repulsion), the phase diagram undergoes a radical transformation. Notably, an insulator displaying a Kekulé distortion at the scale of the single-layer graphene becomes the most stable at charge neutrality. This then serves as a parent state for all the insulators at different integer fillings, which additionally exhibit topological features. This scenario, only realized by introducing these peculiar optical phonons in the picture, has been subsequently confirmed experimentally through state-of-the-art scanning tunneling microscopy (STM) measurements [28], which indeed detected a local Kekulé distortion at $\nu = \pm 2$.

Moving beyond the Hartree-Fock approximation, I will present a resonating valence bond scenario, where now the Kekulé distortion oscillates between different geometries. This theoretical framework predicts a insulating states composed of topological $d \pm id$ Cooper pairs which are naturally predisposed to develop superconductivity upon doping, in alignment with experimental evidences [29–31].

1.3 Green's function zeros and topological invariants

The third part of this thesis focuses on the role of Green's function zeros in the topological character of interacting many body ground states. The Green's function, defined as the transition amplitude between an electron created at (imaginary) time zero in position $\mathbf{r}'$ and an electron annihilated at time τ and position $\mathbf{r}$ on the ground state

$$G(\mathbf{r}-\mathbf{r}',\tau) = -i\,\langle\, T_\tau\big(\psi(\mathbf{r},\tau)\psi^\dagger(0,\mathbf{r}')\big)\,\rangle\ ,$$

carries information about the single particle structure of correlated electronic systems, and is at the base of the so called many body perturbation theory in condensed matter.
In the non-interacting case the Green's function takes a rather simple form in momentum and frequency spaces, where it displays poles around the single particle states

$$G_0(\mathbf{k}, i\omega) = \frac{1}{i\omega - \epsilon_{\mathbf{k}}}\,,$$

$\epsilon_{\mathbf{k}}$ is the non-interacting dispersion and the chemical potential is set to zero for simplicity. Once interactions are considered, electronic correlations are fully described by the self energy $\Sigma(\mathbf{k}, i\omega)$, which can be defined via the Dyson equation

$$G(\mathbf{k}, i\omega) = \big(G_0^{-1}(\mathbf{k}, i\omega) - \Sigma(\mathbf{k}, i\omega)\big)^{-1} = \frac{1}{i\omega - \epsilon_{\mathbf{k}} - \Sigma(\mathbf{k}, i\omega)}\,,$$

which relates the non-interacting Green's function to the fully interacting one. In particular, when perturbation theory is valid, the self energy can be expressed in term of a converging power series in the interaction, where the main building blocks are the non-interacting Green's function G_0 and the matrix elements of the interaction.

In this perturbative regime, the imaginary part of the self energy, which accounts for decoherence effects, quickly goes to zero at zero frequency. This ensures that single particle excitations, now called quasiparticles, still survive near the chemical potential. The existence of these quasiparticles, at the root of Fermi liquid theory, implies that the Green's function can be divided into a coherent part that is dominant at low frequencies and behaves like the one of non-interacting

electrons, and an incoherent one, which describes states far away from the chemical potential that quickly decay in a plethora of particle-hole excitations,

$$G(\mathbf{k}, i\omega) = G_{coh}(\mathbf{k}, i\omega) + G_{inc}(\mathbf{k}, i\omega)\,,$$
$$G_{coh}(\mathbf{k}, i\omega) \simeq \frac{Z(\mathbf{k}, 0)}{i\omega - \tilde{\epsilon}_{\mathbf{k}}}\,,$$

where

$$Z(\mathbf{k}, \omega) = \left(1 - \frac{\operatorname{Im}\Sigma(\mathbf{k}, i\omega)}{i\omega}\right)^{-1} \geq 0 \qquad \tilde{\epsilon}_{\mathbf{k}} = \lim_{\omega \to 0} Z(\mathbf{k}, \omega)\Big(\epsilon_{\mathbf{k}} + \operatorname{Re}\Sigma(\mathbf{k}, i\omega)\Big)\,,$$

are the so called quasiparticle residue and dispersion. Moreover, the density of states near the chemical potential, now expressed in real frequencies, is given by

$$A(\mathbf{k}, \omega) \simeq -\frac{1}{2\pi}\operatorname{Im} G_{coh}(\mathbf{k}, \omega + i0^+) = Z(\mathbf{k}, 0)\,\delta(\omega - \tilde{\epsilon}_{\mathbf{k}})\,,$$

which is similar to the one of non-interacting electrons, although the spectral weight is renormalized by Z. In particular, these quasiparticles satisfy the Luttinger theorem, namely their number is the same as the one of non-interacting single particle states. In another words, the Fermi surface of the weakly correlated ground state is exactly the one of the quasiparticles, defined as the locus of points in $\mathbf{k}$ space where

$$\epsilon_{\mathbf{k}} + \operatorname{Re}\Sigma(\mathbf{k}, 0) = 0$$

or, alternatively, where the Green's function has a pole at zero frequency.

However, further increasing the strength of the interaction, the perturbation expansion may fail resulting in a self energy that develops poles near zero frequency. At the $\mathbf{k}$ points in the vicinity of these poles, the system is gapped since the quasiparticle dispersion do not cross the chemical potential and the quasiparticle residue goes quickly at zero approaching zero frequency. Considering a half filled system, the presence of poles of the self energy ensures that a gap is opened in the whole Brillouin Zone: a Mott insulator is realized. In this type of insulators, the localization of electrons and, most importantly, their mutual correlations are the only responsible for its insulating behaviour.

But poles of the self energy are in direct correspondence with zeros of the Green's function, or better zeros of the determinant of the Green's function when various quantum numbers are present such that the Green's function becomes a matrix. These zeros have been for long disregarded as a sole accident of the theory without any physical relevance. Though, they posses an equivalent to the Fermi surface called Luttinger surface, i.e. the locus of points where the Green's function displays zeros at zero frequency, which carries the same non-trivial topology of the Fermi one [32].

Intriguingly, a recent work [33] demonstrated that, since the quasiparticle lifetime is actually corrected with the quasiparticle residue

$$\tau_{\mathbf{k}}^{-1} = -\lim_{\omega \to 0^+} \frac{Z(\mathbf{k}, \omega)\,\operatorname{Im}\Sigma(\mathbf{k}, i\omega)}{\omega^2}$$

Fermi liquid theory can be analytically rederived also in the vicinity of the Luttinger surface [34], implying the presence of quasiparticles now described by the effective Hamiltonian

$$H_*(\mathbf{k}, i\omega) = \sqrt{Z(\mathbf{k}, \omega)}\;(\epsilon_{\mathbf{k}} + \operatorname{Re}\Sigma(\mathbf{k}, i\omega))\;\sqrt{Z(\mathbf{k}, \omega)}$$

which has zero eigenvalues at the Luttinger surface even in non-symmetry breaking Mott insulators [34]. Those quasiparticles have the same physical properties as conventional ones at a Fermi surface, but are incompressible [35] and do not contribute to charge transport [34], realizing what could be regarded as a neutral Fermi surface. Interestingly, the presence of a Luttinger surface also implies the breakdown of Luttinger's theorem [35].

This picture becomes even more fascinating when topology is taken into account. Starting from an uncorrelated topological insulator and increasing the interaction, it has been proposed [36, 37] that edge poles, i.e. chiral edge states, may transform into edge zeros without the closure of the insulating gap. This prompted the interest in the interplay between the topological character of a strongly correlated insulator and the properties of the Green's function zeros. In particular, a recent work pointed out that Mott insulators can have non-trivial topological bands of zeros lying inside the insulating gap, clarifying how a possible bulk-boundary correspondence could emerge also for the zeros [38].

Further insight can be gained noticing that every topological invariant of an interacting systems can be written as a product of logarithmic derivative of the Green's function [39–43]

$$G(\mathbf{k}, i\omega)\, \partial_\nu\, G^{-1}(\mathbf{k}, i\omega) = -G^{-1}(\mathbf{k}, i\omega)\, \partial_\nu\, G(\mathbf{k}, i\omega)\,,$$

where ν can be the frequency, the momentum or other parameters of the Hamiltonian. Just by a quick inspection it is straightforward to understand that G and G^{-1} are interchangeable, so that zeros and poles of the Green's function may play, apart from a minus sign, the same role in the topological nature of a strongly correlated insulator. However, up to now, a comprehensive analysis of the zeros contribution to these topological invariants is largely lacking.

Another open problem is the connection between these topological invariants and the actual response functions of the system. For example, is it still true that the two dimensional Chern number of a topological insulator with Green's function zeros corresponds to the quantized value of the transverse conductivity?

In this chapter, I will try to partially fill this gap. In particular I will demonstrate that the first Chern number of an interacting insulator without a Luttinger surface reduces exactly to the TKNN formula calculated on the quasiparticle Hamiltonian at zero frequency $H_*(\mathbf{k}, 0)$. In the perturbative case, this reproduces the results of Zhong and Zhang [42], since $\sqrt{Z(\mathbf{k}, 0)} \sim 1$ and the quasiparticle Hamiltonian almost reduces to the topological Hamiltonian $H_{topo}(\mathbf{k}) = -G^{-1}(\mathbf{k}, 0)$. However, when perturbation theory breaks down and zeros of the Green's function appear, the quasiparticle Hamiltonian describes low energy excitations which are almost entirely determined by the properties of the zeros of the Green's function rather than the poles. Elaborating on that result, I found that deep in the Mott phase the value of the first Chern number is entirely determined by the topology of the in-gap zeros of the Green's function.

In addition, I will demonstrate, using the Streda formula, that in scenarios where perturbation theory breaks down and the Luttinger theorem fails, a direct correspondence between the first Chern number and transverse conductivity may also falter. This breakdown occurs due to the emergence of non-trivial many-body corrections, which become non-zero outside the perturbative regime and can disrupt the one-to-one correspondence between these two physical quantities.

These results, obtained in two dimensions but easily generalizable in any dimensions, shine light on a largely not understood subject and demonstrate how strongly correlated systems can host topological phenomena without any non-interacting counterpart.

1.4 Neutral quasiparticles in topological Kondo insulators

In the concluding segment of this thesis, I will present preliminary results concerning the potential significance of Green's function zeros in elucidating the enigmatic dualistic behavior, alternating between metallic and insulating, exhibited by topological Kondo insulators (TKIs).

To provide readers with the essential context, I a going to first delve into the key characteristics of Kondo insulators. In these materials, the near-Fermi energy band structure is primarily dominated by an itinerant metallic band which interplays with a more localized and strongly correlated counterpart. At elevated temperatures, Kondo insulators display metallic behavior, with transport properties predominantly governed by the itinerant electrons. As the temperature decreases below a certain value, an energy gap emerges, causing the system to transition into an insulating state. This phenomenon is typically interpreted through the lens of the Kondo effect: at low temperature the localized electrons get promoted into the conduction band and that opens a hybridisation gap making the system insulating.

In light of these considerations, Kondo insulators are often successfully modeled using a tight-binding Hamiltonian, wherein an itinerant band hybridizes on-site with a flat and highly interacting one, known as the periodic Anderson model (PAM).

Topological Kondo insulators, exemplified by materials such as SmB_6 and YbB_{12}, share the same characteristic gap opening at low temperatures. However, they also exhibit a distinct feature: the emergence of metallic edge states with apparent topological origins [44–51]. In these materials, the low energy properties are primarily influenced by the d- and f-orbitals of the rare earth atoms, whereas the boron orbitals reside well below the chemical potential, serving as a structural stabilizer. Notably, the high-energy shells of the d- and f-orbitals implies strong spin-orbit coupling, leading to significant hybridization between the two. The odd parity of this orbital hybridization, along with the opposed parity of d- and f-orbitals, enables a nearest-neighbor band mixing with just the right symmetry to sustain a topological insulator.

Consequently, a slightly modified periodic Anderson model has been proposed to describe these materials [52], in which one or more itinerant d-orbitals hybridize with the correlated f-orbitals in adjacent cells. By tuning the model parameters to achieve a topological Hamiltonian, one can explain both the emergence of the gap below a Kondo-like temperature and the appearance of genuine topological chiral edge states.

Nevertheless, topological Kondo insulators present puzzling and counterintuitive features emerging in the insulating phase. Notably, their heat capacity, heat transport properties, and quantum oscillations mimic those of metals [53–64] suggesting the existence of an analogue to a bulk Fermi surface; a phenomenon at odds with the conventional Kondo insulators.

A promising interpretation of these effects is the presence of a 'neutral' Fermi surface that displays Landau levels quantization [65–67], although the possible mechanism at the basis of its formation is still controversial.
Other theoretical explanations have been proposed, involving the role of excitons and magneto-excitons [68], the possibility of quantum oscillations in narrow gap insulators [69–71], the enhancement of quantum oscillations in Kondo insulators [72], the interplay between surface states and the Kondo breakdown [73]. These explanations predict, however, a strong deviation from the Lifshitz-Kosevich expression for quantum oscillations, at odd with experimental evidences [61,64].

In this chapter, I will explore an alternative picture involving the presence of zeros of the Green's

function forming a Luttinger surface. As previously discussed, this surface could potentially host gapless excitations that resemble metallic quasiparticles while exerting no influence on charge transport properties [74–76]. Such a framework implies the existence of a finite single-particle gap in the density of states, coexisting with 'neutral' fermionic quasiparticles within the gap. These quasiparticles may provide a suitable description for the observed Fermi liquid properties and quantum oscillations in topological Kondo insulators.

To identify the presence of a Luttinger surface, I conducted dynamical cluster approximation (DCA) calculations. This approach allows for the determination of non-local contribution to the self-energy, which is calculated at some $\mathbf{k}$ points within the Brillouin zone. Subsequently, smooth lattice properties can be derived through a meticulous periodization of the self-energy, ultimately revealing the locus in $\mathbf{k}$ space where it exhibits zero-energy poles hallmark of the Luttinger surface.

I will begin my analysis by focusing on the model discussed earlier [52], in which only the f-electrons exhibit interactions. For small interaction strengths, the system closely resembles a weakly correlated topological insulator that can be adiabatically connected to a non-interacting one. As the strength of the interactions increases, the f-bands progressively localize, eventually realizing an heavy fermion system either metallic or insulating but with a minuscule gap. However, both of these scenario are at odd with the experimental picture and thus incongruity necessitates a reexamination of the TKI model.

A common feature among these materials is the shared origin of the d- and f-orbitals within the same atom. Consequently, the matrix elements of the local Coulomb repulsion involving the d-orbitals are of comparable magnitude to those within the f-subspace. This indicates that the correlation of the d-orbitals could play a relevant role in the actual electronic structure of the system, and the assumption that only the interaction between the f-orbitals is relevant may not be accurate enough to describe these kind of materials.

By incorporating these terms into the model Hamiltonian, I will observe that, for small interaction strengths, the system once again resembles a weakly correlated topological insulator, with interactions primarily serving to renormalize the parameters of the non-interacting Hamiltonian. As the interaction strength is further increased, both orbitals simultaneously undergo localization. The system can now accommodate a Luttinger surface, which can exhibit characteristics of both d- and f-orbitals depending on the model parameters, all while maintaining an insulating state. These results thus support the idea that TKI can instead be Mott insulators with a Luttinger surface, which would explain the peculiar metal-insulator dichotomy of these materials.

Lastly, I will discuss the interplay between the presence of a Luttinger surface, i.e., zeros of the Green's function, and the topology of the ground state, also in light of the analytical results obtained in the previous chapter of the present thesis.

CHAPTER 2

EXCITON CONDENSATION AND TOPOLOGY IN QSHI

2.1 Introduction

The physics of excitons in topological insulators has attracted considerable interest in the last decade, see, not as an exhaustive list, Refs. [7, 77–83], recently renewed [84] by the evidence of a quantum spin Hall effect [85–87] and excitonic condensation [5, 6] in two-dimensional transition metal dichalcogenides.
More precisely, a consistent part of the research activity has focused into the possibility of an exciton condensation in thin samples of topological insulators [77–79, 82, 88–90], much in the spirit of what was proposed [91, 92] and observed [4] in bilayer graphene.
In addition, the puzzling properties of the purported topological Kondo insulator SmB_6 [93–95] prompted interest in the excitons of such material [7, 8, 80, 81, 96, 97] as partly responsible for its anomalous behaviour.

Even though evidences of excitons exist also in the three-dimensional topological insulator Bi_2Se_3 [83], besides those in the still controversial SmB_6, a systematic study in model topological insulators is largely lacking [96, 98–100]. The main goal of this chapter is to partly fill this gap. Specifically, I consider the prototypical model of a Quantum Spin Hall Insulator (QSHI) introduced by Bernevig, Hughes and Zhang [9], and add a local interaction compatible with the symmetries, which, e.g., allow for a dipole-dipole term. I deal with such an interaction in a conserving mean-field scheme. Namely, I assume the Hartree-Fock expression of the self-energy functional to compute the single-particle Green's function. Next, I calculate the excitons by solving the Bethe-Salpeter equations for the response functions, using as irreducible vertex the functional derivative of the Hartree-Fock self-energy functional with respect to the Green's function; what is often called random phase approximation plus exchange [101].
The main result of this chapter is that, starting from the non-interacting QSHI, branches of excitons that transform into each other under time reversal detach from the continuum of particle-hole excitations, and gradually soften upon increasing interaction strength. When the latter exceeds a critical value, those excitons become massless, and thus condense through a second order critical

point, which coincides with that obtained directly through the Hartree-Fock calculation not forcing any symmetry. Such symmetry broken phase is still insulating, and displays magnetoelectric effects. Upon further increasing interaction, it eventually gives in to the non-topological symmetry invariant insulator via another second order transition. None of those transitions is accompanied by any gap closing; therefore uncovering a path between the QSHI and the trivial insulator that does not cross any gapless point [102–104], thanks to the interaction-driven spontaneous breakdown of time reversal symmetry.
I also find that, approaching the excitonic insulator from the QSHI, the excitons themselves may acquire a non trivial topology signalled by a non-zero Chern number, suggestive of the existence of chiral exciton edge modes. In addition, there are evidences that, in open boundary geometries, exciton condensation occurs at the surface earlier than in the bulk, which also foresees the existence of non-chiral surface excitons that go soft before the bulk ones [105–107].
These findings may have observable consequences that I discuss, some of which not in disagreement with existing experimental evidences.

2.2 The model Hamiltonian

I shall consider the model introduced by Bernevig, Hughes and Zhang, after them named BHZ model, to describe the QSHI phase in HgTe quantum wells [9]. The BHZ model involves two spinful Wannier orbitals per unit cell, which transform like s-orbitals, $|s\,\sigma\rangle$, where $\sigma =\uparrow,\downarrow$ refers to the projection of the spin along the z-axis, and like the $J = 3/2$, $J_z = \pm 3/2$ spin-orbit coupled combinations of p-orbitals, i.e.,

$$\begin{aligned} |p_x + ip_y\uparrow\rangle &= |p_{+1}\uparrow\rangle \equiv |p\uparrow\rangle\ , \\ |p_x - ip_y\downarrow\rangle &= |p_{-1}\downarrow\rangle \equiv |p\downarrow\rangle\ . \end{aligned} \tag{2.1}$$

I introduce two sets of Pauli matrices, σ_a and τ_a, $a = 0,\ldots,3$, with $a = 0$ denoting the identity, which act, respectively, in the spin, $\uparrow$ and $\downarrow$, and orbital, s and p, spaces.
With those definitions, the BHZ tight-binding Hamiltonian on a square lattice includes all onsite potentials and nearest neighbour hopping terms that are compatible with inversion, time reversal and C_4 symmetry [108], and reads

$$\mathcal{H}_0 = \sum_{\mathbf{k}} \mathbf{\Psi}^\dagger_{\mathbf{k}}\, \hat{H}_0(\mathbf{k})\, \mathbf{\Psi}_{\mathbf{k}} = \sum_{ij} \mathbf{\Psi}^\dagger_i\, \hat{H}_0(\mathbf{R}_i - \mathbf{R}_j)\, \mathbf{\Psi}_j, \tag{2.2}$$

at density corresponding to two electrons per site, where

$$\mathbf{\Psi}_{\mathbf{k}} = \begin{pmatrix} s_{\mathbf{k}\uparrow} \\ s_{\mathbf{k}\downarrow} \\ p_{\mathbf{k}\uparrow} \\ p_{\mathbf{k}\downarrow} \end{pmatrix}\ , \quad \mathbf{\Psi}_i = \begin{pmatrix} s_{i\uparrow} \\ s_{i\downarrow} \\ p_{i\uparrow} \\ p_{i\downarrow} \end{pmatrix}\ , \tag{2.3}$$

are four component spinors in momentum, $\mathbf{\Psi}_{\mathbf{k}}$, and real, $\mathbf{\Psi}_i$, space, with i labelling the unit cell at position $\mathbf{R}_i$. $\hat{H}_0(\mathbf{k})$ is the 4×4 matrix

$$\begin{aligned} \hat{H}_0(\mathbf{k}) = &\big(M - t\,\epsilon_{\mathbf{k}}\big)\,\sigma_0\otimes\tau_3 - t'\,\epsilon_{\mathbf{k}}\,\sigma_0\otimes\tau_0 \\ &+ \lambda\,\sin k_x\,\sigma_3\otimes\tau_1 - \lambda\,\sin k_y\,\sigma_0\otimes\tau_2\,, \end{aligned} \tag{2.4}$$

with $\mathbf{k} = \big(k_x, k_y\big)$ and $\epsilon_{\mathbf{k}} = \big(\cos k_x + \cos k_y\big)$ while $\hat{H}_0(\mathbf{R}_i - \mathbf{R}_j)$ its Fourier transform in real space. The parameters $t' - t$, $t' + t$ and λ correspond, respectively, to the $s - s$, $p - p$ and $s - p$ nearest neighbour hybridisation amplitudes. Finally, M describes an onsite energy difference between the two orbitals.

Hereafter, I shall analyse the Hamiltonian (2.4) for $M > 0$, $t' = 0.5\,t$ and $\lambda = 0.3\,t$. The precise values of the latter two are not crucial to the physics of the model. What really matters is the relative magnitude of M and t, and the finiteness of λ. Therefore, for sake of simplicity, I shall set $t = 1$ as the unit of energy.

The band structure can be easily calculated and yields two bands, each degenerate with respect to the spin label σ; a conduction and a valence band, with dispersion $\epsilon_c(\mathbf{k})$ and $\epsilon_v(\mathbf{k})$, respectively, which read

$$\epsilon_c(\mathbf{k}) = -t'\,\epsilon_{\mathbf{k}} + E_{\mathbf{k}}\,, \quad \epsilon_v(\mathbf{k}) = -t'\,\epsilon_{\mathbf{k}} - E_{\mathbf{k}}\,, \tag{2.5}$$

where

$$E_{\mathbf{k}} = \sqrt{\big(M - \epsilon_{\mathbf{k}}\big)^2 + \lambda^2\,\sin^2 k_x + \lambda^2\,\sin^2 k_y}\ . \tag{2.6}$$

With this choice of parameters, these bands describe a direct gap semiconductor for any $M \neq 2$. At the high symmetry points in the Brillouin Zone (BZ), the bands have a defined orbital character, i.e., a defined parity under inversion. Specifically, at $\mathbf{\Gamma} = (0, 0)$,

$$\epsilon_c(\mathbf{\Gamma}) = -2t' + \big|M - 2\big|\,, \quad \epsilon_v(\mathbf{\Gamma}) = -2t' - \big|M - 2\big|\,, \tag{2.7}$$

valence and conduction bands have, respectively, s and p orbital character if $M < 2$, and vice versa if $M > 2$. On the contrary, at the zone boundary points $\boldsymbol{M} = (\pi, \pi)$, $\boldsymbol{X} = (\pi, 0)$, and $\boldsymbol{Y} = (0, \pi)$,

$$\begin{aligned} \epsilon_c(\boldsymbol{M}) &= 2t' + \big(M + 2\big)\,, \quad \epsilon_v(\boldsymbol{M}) = 2t' - \big(M + 2\big)\,, \\ \epsilon_c(\boldsymbol{X}) &= \epsilon_c(\boldsymbol{Y}) = M\,, \qquad\quad \epsilon_v(\boldsymbol{X}) = \epsilon_v(\boldsymbol{Y}) = -M\,, \end{aligned} \tag{2.8}$$

the valence band is p and the conduction one s for any value of M. It follows that, if $M < 2$, there is an avoided band crossing, due to $\lambda \neq 0$, moving from $\mathbf{\Gamma}$ towards the BZ boundary, while, if $M > 2$, each band has predominantly a single orbital character, s the conduction band and p the valence one, see Fig. 2.1. At $M = 2$ the gap closes at $\mathbf{\Gamma}$, around which the dispersion becomes Dirac-like,

$$\epsilon_c(\mathbf{k}) \simeq +\lambda\,\big|\boldsymbol{k}\big|\,, \quad \epsilon_v(\mathbf{k}) \simeq -\lambda\,\big|\boldsymbol{k}\big|\,. \tag{2.9}$$

The transition between the two insulating phases is known to have topological character [9].

I note that the Hamiltonian $\hat{H}_0(\mathbf{k})$ commutes with σ_3, i.e., is invariant under $U(1)$ spin rotations around the z-axis, as well as under inversion and time reversal, respectively represented by the operators

$$\begin{aligned} \mathcal{I}:\ &\hat{H}_0(\mathbf{k}) = \sigma_0 \otimes \tau_3\ \hat{H}_0(-\mathbf{k})\ \sigma_0 \otimes \tau_3\,, \\ \mathcal{T}:\ &\hat{H}_0(\mathbf{k}) = \big(-i\sigma_2 \otimes \tau_0\big)\ \hat{H}_0^*(-\mathbf{k})\ \big(i\sigma_2 \otimes \tau_0\big)\,. \end{aligned} \tag{2.10}$$

In addition, it is invariant under spatial, i.e., not affecting spins, C_4 rotations, which correspond to

$$\mathcal{C}_4:\ \hat{H}_0(\mathbf{k}) \quad = \mathrm{e}^{-i\,\frac{\pi}{2}\,L_3}\ \hat{H}_0\big(\mathrm{C}_4(\mathbf{k})\big)\ \mathrm{e}^{\,i\,\frac{\pi}{2}\,L_3}\,, \tag{2.11}$$

where $\mathrm{C}_4(\mathbf{k}) = \big(k_y, -k_x\big)$, and the z-component of the angular momentum operator is

$$L_3 = \sigma_3 \otimes \frac{\tau_0 - \tau_3}{2}\,. \tag{2.12}$$

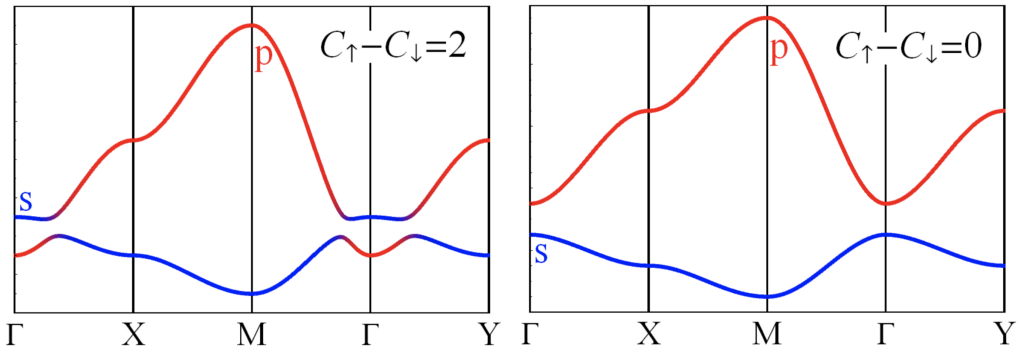

Figure 2.1: Band structure of the BHZ model in the topological, left panel, and trivial, right panel, regimes. Blue and red colours indicate, respectively, even (s orbital character) and odd (p orbital character) parity under inversion.

Evidently, since the Hamiltonian is also invariant under spin $U(1)$ rotations, with generator $S_3 = \sigma_3 \otimes \tau_0/2$, it is also invariant under $\pi/2$ rotations with generator the total angular momentum along z, i.e., $J_3 = L_3 + S_3$, which provides a better definition of C_4.
I observe that, if C_σ is the Chern number of the spin-σ valence-band electrons, then invariance under both inversion and time reversal entails a vanishing $\left(C_\uparrow + C_\downarrow\right)$, which is proportional to the transverse charge-conductance, but a possibly non zero $\left(C_\uparrow - C_\downarrow\right)$, which would correspond to a finite transverse spin-conductance, thus the nontrivial topology of a QSHI [109]. Specifically, $\left(C_\uparrow - C_\downarrow\right) \neq 0$ occurs when $M < 2$ [9,102], not surprisingly in view of the avoided band crossings. I emphasise that a robust topological invariant can be defined provided spin $U(1)$ symmetry is preserved.
So far I have discussed the main properties of the non-interacting Hamiltonian (2.2). However, physically, electrons unavoidably interact with each other. I shall therefore add to the non-interacting Hamiltonian (2.2) a local Coulomb interaction $U_{\rm int}$, thus neglecting its long range tail, which includes, besides monopoles terms, also a dipole-dipole interaction $U_{\rm dip}$, which is here allowed by symmetry. Specifically,

$$U_{\rm int} = U + U_{\rm dip}\,, \tag{2.13}$$

where

$$U = \sum_i \left(U_s\, n_{is\uparrow} n_{is\downarrow} + U_p\, n_{ip\uparrow} n_{ip\downarrow} + V\, n_{is} n_{ip} \right), \tag{2.14}$$

includes monopole terms, while the dipole-dipole interaction, projected onto the basis of single-particle wavefunctions, reads

$$U_{\rm dip} = \frac{J}{2} \sum_i \left[\left(\mathbf{\Psi}_i^\dagger\, \sigma_0 \otimes \tau_1\, \mathbf{\Psi}_i \right)^2 + \left(\mathbf{\Psi}_i^\dagger\, \sigma_3 \otimes \tau_2\, \mathbf{\Psi}_i \right)^2 \right]. \tag{2.15}$$

All coupling constants, U_s, U_p, V and J, are positive, $n_{is\sigma} = s_{i\sigma}^\dagger\, s_{i\sigma}$, $n_{ip\sigma} = p_{i\sigma}^\dagger\, p_{i\sigma}$, and $n_{is(p)} = n_{is(p)\uparrow} + n_{is(p)\downarrow}$. Hereafter, in order to reduce the number of independent parameters and thus simplify the analysis, I shall take $U_s = U_p = U$. Moreover, the numerical solution will be carried out with the further simplification $U = V$.

I end mentioning that a calculation similar to the one I am going to present has been performed by Chen and Shindou [99], though in the magnetised BHZ model, which includes just two orbitals: $|s\uparrow\rangle$ and, differently from the time-reversal invariant case, see Eq. (2.1), the $J = 3/2$, $J_z = +1/2$ orbital $|p_+\downarrow\rangle$. Physically, this correspond to consider an anomalous quantum Hall insulator rather than a QSHI.

2.3 Methods and approximations

2.3.1 Hartree-Fock approximation

The simplest way to include the effects of a not too strong interaction is through the Hartree-Fock approximation (HF), which amounts to approximate the self-energy functional simply by the Hartree and Fock diagrams. For sake of simplicity, I shall introduce the HF approximation under the assumption of unbroken translational symmetry, so that the lattice total momentum is a good quantum number. Whenever needed, I will mention what changes when translational symmetry is broken. Within the HF approximation, if

$$\hat{G}_0(i\epsilon, \mathbf{k})^{-1} = i\epsilon - \hat{H}_0(\mathbf{k})\,, \tag{2.16}$$

is the inverse of the non-interacting 4×4 Green's function matrix at momentum $\mathbf{k}$ and in Matsubara frequencies, $i\epsilon$, the interacting Green's function is

$$\hat{G}(i\epsilon, \mathbf{k})^{-1} = \hat{G}_0(i\epsilon, \mathbf{k})^{-1} - \hat{\Sigma}_{HF}\big[\hat{G}\big]\,, \tag{2.17}$$

where, in the specific case under consideration, the self-energy within the HF approximation is functional of the local Green's function

$$\hat{\Sigma}_{HF}\Big[\hat{G}(\mathbf{R}_i, \mathbf{R}_i)\Big] = \sum_{\alpha,a=0}^{3} \sigma_\alpha \otimes \tau_a\, \Gamma^0_{\alpha a}\, \Delta_{\alpha a}(\mathbf{R}_i)\,, \tag{2.18}$$

with

$$\begin{aligned} \Delta_{\alpha a}(\mathbf{R}_i) &\equiv T\sum_{\epsilon} \mathrm{e}^{i\epsilon\, 0^+}\ \mathrm{Tr}\Big(\hat{G}(i\epsilon, \mathbf{R}_i, \mathbf{R}_i)\, \sigma_\alpha \otimes \tau_a\Big) \\ &= \langle\, \mathbf{\Psi}_i^\dagger\, \sigma_\alpha \otimes \tau_a\ \mathbf{\Psi}_i\ \rangle \equiv \langle\, \mathrm{O}_{\alpha a}(\mathbf{R}_i)\,\rangle \in \mathbb{R}\,, \end{aligned} \tag{2.19}$$

which become independent of the site coordinates $\mathbf{R}_i$ if translational symmetry holds, i.e., $\Delta_{\alpha a}(\mathbf{R}_i) \to \Delta_{\alpha a}$. The Dyson equation (2.17), together with (2.18) and (2.19), yield a self-consistency condition that has to be solved. $\Gamma^0_{\alpha a}$ are the irreducible scattering amplitudes in the HF approximation, and,

through Eq. (2.13), their expressions can be readily derived:

$$\begin{aligned}
\Gamma^0_{00} &= \frac{U+2V-2J}{4}\,, & \Gamma^0_{03} &= \frac{U-2V+2J}{4}\,,\\
\Gamma^0_{01} &= -\frac{V-4J}{4}\,, & \Gamma^0_{02} &= -\frac{V}{4}\,,\\
\Gamma^0_{10} &= \Gamma^0_{20} = -\frac{U}{4}\,, & \Gamma^0_{30} &= -\frac{U+2J}{4}\,,\\
\Gamma^0_{11} &= \Gamma^0_{21} = -\frac{V+2J}{4}\,, & \Gamma^0_{31} &= -\frac{V}{4}\,,\\
\Gamma^0_{12} &= \Gamma^0_{22} = -\frac{V-2J}{4}\,, & \Gamma^0_{32} &= -\frac{V-4J}{4}\,,\\
\Gamma^0_{13} &= \Gamma^0_{23} = -\frac{U}{4}\,, & \Gamma^0_{33} &= -\frac{U-2J}{4}\,.
\end{aligned} \tag{2.20}$$

I note that the scattering amplitudes posses the same spin $U(1)$ symmetry of the non-interacting Hamiltonian, namely, $\Gamma^0_{1a} = \Gamma^0_{2a} \neq \Gamma^0_{3a}$, $a = 0, \ldots, 3$.

The expectation values $\Delta_{00}(\mathbf{R}_i) = \langle n_{is} + n_{ip} \rangle$ and $\Delta_{03}(\mathbf{R}_i) = \langle n_{is} - n_{ip} \rangle$, which measure the local density and orbital polarisation, respectively, are finite already in absence of interaction. In this case, the effects of the scattering amplitudes Γ^0_{00} and Γ^0_{03} treated within HF are, respectively, to shift the chemical potential, which can be discarded since the density is fixed at half filling, and renormalise upward the value of M, thus enlarging the stability region of the non topological phase.

On the contrary, all other expectation values $\Delta_{\alpha a}(\mathbf{R}_i)$, $(\alpha, a) \neq (0,0), (0,3)$, break one or more symmetries of the non-interacting Hamiltonian, and therefore vanish identically in the non interacting case. They could become finite should interaction be strong enough to lead to spontaneous symmetry breaking. I expect this should primarily occur in those channels whose scattering amplitudes are the most negative ones, being $\Delta_{\alpha a}(\mathbf{R}_i)$ real by definition. If $V \simeq U$, as I shall assume in the following numerical calculations, the dominant symmetry breaking channels are therefore those with $(\alpha, a) = (3,0)$, $(1,1)$, $(2,1)$. I emphasise that the dipolar coupling constant J plays an important role in splitting the large degeneracies of the scattering amplitudes in (2.20) that exist at $J = 0$.

Specifically,

$$\Delta_{30}(\mathbf{R}_i) = \langle \mathbf{\Psi}_i^\dagger \, \sigma_3 \otimes \tau_0 \, \mathbf{\Psi}_i \rangle = \sum_{l=s,p} \langle \, n_{il\uparrow} - n_{il\downarrow} \, \rangle \,, \tag{2.21}$$

corresponds to a spontaneous spin polarisation along the z-axis, which breaks time reversal symmetry. I shall investigate two possible magnetic orders, $\Delta_{30}(\mathbf{R}_i) = \Delta_{30}\, \mathrm{e}^{i\boldsymbol{Q}\cdot\mathbf{R}_i}$, with $\mathbf{Q} = (0,0)$ or $\mathbf{Q} = (\pi, \pi)$, corresponding, respectively, to ferromagnetism or antiferromagnetism. I point out that the latter implies a breakdown of translational symmetry, in which case the Green's function is not anymore diagonal in $\mathbf{k}$, but depends on it as well as on $\mathbf{k} + \mathbf{Q}$, so it becomes an 8×8 matrix, and Eq. (2.17) must be modified accordingly.

On the contrary,

$$\begin{aligned}
\Delta_{11}(\mathbf{R}_i) &= \langle \mathbf{\Psi}_i^\dagger \, \sigma_1 \otimes \tau_1 \, \mathbf{\Psi}_i \rangle = \sum_{\sigma=\uparrow,\downarrow} \langle s^\dagger_{i\sigma} \, p_{i-\sigma} + p^\dagger_{i\sigma} \, s_{i-\sigma} \rangle \,,\\
\Delta_{21}(\mathbf{R}_i) &= \langle \mathbf{\Psi}_i^\dagger \, \sigma_2 \otimes \tau_1 \, \mathbf{\Psi}_i \rangle = -i \sum_{\sigma=\uparrow,\downarrow} \sigma \, \langle s^\dagger_{i\sigma} \, p_{i-\sigma} + p^\dagger_{i\sigma} \, s_{i-\sigma} \rangle \,,
\end{aligned} \tag{2.22}$$

describe a spin-triplet exciton condensate polarised in the plane. Since the insulator has a direct gap, excitons condense at $\mathbf{Q} = \mathbf{0}$, namely $\Delta_{\alpha 1}(\mathbf{R}) = \Delta_{\alpha 1}$, and $\alpha = 1, 2$. Moreover, because $\Gamma^0_{11} = \Gamma^0_{21}$, if I write

$$\Delta_{11} = \Delta \cos\phi\,, \quad \Delta_{21} = \Delta \sin\phi\,, \tag{2.23}$$

I expect to find a solution with the same amplitude Δ for any value of ϕ, which reflects the spin $U(1)$ symmetry. At any given ϕ, such exciton condensation would break spin $U(1)$, inversion and time reversal symmetry.

The emergence of an exciton condensate is therefore accompanied by a spontaneous spin $U(1)$ symmetry breaking. As previously mentioned, such breakdown prevents the existence of the strong topological invariant that characterises the QSHI phase. Specifically, since the z-component of the spin is not anymore a good quantum number, the counter propagating edge states of opposite spin are allowed to couple each other, which turns their crossing into an avoided one [102]. The boundary thus becomes insulating, spoiling the topological transport properties of the QSHI.

I shall study this phenomenon performing an HF calculation in a ribbon geometry with open boundary conditions (OBC) along x, but periodic ones along y. Consequently, the non-interacting BHZ Hamiltonian looses translational invariance along the x-direction, while keeping it along y, so that the Green's function becomes a $4N_x \times 4N_x$ matrix for each momentum k_y, with N_x the number of sites along x. A further complication is that HF self-energy in Eq. (2.17) unavoidably depends on the x-coordinate of each site, which enlarges the number of self-consistency equations to be fulfilled. However, since those equations can be easily solved iteratively, I can still numerically afford ribbon widths, i.e., values of N_x, which provide physically sensible results with negligible size effects.

The OBC calculation gives access not only to the states that may form at the boundaries, but also, in the event of a spontaneous symmetry breaking, to the behaviour of the corresponding order parameter moving from the edges towards the bulk interior. In practice, I shall investigate such circumstance only in the region of Hamiltonian parameters when the dominant instability is towards the spin-triplet exciton condensation.

2.3.2 Bethe-Salpeter equation

If I start from the QSHI, $M < 2$, and adiabatically switch on the interaction (2.13), I expect that such phase will for a while survive because of the gap, till, for strong enough interaction, it will eventually give up to a different phase. I already mentioned that the first effect of interaction is to renormalise upward M, thus pushing the topological insulator towards the transition into the non topological one. Beside that, a repulsive interaction can also bind across gap particle-hole excitations, i.e., create excitons.

A direct way to reveal excitons is through the in-gap poles of linear response functions. Within the HF approximation for the self-energy functional, the linear response functions must be calculated solving the corresponding Bethe-Salpeter (BS) equations using the HF Green's functions together with the irreducible scattering amplitudes in Eq. (2.20), which are actually the functional derivatives of $\hat{\Sigma}_{HF}[\hat{G}]$ with respect to $\hat{G}$.

If the interaction is indeed able to stabilise in-gap excitons, their binding energy must increase with increasing interaction strength. It is therefore well possible that the excitons touch zero energy at a critical interaction strength, which would signal an instability towards a different, possibly

symmetry-variant phase. Consistency of the approximation requires that such instability should also appear in the unconstrained HF calculation as a transition from the topological insulator to another phase, especially if such transition were continuous. I shall check that is indeed the case.

With my notations, see Eqs. (2.19) and (2.20), a generic correlation function will be defined as

$$\chi_{\alpha a;\beta b}(\tau,\mathbf{R}) \equiv -\big\langle\, T_\tau\Big(\, \mathrm{O}_{\alpha a}(\tau,\mathbf{R})\, \mathrm{O}_{\beta b}(0,\mathbf{0})\,\Big)\,\big\rangle\,, \tag{2.24}$$

where T_τ is the time-ordering operator, and the operators $\mathrm{O}_{\alpha a}(\mathbf{R}_i) = \mathbf{\Psi}_i^\dagger \sigma_\alpha \otimes \tau_a \mathbf{\Psi}_i$ are evolved in imaginary time τ. Spin $U(1)$ symmetry implies that the z-component S_z of the total spin is conserved. It follows that the only non zero correlation functions $\chi_{\alpha a;\beta b}$ have α and β either 0 and 3, corresponding to $S_z = 0$, or 1 and 2, satisfying

$$\begin{aligned} \chi_{1a;1b}(\tau,\mathbf{R}) &= \chi_{2a;2b}(\tau,\mathbf{R})\,, \\ \chi_{1a;2b}(\tau,\mathbf{R}) &= -\chi_{2a;1b}(\tau,\mathbf{R})\,, \end{aligned} \tag{2.25}$$

whose combinations $\chi_{1a;1b} \pm i\,\chi_{1a;2b}$ describe the independent propagation of $S_z = \pm 1$ particle-hole excitations. The Fourier transform $\chi_{\alpha a;\beta b}(i\omega,\mathbf{q})$, in momentum and in Matsubara frequencies, are obtained through the solution of a set of BS equations

$$\chi_{\alpha a;\beta b}(i\omega,\mathbf{q}) = \chi^{(0)}_{\alpha a;\beta b}(i\omega,\mathbf{q}) + \sum_{\gamma c} \chi^{(0)}_{\alpha a;\gamma c}(i\omega,\mathbf{q})\, \Gamma^0_{\gamma c}\, \chi_{\gamma c;\beta b}(i\omega,\mathbf{q})\,, \tag{2.26}$$

where

$$\begin{aligned} \chi^{(0)}_{\alpha a;\beta b}(i\omega,\mathbf{q}) = \frac{1}{N}\sum_{\mathbf{k}} T \sum_{\epsilon} \\ \mathrm{Tr}\Big(\sigma_\alpha \otimes \tau_a\, \hat{G}(i\epsilon + i\omega, \mathbf{k}+\mathbf{q})\, \sigma_\beta \otimes \tau_b\, \hat{G}(i\epsilon,\mathbf{k})\Big)\,. \end{aligned} \tag{2.27}$$

In Eq. (2.27), N is the number of sites, and $\hat{G}(i\epsilon,\mathbf{k})$ the HF Green's function matrices. I shall perform the above calculation at zero temperature without allowing in the HF calculation any symmetry breaking. With this assumption, the HF Green's function reads

$$\hat{G}(i\epsilon,\mathbf{k}) = \frac{(i\epsilon + t'\epsilon_{\mathbf{k}})\, \sigma_0 \otimes \tau_0 + \hat{H}_{HF}(\mathbf{k})}{\big(i\epsilon - \epsilon_c(\mathbf{k})\big)\big(i\epsilon - \epsilon_v(\mathbf{k})\big)} \tag{2.28}$$

where $\hat{H}_{HF}(\mathbf{k})$, $\epsilon_c(\mathbf{k})$ and $\epsilon_v(\mathbf{k})$ are those in equations (2.4) and (2.5), with M in (2.4) and (2.6) replaced by an effective M_{HF} determined through the self-consistency equation

$$M_{HF} = M - \frac{2\,\Gamma^0_{03}}{N} \sum_{\mathbf{k}} \frac{M_{HF} - \epsilon_{\mathbf{k}}}{E_{\mathbf{k}}}\,. \tag{2.29}$$

For $V \simeq U$, $\Gamma^0_{03} < 0$ so that, since the sum over $\mathbf{k}$ is positive, $M_{HF} > M$, as anticipated.
In short notations, and after analytic continuation on the real axis from above, $i\omega \to \omega + i\eta$, with $\eta > 0$ infinitesimal, the physical response functions are obtained through the set of linear equations

$$\hat{\chi}(\omega,\mathbf{q}) = \Big[\, \mathbb{1} - \hat{\chi}^{(0)}(\omega,\mathbf{q})\, \hat{\Gamma}^{\,0}\,\Big]^{-1}\, \hat{\chi}^{(0)}(\omega,\mathbf{q})\,. \tag{2.30}$$

The excitons are in-gap solutions $\omega_i(\mathbf{q})$, i.e.,

$$\omega_i(\mathbf{q}) < \omega_{\min}(\mathbf{q}) \equiv \min_{\mathbf{k}} \Big(\epsilon_c(\mathbf{k}+\mathbf{q}) - \epsilon_v(\mathbf{k})\Big)\,, \tag{2.31}$$

of the equation

$$\det\left[\, \mathbb{1} - \hat{\chi}^{(0)}\big(\omega_i(\mathbf{q}), \mathbf{q}\big)\, \hat{\Gamma}^{\,0} \,\right] = 0\,, \tag{2.32}$$

and have either z-component of the spin $S_z = 0$, if they appear in the channels with $\alpha, \beta = 0, 3$, or $S_z = \pm 1$, in the channels with $\alpha, \beta = 1, 2$. For $\omega \simeq \omega_i(\mathbf{q})$, the response functions can be expanded in Laurent series [99]

$$\hat{\chi}(\mathbf{q}, \omega) = \sum_i \frac{A_i(\mathbf{q})}{\omega - \omega_i(\mathbf{q}) + i\eta}\, |\psi_i(\mathbf{q})\rangle \langle \psi_i(\mathbf{q})| + \dots\,, \tag{2.33}$$

where $|\psi_i(\mathbf{q})\rangle$ is the exciton wavefunction and $A_i(\mathbf{q})$ its spectral weight. This allows computing the exciton Chern number through the integral of the Berry curvature

$$\begin{aligned} C_i &= \frac{1}{2\pi} \int d^2\mathbf{q}\ \Omega_i(\mathbf{q})\,, \\ \Omega_i(\mathbf{q}) &= \mathrm{Im}\ \langle\, \partial_x \psi_i(\mathbf{q}) \mid \partial_y \psi_i(\mathbf{q}) \,\rangle\ . \end{aligned} \tag{2.34}$$

The curvature is even under inversion and odd under time reversal; if a system is invariant under both, the Chern number thus vanishes by symmetry.
I observe that all the excitons are invariant under inversion, but, while the $S_z = 0$ ones are also invariant under time reversal, the latter maps onto each other the $S_z = +1$ and $S_z = -1$ excitons. Accordingly, only the $S_z = \pm 1$ excitons can have non-zero Chern numbers, actually opposite for opposite S_z, while the $S_z = 0$ excitons are constrained to have trivial topology. I stress that such result, being based only upon symmetry considerations, remains valid for every inversion symmetric QSHI, and not only in the context of the interacting BHZ model.
The exciton Chern number does not seem to be directly related to any quantised observable. Nonetheless, as pointed out in Refs. [99, 110], a nonzero C_i ensures the presence of chiral exciton modes localised at the edges of the sample, which may have direct experimental consequences.

2.4 Results

In the preceding sections I have introduced a conserving mean-field scheme to consistently calculate both the phase diagram and the linear response functions. Now, I move to present the numerical results obtained by that method at zero temperature and with Hamiltonian parameters $t' = 0.5$, $\lambda = 0.3$, $V = U = U_s = U_p$ and $J = U/16$, see equations (2.4), (2.13), (2.14) and (2.15). The value of J is estimated from 1s and 2p hydrogenoic orbitals, which may provide a reasonable estimate of the relative order of magnitude between the dipole interaction and the monopole one.

2.4.1 Hartree-Fock phase diagram

The HF phase diagram is shown in Fig. 2.2. As I previously mentioned, the interaction effectively increases M, thus pushing the transition from the topological insulator (QSHI) to the non topological one (Band Insulator) to lower values of M the larger U. This is precisely what happens for $M \gtrsim 1.1$: U increases the effective M_{HF}, see eq. (2.29), until $M_{HF} = 2$. At this point the gap closes and, for still larger U, the QSHI turns into the trivial Band Insulator.

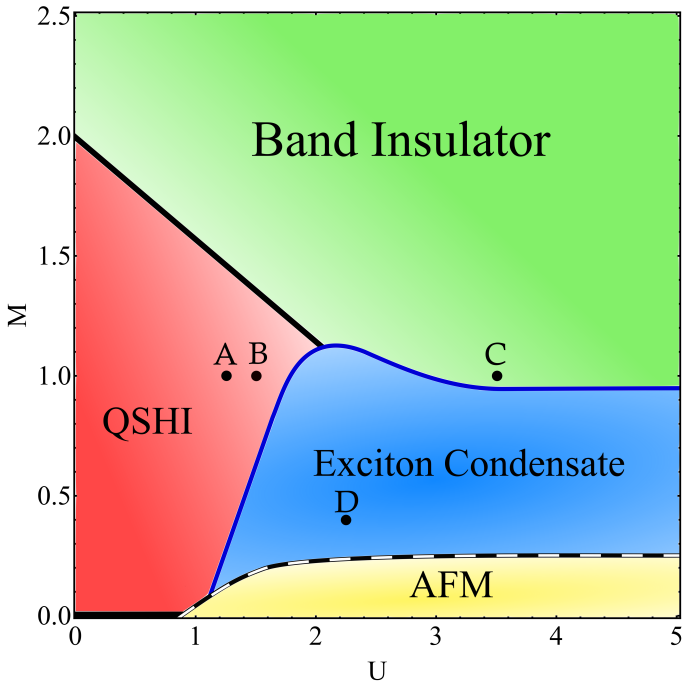

Figure 2.2: Hartree-Fock phase diagram at $\lambda = 0.3$, $t' = 0.5$, $U_s = U_p = V = U$ and $J = U/16$. The topological insulator is denoted as QSHI, while the non topological one as Band Insulator. For small value of M, AFM is stabilised upon increasing U. For larger values of M, U stabilises a symmetry broken phase with Exciton Condensate. The thick black line that separates the QSHI from the Band Insulator, as well as that at $M = 0$ extending from $U = 0$ to the AFM phase, indicate a gapless metallic phase. The transition between the Exciton Insulator and the QSHI or the Band Insulator is continuous, while the transition into the AFM insulator is first order.

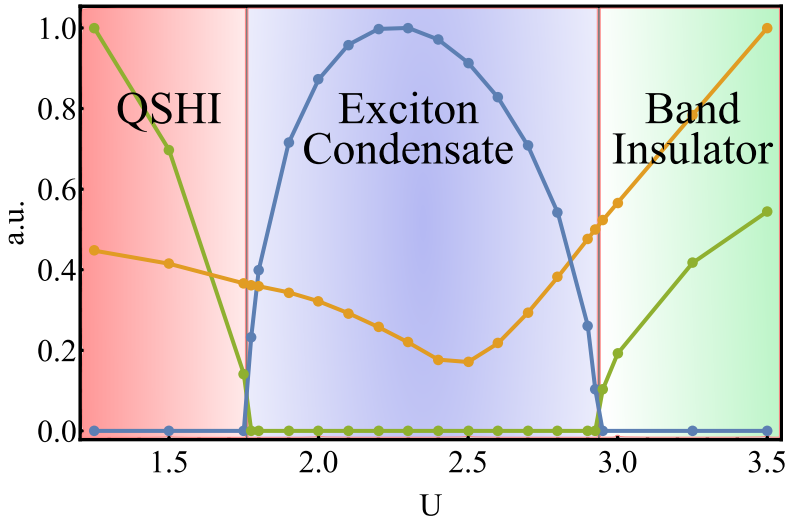

Figure 2.3: Order parameter Δ of Eq. (2.23) (blue), lowest $S_z = \pm 1$ exciton energy at $\mathbf{Q} = \mathbf{0}$ (green), and band gap (orange) along the path A to C in Fig. 2.2 ($M = 1$, $U \in [1.25, 3.5]$), i.e., from the topological to the trivial insulator crossing the exciton insulator. I note that the intermediate phase emerges exactly when the exciton becomes massless, as well as that the band gap never vanishes.

For very small $M \lesssim 0.2$, upon increasing U the QSHI gives in to an antiferromagnetic insulator (AFM), characterised by finite order parameters $\Delta_{30}(\mathbf{R}_i) = \Delta_{30}\, e^{i\boldsymbol{Q}\cdot\mathbf{R}_i}$, see Eq. (2.21), with $\mathbf{Q} = (\pi, \pi)$, thus magnetised along z. HF predicts such transition to be of first order, in accordance to more accurate dynamical mean field theory calculations [111], which also explains why I do not find any precursory softening of $S_z = 0$ exciton at $\mathbf{Q}$.

More interesting is what happens for $0.2 \lesssim M \lesssim 1.1$. Here, increasing the interaction U drives a transition into a phase characterised by the finite order parameter in Eq. (2.23), thus by a spontaneous symmetry breaking of spin $U(1)$, time reversal and inversion symmetry. The breaking of time reversal allows the system moving from the QSHI to the Band Insulator without any gap closing [102–104], see Fig. 2.3. I note that the transition into the symmetry variant phase happens to be continuous, at least within HF. As I mentioned, consistency of this approach implies that this transition must be accompanied by the softening of the excitons whose condensation signals the birth of the symmetry breaking. These excitons are those with $S_z = \pm 1$, and indeed get massless on both sides of the transition, see Fig. 2.3.

The HF numerical results in the ribbon geometry with OBC along x show that electron correlations get effectively enhanced near the boundaries, [105–107] unsurprisingly because of the reduced coordination [112]. Indeed, the order parameter is rather large at the edges, and, moving away from them, decays exponentially towards its bulk value, as expected in an insulator. Remarkably, even when the bulk is in the QSHI stability region, a finite symmetry breaking order parameter exponentially localised at the surface layer may still develop, see Fig. 2.4 that refers to the point B in the phase diagram of Fig. (2.2). In the specific two dimensional BHZ model that I study, such phenomenon is an artefact of the Hartree-Fock approximation, since the spin $U(1)$ symmetry can-

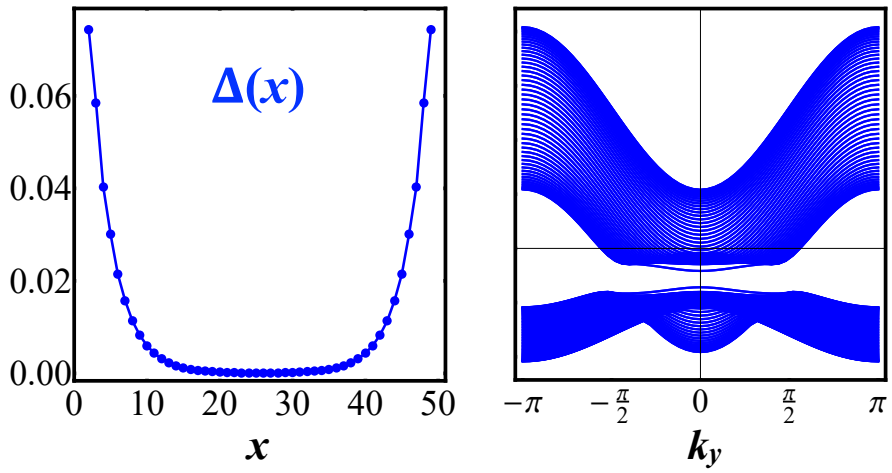

Figure 2.4: Left panel: exciton condensation order parameter $\Delta(x)$ in Eq. (2.23) as function of the x-coordinate in a ribbon geometry with $N_x = 50$ sites, calculated at point B in Fig. 2.2 ($M = 1$, $U = 1.5$). Right panel: The ribbon band structure as function of the momentum k_y. I note that, even though the condensate is exponentially localised at the edges of the system, still it has a strong effect on the single-particle edge states: a gap opens between the two branches, preventing topological spin transport.

not be broken along the one dimensional edges. Nonetheless, the enhanced quantum fluctuations, while preventing a genuine symmetry breaking, should all the same substantially affect the physics at the edges.

I end the discussion of the Hartree-Fock phase diagram by comparing my results with those obtained by Xue and MacDonald [104]. These authors, too, apply the HF approximation to study the BHZ model but in the continuum limit and in presence of a long range Coulomb interaction. They also find a path between the topological insulator and the trivial one that crosses another insulating phase characterised by spontaneous time reversal symmetry breaking, which, they argue, further breaks C_4 symmetry, thus being nematic. The HF band structure that I find in the exciton condensate phase is instead perfectly C_4 invariant, which might apparently indicate that my phase and that of Ref. [104] are different. In reality, I believe the two phases are just the same phase. Indeed, while it is true that the order parameter (2.23) is not invariant under the C_4 symmetry of Eq. (2.11) that changes $\phi \to \phi - \pi/2$, such shift can be reabsorbed by a $-90°$ spin $U(1)$ rotation. In other words, the order parameter (2.23) is invariant under a magnetic C_4' symmetry of the Hamiltonian, whose generator of $\pi/2$ rotations is $L_3 - S_3$ times the rotation of $\mathbf{k}$. Due to such residual symmetry, the band structure as well as the magnetoelectric tensor discussed later in section 2.4.3 do not show nematicity.

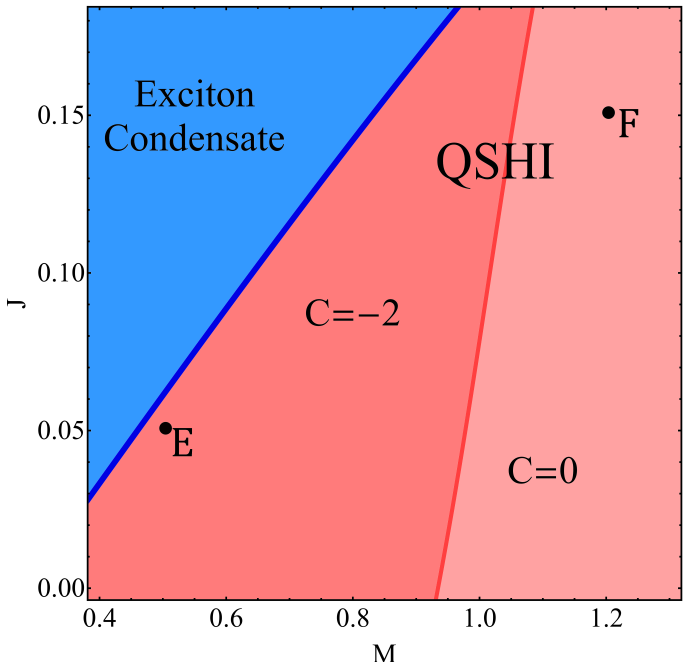

Figure 2.5: Chern number of the most bound exciton with $S_z = -1$ at $\lambda = 0.3$, $t' = 0.5$, $U_s = U_p = V = 1.5$, as function of M and J close to the transition from the QSHI to the symmetry broken phase.

2.4.2 Excitons and their topological properties

The mechanism that triggers exciton topology is similar to the band inversion in the single-particle case: a topological exciton is composed by particle-hole excitations that have different parity under inversion in different regions of the BZ. In this case study four possible orbital channels τ_a, $a = 0, \ldots, 3$, are allowed, each possessing a well defined parity: τ_1 and τ_2 odd, while τ_0 and τ_3 even. In the non-topological insulator, the $S_z = \pm 1$ excitons have the same parity character at all inversion invariant **k**-points, $\boldsymbol{\Gamma}$, $\boldsymbol{M}$, $\boldsymbol{X}$ and $\boldsymbol{Y}$, and thus are topologically trivial. On the contrary, in the QSHI, the highly mixed bands entail that all channels have finite weight in the exciton, which may acquire non trivial topology when its symmetry under parity changes among the inversion invariant **k**-points, thus entailing one or more avoided crossings.

In Fig. 2.5 I show the Chern number of the lowest energy exciton branch with $S_z = -1$ calculated through Eq. (2.34) with $U_s = U_p = V = 1.5$ as function of M and J along the way from the QSHI to the symmetry broken phase where excitons condense. I observe that the dipole-dipole interaction J favours not only the instability of the $S_z = \pm 1$ excitons, but also their non trivial topology, signalled by a non zero Chern number. In Fig. 2.6 I show for the two points E and F in Fig. 2.5 the $S_z = -1$ exciton bands, $\omega_i(\mathbf{q})$, $i = 1, 2$ along high-symmetry paths in the BZ, together with the continuum of $S_z = -1$ particle-hole excitations, bounded from below by $\omega_{\min}(\mathbf{q})$, see Eq. (2.31). The upper branch is very lightly bound, and almost touches the continuum, unlike the lower branch, whose binding energy is maximum at the $\boldsymbol{\Gamma}$ point where, eventually, the condensation

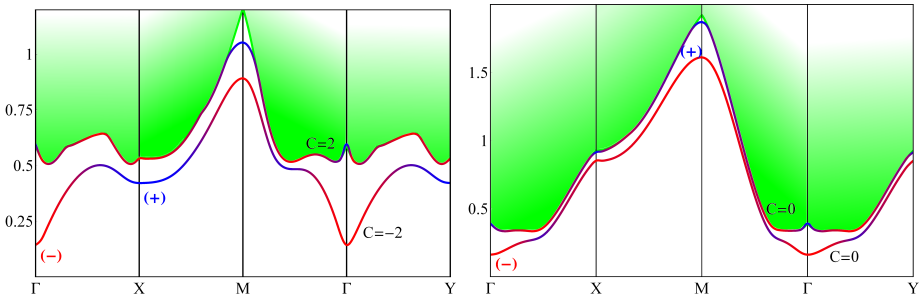

Figure 2.6: $S_z = -1$ exciton dispersion along high-symmetry paths in the Brillouin zone, calculated for the two points E, top panel, and F, bottom panel, in Fig. 2.5. The green shaded regions are the particle-hole continuum. The blue and red colours of the curves indicate even (+) and odd (-) parity under inversion, while C is the corresponding Chern number.

will take place. The blue and red colours indicate, respectively, even (+) and odd (-) parity character under inversion. I note that at point F in Fig. 2.5 both exciton bands have vanishing Chern number, signalled by the same parity character at all inversion-invariant **k**-points. On the contrary, at point E, close to the transition, the two exciton branches change parity character among the high-symmetry points, and thus acquire finite and opposite Chern numbers, $C = \pm 2$.

For completeness, in Fig. 2.7 I show at the same points E and F of Fig. 2.5 the dispersion of the $S_z = 0$ excitons. Since they are invariant under time reversal, I also indicate their symmetry, even (black dots) or odd (yellow dots), which correspond, respectively, to the spin singlet and spin triplet with $S_z = 0$ components of the exciton.
Comparing Fig. 2.7 with 2.6, I note that the $S_z = 0$ excitons are far less bound than the $S_z = -1$ ones. However, it is conceivable that the inclusion of the long range part of the Coulomb interaction could increase the binding energy of the $S_z = 0$ excitons, even though it is likely that the $S_z = \pm 1$ excitons would still be lower in energy.

Moving to the sample surface at point E I expect two phenomena to occur. First, chiral exciton edge modes should appear, and connect the two branches with opposite Chern numbers, in analogy with the single particle case, and as thoroughly discussed by the authors of Ref. [99] in the magnetised BHZ model. In addition, my previous results in the ribbon geometry, showing that the exciton condensate appears on the surface earlier than the bulk, suggest the existence of genuine surface excitons, more bound than their bulk counterparts, definitely in the $S_z = \pm 1$ channel, but possibly also in the $S_z = 0$ one.
Both the chiral exciton edge modes as well as the surface excitons may potentially have important effects on the physical behaviour at the boundaries. First of all, since the most bound ones correspond to coherent $S_z = \pm 1$ particle-hole excitations, they may provide efficient decay channels for the single-particle edge modes, which are counter propagating waves with opposite $S_z = \pm 1/2$. Experimental evidences of such phenomenon in the purported topological Kondo insulator SmB_6 have been indeed observed [7,8], and previously attributed to scattering off bulk excitons [96]. This is well possible, but should be much less efficient than the scattering off surface exciton modes, which I propose as an alternative explanation. Furthermore, the presence of odd-parity excitons localised at the surface might have direct consequences on the surface optical activity, which could

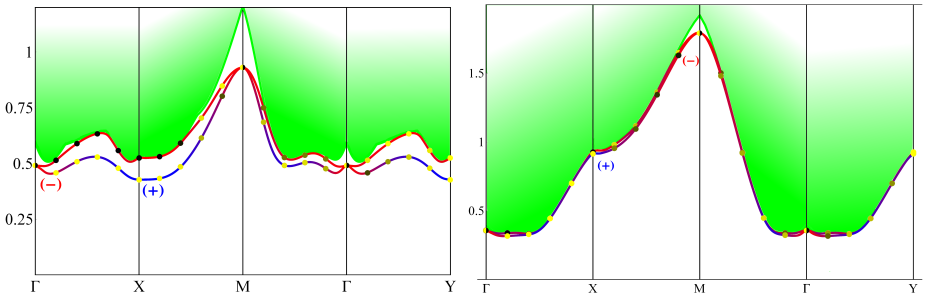

Figure 2.7: Same as Fig. 2.6 but for the $S_z = 0$ excitons. Black and yellow dots indicate that the excitons are, respectively, even and odd under time reversal.

be worth investigating.

2.4.3 Exciton condensate and magnetoelectricity

Since the order parameter in the phase with exciton condensation breaks spin $U(1)$ symmetry, inversion $\mathcal{I}$ and time reversal $\mathcal{T}$, but not $\mathcal{T} \times \mathcal{I}$, it is eligible to display magnetoelectric effects, which can be experimentally detected.
The free energy density expanded up to second order in the external electric and magnetic fields, both assumed constant in space and time, can be written as

$$F(\mathbf{E}, \mathbf{B}) = F_0 - \frac{1}{2}\, \boldsymbol{E} \cdot \hat{\chi}_e\, \boldsymbol{E} - \frac{1}{2}\, \boldsymbol{B} \cdot \hat{\chi}\, \boldsymbol{B} - \boldsymbol{E} \cdot \hat{\alpha}\, \boldsymbol{B}\,, \tag{2.35}$$

where $\hat{\chi}_e$, $\hat{\chi}$ and $\hat{\alpha}$ are the electric polarisability, magnetic susceptibility, and magnetoelectric tensors, respectively. The magnetization, $\boldsymbol{M}$, and polarization, $\boldsymbol{P}$, are conjugate variables of the fields, namely

$$\begin{aligned} \boldsymbol{M} &= -\frac{\partial F}{\partial \boldsymbol{B}} = \hat{\chi}\, \boldsymbol{B} + \hat{\alpha}\, \boldsymbol{E}\,, \\ \boldsymbol{P} &= -\frac{\partial F}{\partial \boldsymbol{E}} = \hat{\chi}_e\, \boldsymbol{E} + \hat{\alpha}\, \boldsymbol{B}\,. \end{aligned} \tag{2.36}$$

I observe that, since $\boldsymbol{E}$ and $\boldsymbol{B}$ have opposite properties under inversion and time reversal, a non-zero $\hat{\alpha}$ is allowed only when both symmetries are broken, but not their product.
Since the exciton condensate Eq. (2.23) is spin-polarised in the $x-y$ plane, with azimuthal angle ϕ, and involves dipole excitations $s \leftrightarrow p_{\pm 1}$, see Eq. (2.1), I restrict my analysis to fields $\boldsymbol{E}$ and $\boldsymbol{B}$ that have only x and y components, which allows us discarding the electromagnetic coupling to the electron charge current. Consequently, the magnetoelectric tensor $\hat{\alpha}$ of interest will be a 2×2 matrix with components α_{ij}, $i, j = x, y$.

In the exciton condensed phase, which is insulating, the coupling to the planar electric field is via the polarisation density, namely, in proper units,

$$\delta H_E = -\sum_i \boldsymbol{\Psi}_i^\dagger \left(E_x\, \hat{d}_x + E_y\, \hat{d}_y \right) \boldsymbol{\Psi}_i\,, \tag{2.37}$$

with dipole operators

$$\hat{d}_x = \sigma_0 \otimes \tau_1\,, \quad \hat{d}_y = \sigma_3 \otimes \tau_2\,. \tag{2.38}$$

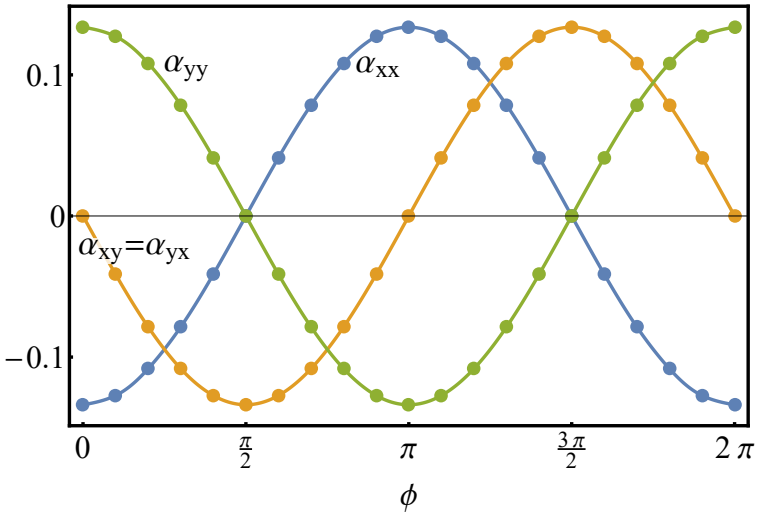

Figure 2.8: Components of the magnetoelectric tensor $\hat{\alpha}$ calculated at the point D in Fig. 2.2 ($M = 0.5$, $U = 2$). The data fit perfectly with the expression in Eq. (2.41).

Moreover, as the orbitals $|s\,\sigma\rangle$ have physical total momentum $J_z = L_z + S_z = \pm 1/2$, while $|p\,\sigma\rangle$ have $J_z = \pm 3/2$, the in-plane magnetic field only couples to the magnetic moment of the s-orbitals. Specifically,

$$\delta H_B = -\sum_i \mathbf{\Psi}_i^\dagger \left(B_x\, \hat{m}_x + B_y\, \hat{m}_y \right) \mathbf{\Psi}_i \,, \tag{2.39}$$

where

$$\hat{m}_x = \sigma_1 \otimes \frac{\tau_0 + \tau_3}{2} \,, \quad \hat{m}_y = \sigma_2 \otimes \frac{\tau_0 + \tau_3}{2} \,. \tag{2.40}$$

Since I am interested in the effects of the external fields once the the symmetry has been broken, I performed a non self-consistent calculation with the HF self-energy calculated at $\boldsymbol{E} = \boldsymbol{B} = \mathbf{0}$. The finite magnetoelectric effect in the presence of the exciton condensate is indeed confirmed, see Fig. 2.8 where I show the components of $\hat{\alpha}$ as function of the azimuthal angle ϕ in Eq. (2.23), and which I find to behave as

$$\hat{\alpha} = \alpha_0 \begin{pmatrix} -\cos\phi & -\sin\phi \\ -\sin\phi & \cos\phi \end{pmatrix} \,, \tag{2.41}$$

where α_0 is proportional to the amplitude Δ of the order parameter, see Eq. (2.23), and thus vanishes when the symmetry is restored.

I remark that the magnetoelectric tensor (2.41) has the form predicted for the magnetic point group $4'$ [113], thus not showing signals of the nematic order proposed in Ref. [104], as earlier discussed in section 2.4.1.

2.5 Discussion

In this chapter I have studied within a conserving mean-field scheme the role of a local electron repulsion in the prototype BHZ model of a quantum spin Hall insulator [9], whose symmetries allows, besides the conventional monopole components of Coulomb interaction, also a dipolar one, which I find to play a rather important role.
In absence of interaction, the BHZ model displays, as function of a mass parameter $M > 0$, two insulating phases, one topological at $M < M_c$, and another non-topological above M_c, separated by a metal point with Dirac-like dispersion at $M = M_c$. The primary effect of Coulomb interaction, namely the level repulsion between occupied and unoccupied states, pushes the critical M_c to lower values, thus enlarging the stability region of the non-topological insulator. Besides that, and for intermediate values of M, the mean field results predict that interaction makes a new insulating phase to intrude between the topological and non-topological insulators, uncovering a path connecting the latter two that does not cross any metal point. In this phase, inversion symmetry and time reversal are spontaneously broken, though their product is not, implying the existence of magnetoelectric effects. The approach to this phase from both topological and non-topological sides is signalled by the softening of two exciton branches, related to each other by time-reversal and possessing, for $M \lesssim 1$ with the parameters of Fig. 2.2, finite and opposite Chern numbers. This phase can therefore be legitimately regarded as a excitonic condensate.
Since, starting from the quantum spin Hall insulator, the softening of those excitons and their eventual condensation occurs upon increasing the interaction, it is rather natural to expect those phenomena to be enhanced at the surface layers. Indeed, the mean field approach in a ribbon geometry predicts the surface instability to precede the bulk one. Even though a genuine exciton condensation at the surface layer might be prevented by quantum and thermal fluctuations, still it would sensibly affect the physics at the surface. The simplest consequence I may envisage is that the soft surface excitons would provide an efficient decay channel for the chiral single-particle edge modes, as indeed observed in the supposedly three-dimensional topological Kondo insulator SmB_6 [7, 8]. In addition, other important consequences on the transport properties and optical activity at the surface cannot be excluded.

I believe that going beyond the approximations assumed throughout this paper should not significantly alter the main results. RPA plus exchange allows accessing in a simple way collective excitations, though it ignores their mutual interaction. I expect that the latter would surely affect the precise location of the transition points, but not wash out the exciton condensation.
Moreover, the inclusion of the neglected long range tail of Coulomb interaction would introduce two terms: the standard monopole-monopole charge repulsion, proportional to $1/r$, and a dipole-dipole interaction decaying as $1/r^3$. The former is expected to increase the exciton binding energy, though without distinguishing between spin singlet and triplet channels. Therefore, the conclusion that the $S_z = \pm 1$ excitons soften earlier than the $S_z = 0$ ones should remain even in presence of the $1/r$ tail of Coulomb interaction. The dipole-dipole interaction might instead favour an inhomogeneous exciton condensation. However, I suspect that the $1/r^3$ decay in two dimensions is not sufficient to stablize domains.

To conclude, I believe that my results, though obtained by a mean field calculation and for a specific model topological insulator, catch sight of still not fully explored effects of electron electron interaction in topological insulators, which might be worth investigating experimentally, as well as

theoretically in other models and, eventually, by means of more reliable tools [114, 115].

CHAPTER 3

MOIRÉ PHONONS AND LOCAL KEKULÉ ORDER IN TBLG

3.1 Introduction

Atomic relaxation in magic angle twisted bilayer graphene (TBLG) is responsible [116–121] of the gap opening between the four flat bands and all other upper and lower ones. Moreover, scattering by acoustic phonons has been invoked [122, 123] to explain the anomalous linear in temperature resistivity of the normal metal phases [124], and both acoustic [122,125–128] and optical [129] modes have been explored as possible mechanisms of the observed superconductivity [12, 13, 15, 19, 20, 26]. In spite of all that, the role of lattice degrees of freedom in the insulating phases of TBLG at integer fillings $\nu = \pm n$, $n = 0, \ldots, 3$, of the flat bands [11–23] has been mostly overlooked in favour of Coulomb interaction [130–139], which struggles to explain superconductivity [128, 140–142], and, especially, the anomalous quantum Hall effect [24, 25] as well as the emergent Kekulé pattern recently observed at $\nu = \pm 2$ [28].

The major importance of the electron-phonon coupling also emerged from Ref. [27] that theoretically uncovered special, almost non dispersive, optical modes, later observed by nano-Raman spectroscopy [144], which are so strongly coupled to the electrons that atomic displacements as small as 5mÅ are sufficient to open sizeable gaps in the flat bands at all integer ν. Those phonons derive from the 1360 cm^{-1} A_1 and B_1 TO modes of a single-layer graphene at the $\mathbf{K}$ point, see Fig. 3.1**b**, superimposed with a long wavelength modulation driven by the van der Waals inter-layer interaction that makes these modes exist throughout the whole reduced Brillouin zone (RBZ) of the moirè superlattice and be localized into the AA stacked regions and the domain walls separating AB from BA stacked ones. Remarkably, these special phonons have the same twofold accidental degeneracy of the flat bands along the $\boldsymbol{\Gamma} \to \mathbf{K} \to \boldsymbol{M}$ high-symmetry path in the RBZ that reflects the emerging $U_v(1)$ valley symmetry [10, 27]. Because of that, the $U_v(1)$ symmetric electron-phonon coupling effectively realises a Jahn-Teller model, which explains the efficacy of a static distortion on lifting the accidental degeneracy.

However, systematic theoretical studies of the lattice contribution to the phase diagram of TBLG are lacking. Indeed, Ref. [27] describes a realistic frozen-phonon tight-binding calculation

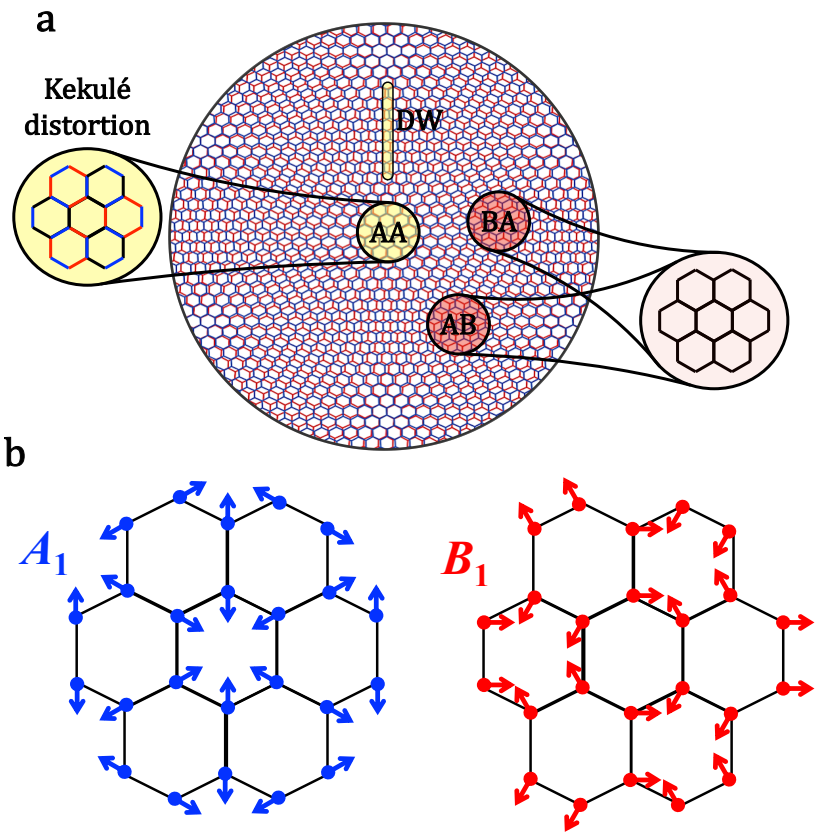

Figure 3.1: **Kekulé-like distortion that stabilises a non- magnetic insulator at charge neutrality**. Panel **a**: Kekulé-like distortion that stabilises a non-magnetic insulator at charge neutrality. Such distortion is driven by moiré optical modes at the $\mathbf{\Gamma}$ point with A_1 and B_1 symmetry, which correspond to long-wavelength modulations of the single-layer graphene A_1 and B_1 modes shown in panel **b**. The moiré optical phonons, and thus the Kekulé distortion, mainly affect the AA stacked regions and the domain walls (DW), both shown in yellow in panel **a**, separating Bernal stacked AB and BA regions, shown in red, the latter remaining almost unaffected [27]. I emphasise that the lattice displacement occurs at the zone center of the reduced Brillouin zone and on the atomic scale of graphene, which distinguishes it from the Kekulé state discussed in Ref. [143].

that neglects Coulomb repulsion and can only access states with broken $U_v(1)$ and, eventually, broken spatial symmetries when the frozen-phonon is not at the $\mathbf{\Gamma}$ point, but not the observed Chern insulators with spontaneously broken time-reversal symmetry. Filling this gap is actually the scope of this work. Specifically, upon integrating out phonons one obtains an effective electron-electron attraction that can be assumed instantaneous since the flat-band width is a lot smaller than the phonon frequency. I treat this interaction on an equal footing with Coulomb repulsion, investigating their mutual interplay and its effect on the phase diagram by means of Hartree-Fock

and projected BCS-wavefunctions calculations.

Before discussing my findings, I believe worth placing them within the general context of correlation effects in graphene. I recall that interaction strength in graphene is sizeable but yet not enough to stabilise a correlated insulator at charge neutrality [145]. An isotropic strain above 8-10% that expands all C-C bonds has been shown to stabilise [146] both an antiferromagnetic insulator and a Kekulé valence-bond (KVB) one, with the latter lower in energy than the former. The Kekulé distortion involves just the above mentioned A_1 and B_1 modes of graphene, whose positive interplay with Coulomb repulsion thus favours the KVB insulator instead of the antiferromagnetic one expected from Coulomb repulsion alone. In light of the vanishingly small Fermi velocity at the Dirac cones in magic-angle TBLG, whose Bloch waves are primarily localised into the AA stacked regions just like the A_1 and B_1 moiré phonons, it is not unlikely that also in this case those phonons cooperate with Coulomb repulsion to stabilise a KVB insulator, with the distortion discussed in Ref. [27] and shown schematically in Fig. 3.1**a**.

That is precisely what I find within Hartree-Fock approximation. I, hereafter, denote such space-selective Kekulé distortion at the zone-center of the moiré Brillouin zone a static Kekulé valence bond (S-KVB) distortion. The corresponding S-KVB insulator at charge neutrality seeds the cascade of symmetry-breaking mean-field insulating states at all other integer fillings.
Since the AA regions are quite far apart from each other, as testified by the tiny dispersion of the A_1 and B_1 modes in TBLG [27], it is well possible that a resonating rather than static Kekulé valence bond (R-KVB) insulator is stabilised, in which each AA region is instantaneously distorted along A_1 or B_1 but dynamically the symmetry is restored.
Since the electron-phonon coupling realises a Jahn-Teller model, S-KVB and R-KVB correspond to static and dynamic Jahn-Teller effect, respectively. Such R-KVB state thus effectively realises a Jahn-Teller-Mott insulator [147]. The close analogy with Anderson's resonating valence bond scenario [148] for cuprates also suggests that the Jahn-Teller-Mott insulator is prone to become a superconductor upon doping; a phonon mediated superconductivity not hindered by Coulomb repulsion [148–150]. I will show that such superconductor is likely to have chiral or nematic d-wave symmetry, in accordance with the analysis of Ref. [129] where the same TO phonons of graphene have been considered as driving mechanism of superconductivity in TBLG.

3.2 Model Hamiltonian and interaction

I consider two AA stacked graphene layers, and rotate around the perpendicular axis layer 1 by $+\theta/2$ and layer 2 by $-\theta/2$, at magic angle $\theta = 1.08°$. The band structure is described through the Bistritzer-MacDonald continuum model [10], using the conventions of Ref. [151]. Specifically, I define four component spinors in momentum space $\Psi_{\mathbf{k},\mathbf{Q}_a,\sigma}$ and $\Psi_{\mathbf{k},\mathbf{Q}_b,\sigma}$, two components corresponding to sublattices A and B of a graphene layer, and the other two to the valley index $\eta = \pm 1$, where σ is the spin, $\mathbf{k}$ runs within the first RBZ, while $\mathbf{Q}_a$ and $\mathbf{Q}_b$ identify the two sublattices in reciprocal space, see Fig. 3.2. The operator $\Psi_{\mathbf{k},\mathbf{Q}_a,\sigma}$ is defined close to the Dirac point $\mathbf{K}$ on layer 1 and $-\mathbf{K}$ on layer 2 for $\eta = +1$ and $\eta = -1$, respectively, while in $\Psi_{\mathbf{k},\mathbf{Q}_b,\sigma}$ the two layers are interchanged. Moreover, the sublattice components of the spinors with $\eta = +1$ and $\eta = -1$ are inverted [151]. It is implicitly assumed that the longest reciprocal lattice vector kept in the calculation is still much smaller that the distance $2|\mathbf{K}|$ between the two valleys, so that the chosen

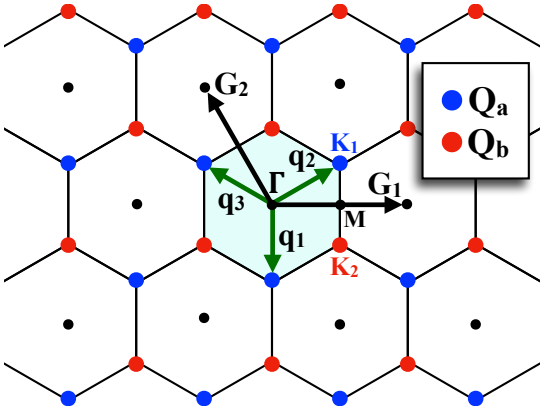

Figure 3.2: **Reciprocal lattice space**. The two sublattices $\mathbf{Q}_a$, blue dots, and $\mathbf{Q}_b$, red dots, of the reduced Brillouin zones, in light cyan the first one, can be generated, e.g., through $\mathbf{Q}_a = \mathbf{q}_1 + \boldsymbol{G}$ and $\mathbf{Q}_b = -\mathbf{q}_1 + \boldsymbol{G}$, where $\boldsymbol{G} = n\boldsymbol{G}_1 + m\boldsymbol{G}_2$ is any reciprocal lattice vector with $\boldsymbol{G}_1$ and $\boldsymbol{G}_2$ the primitive ones. Also shown are the high symmetry points $\boldsymbol{\Gamma}$, $\mathbf{K}_1$, $\mathbf{K}_2$ and $\boldsymbol{M}$.

basis is not overcomplete.
With those definitions, the non-interacting Hamiltonian can be written as

$$H_0 = \sum_{\mathbf{k}\sigma} \sum_{\mathbf{Q},\mathbf{Q}'} \Psi^\dagger_{\mathbf{k},\mathbf{Q},\sigma}\, \hat{H}^{(0)}_{\mathbf{Q}\mathbf{Q}'}(\mathbf{k})\, \Psi_{\mathbf{k},\mathbf{Q}',\sigma}\,, \tag{3.1}$$

where $\mathbf{Q} = \mathbf{Q}_a \oplus \mathbf{Q}_b$, and, in the zero-angle approximation [10],

$$\begin{aligned} \hat{H}^{(0)}_{\mathbf{Q}\mathbf{Q}'}(\mathbf{k}) &= \delta_{\mathbf{Q},\mathbf{Q}'}\, v_F\, \tau_3 \left(\mathbf{k} - \mathbf{Q}\right) \cdot \boldsymbol{\sigma} + \\ &+ \tau_0 \sum_{i=1}^{3} \left(\delta_{\mathbf{Q}-\mathbf{Q}',q_i} + \delta_{\mathbf{Q}'-\mathbf{Q},q_i}\right) \hat{T}_i(u_0,u_1)\,. \end{aligned} \tag{3.2}$$

Hereafter, the Pauli matrices τ_a and σ_a, $a = 0,1,2,3$, act on the valley and sublattice indices, respectively, $\mathbf{q}_i$, $i = 1,2,3$, are defined in Fig. 3.2, while

$$\begin{aligned} \hat{T}_1(u_0,u_1) &= u_0\, \sigma_0 + u_1\, \sigma_1\,, \\ \hat{T}_{j+1}(u_0,u_1) &= \mathrm{e}^{i\frac{2\pi}{3}\sigma_3}\, \hat{T}_j(u_0,u_1)\, \mathrm{e}^{-i\frac{2\pi}{3}\sigma_3}\,, \qquad j = 1,2\,. \end{aligned} \tag{3.3}$$

Setting as unit length the moiré primitive lattice vector for a twist angle of $1.08°$, I fix $v_F = 40\,\mathrm{meV}$, $u_0 = 76.1\,\mathrm{meV}$ and $u_1 = 103.1\,\mathrm{meV}$.
The charge density operators $\rho_\ell(\mathbf{q}+\boldsymbol{G})$ of each layer $\ell = 1,2$ are diagonal in sublattice and valley indices, and read, for $\mathbf{q} \in \mathrm{RBZ}$,

$$\begin{aligned} \rho_\ell(\mathbf{q}+\mathbf{G}) &= \sum_{\mathbf{k}\mathbf{Q}\sigma} \Psi^\dagger_{\mathbf{k},\mathbf{Q},\sigma}\, \hat{\rho}_\ell(\mathbf{Q})\, \sigma_0\, \Psi_{\mathbf{k}+\mathbf{q},\mathbf{Q}-\mathbf{G},\sigma}\,, \\ \hat{\rho}_\ell(\mathbf{Q}) &= \delta_{\mathbf{Q},\mathbf{Q}_a}\, \frac{\tau_0 - (-1)^\ell\, \tau_3}{2} + \delta_{\mathbf{Q},\mathbf{Q}_b}\, \frac{\tau_0 + (-1)^\ell\, \tau_3}{2}, \end{aligned} \tag{3.4}$$

and thus the Coulomb repulsion can be written as

$$H_C = \frac{1}{2N\Omega_c} \sum_{\mathbf{q},\mathbf{G}} \sum_{\ell\ell'} U_{\ell\ell'}(\mathbf{q}+\mathbf{G})\, \rho^\dagger_\ell(\mathbf{q}+\mathbf{G})\, \rho_{\ell'}(\mathbf{q}+\mathbf{G})\,, \tag{3.5}$$

with N the number of supercells, Ω_c the area of each supercell, $U_{11}(\mathbf{q}) = U_{22}(\mathbf{q})$ and $U_{12}(\mathbf{q}) = U_{21}(\mathbf{q})$ the intra- and inter-layer Fourier transforms of the interaction e^2/r screened by the high-frequency dielectric constant $\epsilon_\infty = 9$ of graphene, and by the presence of a dual metal gate [133] assumed at distance $d_g = 30$ nm. I assume the two graphene layers placed at a distance $d_\ell = 0.335\,\text{nm}$, resulting in

$$U_{\ell\ell'}(\mathbf{q}+\mathbf{G}) = \frac{2\pi e^2}{\epsilon_\infty}\,\frac{\tanh(d_g(q+G))}{q+G}\,\left(e^{-d_\ell(q+G)} + \delta_{\ell\ell'}(1-e^{-d_\ell(q+G)})\right). \tag{3.6}$$

The non-retarded attraction mediated by A_1 and B_1 moiré phonons can be straightforwardly derived from Ref. [152] and is

$$H_P = -\frac{1}{2\omega_0\,N}\sum_{\mathbf{q}}\sum_{a=1,2} L_a^\dagger(\mathbf{q})\,L_a(\mathbf{q})\,, \tag{3.7}$$

where $\omega_0 \simeq 1360\ \text{cm}^{-1}$ is the phonon frequency, neglecting its very weak dispersion [27], and

$$L_a(\mathbf{q}) = \sum_{\sigma\mathbf{k}}\sum_{\mathbf{Q}\mathbf{Q}'} \Psi^\dagger_{\mathbf{k},\mathbf{Q},\sigma}\,\tau_a\,\hat{L}_{\mathbf{Q}\mathbf{Q}'}\,\Psi_{\mathbf{k}+\mathbf{q},\mathbf{Q}',\sigma}\,, \tag{3.8}$$

with

$$\hat{L}_{\mathbf{Q}\mathbf{Q}'} = \gamma\,\delta_{\mathbf{Q},\mathbf{Q}'}\,\sigma_0 \;+\sum_{i=1}^{3}\left(\delta_{\mathbf{Q}-\mathbf{Q}',q_i} + \delta_{\mathbf{Q}'-\mathbf{Q},q_i}\right)\hat{T}_i(g_0,g_1)\,. \tag{3.9}$$

$\hat{T}_i(g_0,g_1)$ are the same as in Eq. (3.3) with u_0 and u_1 replaced by g_0 and g_1. I mention that, since sublattices in valleys +1 and -1 are interchanged, g_0 and g_1 are the modulations induced by the phonons on the intralayer hopping between opposite and equal sublattices, respectively, while γ refers to the interlayer opposite sublattice one. The results of realistic tight-binding calculations with frozen phonon displacement [27] are reproduced by the continuum model [152] fixing $g_1 \simeq g_0/10$ and $\gamma \simeq g_0/2.5$, allowing to parametrise the strength of the phonon-mediated attraction through the single coupling constant $g \equiv g_0^2/\omega_0$, with realistic value $\lesssim 1$ meV.
I remark that $H_0 + H_C$ is invariant under global charge $U(1)$, valley $U_v(1)$ and separate spin $SU(2)$ rotations in each valley, thus a large $U(2)\times U(2)$ symmetry [133]. On the contrary, the full Hamiltonian $H_0 + H_C + H_P$ is only invariant under $U(1)\times U_v(1)$ times the global spin $SU(2)$. The following analysis takes into account just the latter reduced symmetry.

3.3 Mean field phase diagram

3.3.1 Hartree-Fock formalism in TBLG

The simplest way to treat a not-too strong electron-electron interaction is through the Hatree-Fock (HF) approximation, which amounts to truncate the skeleton expansion of the self-energy functional at the first order terms. In the context of TBLG, is more convenient to work with the density matrix rather than the interacting Green's function, differently from Chapter 2. The HF ground state is the solution of the following minimum problem over all density matrices $\hat{C}$ corresponding to Slater determinants

$$\min_{\hat{C}}\ \text{Tr}\left[\hat{C}\,\left(H_0 - \frac{1}{2}\Sigma_{HF}[\hat{C}]\right)\right], \tag{3.10}$$

where H_0 is the non-interacting Hamiltonian and $\Sigma_{HF}[\hat{C}]$ the HF self-energy functional of $\hat{C}$. I performed an all-band HF calculation, thus considering the full $\mathbf{k}$-dependence of the Fock self-energy and embracing the full complexity of the band structure and the effects of remote bands on symmetry breaking states.
To further introduce my method, it is convenient to change notation and write the layer-density operator of Eq. 3.4 as

$$\begin{aligned}\rho_\ell(\mathbf{q}+\mathbf{G}) &= \sum_{\mathbf{k}\sigma,i,j} \Psi^\dagger_{\mathbf{k},i\sigma}\, \hat{\rho}_{\ell,ij}(\mathbf{G})\, \Psi_{\mathbf{k}+\mathbf{q},j,\sigma}\,, \\ \hat{\rho}_{\ell,ij}(\mathbf{G}) &= \left(\left(\delta_{\mathbf{Q},\mathbf{Q}_a}\, \frac{\tau_0 - (-1)^\ell \tau_3}{2} + \delta_{\mathbf{Q},\mathbf{Q}_b}\, \frac{\tau_0 + (-1)^\ell \tau_3}{2} \right) \sigma_0\, \delta_{\mathbf{Q}-\mathbf{G},\mathbf{Q}'} \right)_{ij}\,,\end{aligned} \tag{3.11}$$

where the indexes $i,j = (\mathbf{Q},\eta,\mu),(\mathbf{Q}',\eta',\mu')$ include all the internal degrees of freedom, with $\mu = A,B$ the sublattice, and $\hat{\rho}^\dagger_l(\mathbf{G}) = \hat{\rho}_l(-\mathbf{G})$. Introducing the density matrix

$$\begin{aligned}\hat{C}_{ij}(\mathbf{k},\sigma) &\equiv \langle \Psi^\dagger_{\mathbf{k},j\sigma} \Psi_{\mathbf{k},i\sigma} \rangle\,, \\ \hat{C}_{ij} &= \frac{1}{N} \sum_{\mathbf{k},\sigma} \hat{C}_{ij}(\mathbf{k},\sigma)\,,\end{aligned} \tag{3.12}$$

the HF self-energy can be expressed by means of simple matrix multiplications:

$$\begin{aligned}\hat{\Sigma}^{HF}(\mathbf{k},\sigma) &= \frac{1}{N} \sum_{\mathbf{k},\sigma} \sum_{ij} \Psi^\dagger_{\mathbf{k},i\sigma} \left(\Sigma^H_{ij} + \Sigma^F_{ij}(\mathbf{k},\sigma) \right) \Psi_{\mathbf{k},j\sigma} \\ \Sigma^H_{ij} &= \frac{1}{\Omega_c} \sum_{\mathbf{G}} \sum_{\ell\ell'} U_{\ell\ell'}(\mathbf{G})\, \mathrm{Tr}\left[\hat{\rho}_\ell(-\mathbf{G})\, \hat{C} \right] \hat{\rho}_{\ell',ij}(\mathbf{G})\,, \\ \Sigma^F_{ij}(\mathbf{k},\sigma) &= -\frac{1}{N\Omega_c} \sum_{\mathbf{p},\mathbf{G}} \sum_{\ell\ell'} U_{\ell\ell'}(\mathbf{k}-\mathbf{q}+\mathbf{G}) \left(\hat{\rho}_\ell(-\mathbf{G})\, \hat{C}(\mathbf{q},\sigma)\, \hat{\rho}_{\ell'}(\mathbf{G}) \right)_{ij}\,.\end{aligned} \tag{3.13}$$

A similar, but easier, calculation can be done for the potential generated by the phonon-mediated attraction H_P, obtaining the full HF self-energy.
Treating the full $\mathbf{k}$-dependent Fock potential, thought it ensures robust computational results, can be computationally expensive, especially if the reciprocal lattice is taken big enough not to encounter spurious breaking of the translational symmetry in momentum space, i.e.,

$$H_{\mathbf{Q},\mathbf{Q}'}(\mathbf{k}+\mathbf{G}) = H_{\mathbf{Q}-\mathbf{G},\mathbf{Q}'-\mathbf{G}}(\mathbf{k})\,. \tag{3.14}$$

The only approximation made to reduce this complexity is truncating the $\mathbf{G}$ vectors up to the next nearest neighbours, corresponding to 13 vectors (including $\mathbf{G}=0$) up to a distance 4π in reciprocal space.

Moreover, the continuum model for TBLG hides a subtle complication when applying HF: the inter-layer hopping u_0 and u_1 of the non-interacting Hamiltonian are fitted in order to reproduce density functional theory bands. In this sense, the electrostatic effects of occupied bands for the symmetry-invariant ground state are already included in the non-interacting Hamiltonian. To fix this double counting problem, I subtract to the non-interacting Hamiltonian H_0 the Coulomb HF potential generated by the non-interacting ground state

$$H_0 \to H_0 - \Sigma_{HF}[\hat{C}_0]\,. \tag{3.15}$$

where $\hat{C}_0$ is the density matrix induced by H_0. The variational problem of Eq. 3.10 thus becomes

$$\min_{\hat{C}} \mathrm{Tr}\left[\hat{C}\left(H_0 - \Sigma_{HF}[\hat{C}_0] + \frac{1}{2}\Sigma_{HF}[\hat{C}]\right)\right]. \tag{3.16}$$

The energies of the broken symmetry states are then compared with the non-interacting one. This choice of the reference potential has two main advantages: $\hat{C}_0$ is a local minima of the problem by construction, implying that the HF symmetric state is exactly the original non-interacting one and, moreover, this methodology works for any filling.

3.3.2 Numerical results

Due to the peculiar triple-degree of freedom structure of the flat bands, TBLG can in principle host a constellation of symmetry breaking insulating states. Every electron possesses three distinct flavours: the spin one, endowed with $SU(2)$ symmetry; the valley one with $U_\nu(1)$ and generator τ_3; and the Chern number σ_3 that reflect a $\mathbb{Z}_2$ symmetry.
From the HF prospective, the insulators at integer fillings are constructed by selectively occupying those flavours (or a linear combination) according to their HF energies.
Due to particle-hole symmetry, which is only slightly broken by (3.7), only negative fillings are discussed since the corresponding positive ones are easily obtained by a particle-hole transformation.

Charge neutrality: $\boldsymbol{\nu = 0}$

I start analysing the interplay between Coulomb interaction (3.5) and phonon-mediated attraction (3.7) at charge neutrality, $\nu = 0$, where there is consensus [133, 134, 137, 138] that the Coulomb interaction alone stabilises an insulator that has been denoted as Kramer inter-valley coherent (K-IVC) state [133]. This is characterised by the order parameter

$$\Delta_{\text{K-IVC}}(\varphi) \sim \sigma_3 \left(\cos\varphi\,\tau_1 + \sin\varphi\,\tau_2\right), \tag{3.17}$$

which breaks time-reversal symmetry, $\mathcal{T} \sim \tau_1\sigma_1\mathcal{K}$ with $\mathcal{K}$ the complex conjugation, and valley $U_v(1)$ symmetry, but is invariant under $\mathcal{T}\tau_3$. Moreover, it breaks the $\mathcal{C}_{2x} \sim \sigma_1$ twofold rotation, while is invariant under the generalised

$$\mathcal{C}'_{2z}(\varphi) \equiv \mathrm{e}^{-i\varphi\tau_3}\,\mathcal{C}_{2z} \sim \mathrm{e}^{-i\varphi\tau_3/2}\,\tau_1\,\mathrm{e}^{i\varphi\tau_3/2}. \tag{3.18}$$

I note that the order parameter (3.17) commutes with the Chern number σ_3 [133]. Two electrons with given σ_3 may form a spin-triplet valley-singlet, or a spin-singlet valley-triplet. Eq. (3.17) implies that Coulomb interaction favours the latter, with valley polarisation $\boldsymbol{\tau}$ in the xy-plane, opposite for the two different Chern numbers [133].
The phonon-mediated attraction H_P in Eq. (3.7), which can be roughly written as $-g\big(\boldsymbol{\tau}\cdot\boldsymbol{\tau} - \tau_3^2\big)$, still favours a spin-singlet valley-triplet state. However, among the three $\tau_3 = -1, 0, +1$ components, it lowers the energy of the valley-triplet with $\tau_3 = 0$ for both $\sigma_3 = \pm 1$, thus not breaking any of the symmetries. This corresponds to a pseudo-rotation in the $\tau_1 - \tau_2$ plane: the $U_v(1)$ symmetry is instantaneously broken along a direction in that plane but, on average, dynamically restored. Since these pseudo-rotations describe alternating distortions either along A_1 or B_1 modes, the state can be regarded as a resonating Kekulé valence bond. As such, it cannot be

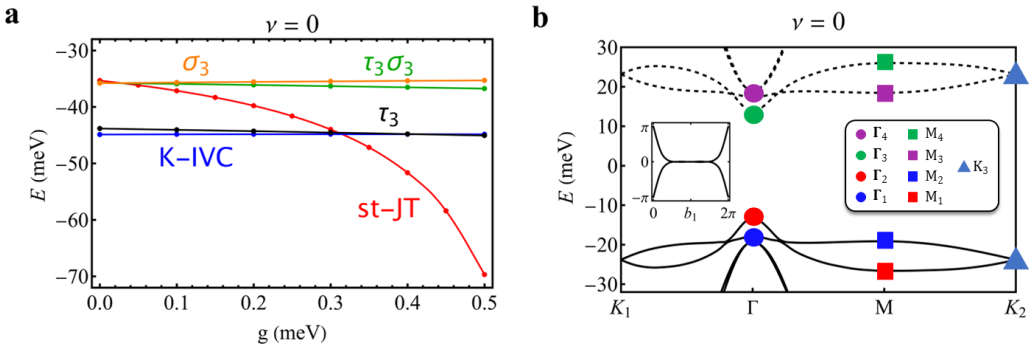

Figure 3.3: **Hartee-Fock results for $\nu = 0$:** Panel **a**: Hartree-Fock energies of the K-IVC and S-KVB variational wavefunctions at charge neutrality, $\nu = 0$, characterised, respectively, by the order parameters Eq. (3.17) and Eq. (3.19), as function of the coupling constant g of the phonon-mediated attraction. In addition, other valley polarized symmetry breaking insulators, characterized by the order parameters σ_3, τ_3 and $\tau_3\sigma_3$ are shown. Panel **b**: Hartree-Fock band structure of the S-KVB state at $g = 0.32\,\text{meV}$ and $\nu = 0$. Solid lines represent valence bands whereas dashed lines conduction ones. Also shown are the symmetry properties of the Bloch waves at the high-symmetry points. In the inset, the Wilson loop of the lowest two flat bands.

represented by a single Slater determinant, hence it is not accessible in HF. It is however possible to study by HF the static counterpart once $U_v(1)$ is explicitly broken through a static distortion along any arbitrary combination of the A_1 or B_1 modes. That amounts to searching for variational wavefunctions with a static Kekulé distortion characterised by the two-component order parameter

$$\Delta_{\text{S-KVB}}(\varphi) \sim \sigma_0 \left(\cos\varphi\, \tau_1 + \sin\varphi\, \tau_2 \right), \tag{3.19}$$

which breaks $U_v(1)$, while it is invariant under $\mathcal{C}_{2x}$, $\mathcal{T}$, and the twofold rotation (3.18). The Fock term of the Coulomb interaction (3.5) may stabilise either order parameters, although $\Delta_{\text{K-IVC}}$ is favoured at charge neutrality [133]. On the contrary, the phonon mediated attraction (3.7) only couples via the Hartree term to $\Delta_{\text{S-KVB}}$.

It is thus reasonable to expect that the cooperation between Coulomb and phonon-mediated interactions may eventually make $\Delta_{\text{S-KVB}}$ prevail over $\Delta_{\text{K-IVC}}$, which is confirmed by the following numerical results. In Fig. 3.3**a**, HF energies of the K-IVC and S-KVB variational states upon increasing the coupling constant g of the attraction are shown, along with other valley-polarized insulating states that however remain always metastable since they are only weakly coupled to the Fock term of H_P. At $g = 0$, K-IVC is the global minimum and S-KVB a local one. Increasing g, the energy of S-KVB lowers and eventually crosses that of K-IVC. For realistic values of g, S-KVB is the stable state, while K-IVC is only metastable. In Fig. 3.3**b** the HF band structure of the S-KVB state at $g = 0.3$ meV is plotted along with the symmetry properties of the Bloch waves, noting that the space group remains $P622$. The band structure describes an insulator with a sizeable gap ~ 30 meV separating the two lower flat bands from the upper two. The Bloch waves of the lower two bands transform like the irreducible representations $\Gamma_1(1)+\Gamma_2(1)$, $M_1(1)+M_2(1)$ and $K_3(2)$, see Fig. 3.3**b**, which hints [151] at a 'fragile' topology, indeed testified by the Wilson

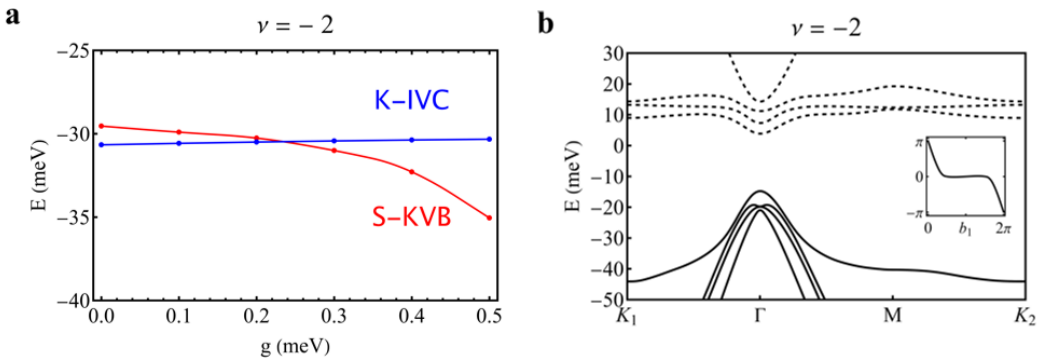

Figure 3.4: **Hartee-Fock results for $\nu = -2$:** Panel **a**: Hartree-Fock energies of the K-IVC and S-KVB variational wavefunctions at half-filling, $\nu = -2$ as function of the coupling constant g of the phonon-mediated attraction. Panel **b**: Hartree-Fock band structure of the S-KVB state at $g = 0.32\,\text{meV}$ and $\nu = -2$. Solid lines represent valence bands whereas dashed lines conduction ones. In the inset, the Wilson loop of the lowest doubly spin-occupied flat band, which indicates a non-zero net Chern number.

loops of the two lower flat bands, see inset of Fig. 3.3**b**. In reality, since the S-KVB state is adiabatically connected to the frozen-phonon insulator of Ref. [27], which was shown to support edge states, that topology is actually robust and implies that the two lower flat bands do have finite and opposite Chern numbers C = ±2.

Half-filling: $\nu = \pm 2$

For integer fillings away from charge neutrality, the sole $U_v(1)$ symmetry-breaking static Kekulé distortion cannot stabilise mean-field insulators, due to the $\mathcal{TC}_{2z}$ protection of the Dirac cones. Therefore additional symmetries must be broken. It can already be anticipated how that occurs by noticing that Jahn-Teller coupling is akin inverted Hund's rules [149, 150, 153] forcing lowest-spin configurations, and that the two occupied flat bands at charge neutrality carry opposite Chern numbers, $\text{C} = \sigma_3 = \pm 1$ per spin [133]. Therefore, if phonon contribution prevails over Coulomb exchange, the Chern number degeneracy is split in the first place by a symmetry-breaking term $\propto \sigma_3$, and only as a last resort spin degeneracy is lifted. At half-filling $\nu = \pm 2$ this corresponds to spin rotationally invariant topological insulators with spin-singlet order parameter

$$\Delta_{\nu=\pm 2}(\varphi) \sim \Delta_{\text{S-KVB}}(\varphi) + \sigma_3\,, \tag{3.20}$$

breaking time-reversal, $\mathcal{C}_{2x}$ and $\mathcal{C}_{2y}$ symmetries, thus leaving just a $P6$ space group.
In the case Coulomb interaction should prevail, K-IVC spin triplet $S = 1$ non-topological insulators [133, 134, 137] should be stabilized.
The former scenario is indeed realized in mean-field, see Fig. 3.4**a** for moderate value of the electron-phonon coupling $g \sim 0.3$ meV, and the resulting Hartree-Fock band structure is shown in Fig. 3.4**b**. As expected, the occupied flat-band has a nonzero winding number of the Wilson loop, suggestive of a topological Chern insulator with Chern number C = ±2.

In reality, this solution, though consistent with experiments [24, 25], is degenerate with other ones at the mean-field level [154]. I observe that the solution whose band structure is shown in panel **b** of Fig. 3.4 can be easily interpreted as deriving from panel **b** of Fig. 3.3 at $\nu = 0$ after the two bands with opposite Chern numbers detach from each other because of the symmetry breaking, and the two electrons occupy the lower one. Since the Chern number per spin of the lowest band can be either $+1$ or -1 depending on the sign of the component $\propto \sigma_3$ of the order parameter (3.20), both signs leading to the same HF energy, and because spin up and down electrons are independent of each other at the mean-field level, I can imagine a situation in which the lowest band has Chern number $+1$ for spin up and -1 for spin down. That corresponds to replacing σ_3 in (3.20) with $s_3\,\sigma_3$, where s_3 is the third Pauli matrix in the spin sector, or, more generally, with any combination of s_1, s_2 and s_3. This solution has the same HF energy as the one with order parameter (3.20), and describes a quantum spin-Hall insulator that also breaks spin $SU(2)$. Even though both solutions are degenerate at the HF level, as first observed in [154], I expect that quantum fluctuations beyond mean-field would tend to restore $SU(2)$ symmetry, eventually stabilising a non-topological insulator. The question about which of the two insulators, topological or not, have lower energy beyond mean-field is an open issue, even though experimental evidence supports the topological one. I will come back to this issue in the context of the resonating valence bond scenario.

Odd fillings: $\nu = -1$ and $\nu = -3$

Insulating solutions at odd fillings $\nu = -1, -3$ and forcing translational symmetry can be stabilised in HF by only assuming that spin $SU(2)$ is broken.
At $\nu = -3$, only one of the eight (including spin) flat bands is occupied, lifting both the Chern number and the spin degeneracy. The S-KVB and the K-IVC insulators collapse into the same state, characterized by an electron with inter-valley coherence occupying one of the four flavours in the spin-Chern subspace. Another possible insulator is spin-valley-Chern polarized (SVCP), thus preserving $U_\nu(1)$ valley symmetry. In this case, the two solutions have a comparable energy already at $g = 0$, see Fig. 3.5**a**. For finite g, the S-KVB becomes unequivocally the ground state, making the result robust under the fine details of the calculation. The spin-polarized bands of the S-KVB insulator are plotted in Fig. 3.4**b**.

At filling $\nu = -1$, three of the eights flat bands are occupied. Since the spin symmetry is broken, one spin projection will have two electrons and the other just one. At the HF level, the two low energy candidates are found by removing an electron to one of the two spin species from the charge neutrality solutions of K-IVC and S-KVB. The minority spin thus resembles the state stabilized at $\nu = -3$, while the majority spin is exactly the one at charge neutrality, but now not doubly occupied. Also in this case, the S-KVB insulator becomes stable for $g \sim 0.3$ meV, see Fig. 3.5**c**, resulting again in a spin-polarized topological insulator whose bands are plotted in Fig. 3.5**d**.

Alignment with hBN

In all the experimental realizations of TBLG, the system is encapsulated or sitting on a hexagonal boron nitrate (hBN) substrate. In the case of perfect alignment between one of the graphene layers and the substrate, the system displays a radically different phase diagram; without superconducting

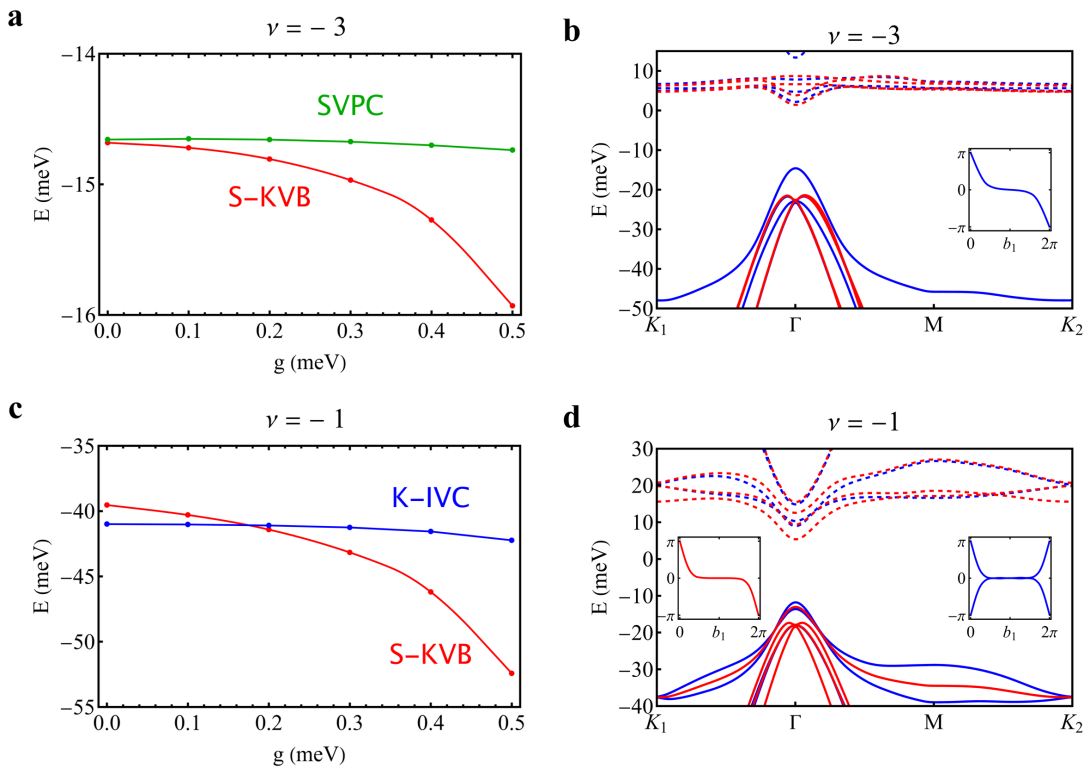

Figure 3.5: **Hartee-Fock results for $\nu = -3$ and $\nu = -1$:** Panel **a-b**: Hartee-Fock energies of the most stable insulators at $\nu = -3$, -1, respectively, as function of the coupling constant g of the phonon-mediated attraction. Panel **c-d**:Hartree-Fock bands of the S-KVB state for $g = 0.32$ meV at $\nu = -3$, -1 respectively. The blue and red bands correspond to majority and minority spins, respectively. In the inset, the Wilson loops of the occupied bands are shown.

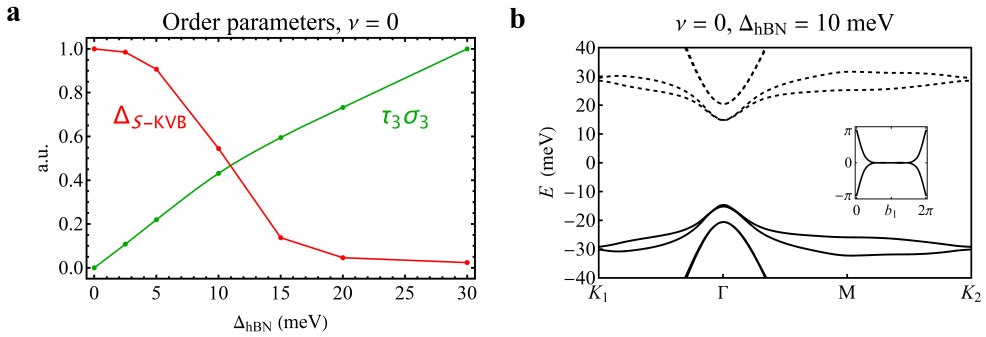

Figure 3.6: **Hartee-Fock results for hBN**: Panel **a** shows the evolution of the order parameters of the S-KVB density matrix increasing the hBN coupling constant. Panel **b** shows the band structure and the Wilson loop of the S-KVB state at $\Delta_{hBN} = 10\,\text{meV}$: the bands and their topology are left almost untouched by the presence of the substrate.

domes and with clear-cut experimental evidences of insulating states only at $\nu = 0$ and $\nu = 3$ [20, 21, 155]. I am thus interested in the case of slight misalignment, to verify if the phase diagram is robust under a small breaking of the C_{2z} symmetry.

Considering a TBLG on top of an hBN substrate, the potential generated by a perfectly aligned hBN can be treated, in first approximation, by including a staggered on-site potential $\sigma_3\,\tau_3$ [156] acting on the bottom graphene layer. Reminding that the bottom layer correspond to the ($\mathbf{Q}_b$, $\eta = +1$) and ($\mathbf{Q}_a$, $\eta = -1$) points, the external potential can be written as

$$V_{\text{hBN}} = \frac{\Delta_{hBN}}{2}\,\delta_{\mathbf{Q}\mathbf{Q}'}\,\left(\,\sigma_3\,\tau_3 + (\delta_{\mathbf{Q},\mathbf{Q}_b} - \delta_{\mathbf{Q},\mathbf{Q}_a})\,\sigma_3\,\right)\,, \tag{3.21}$$

where $\Delta_{hBN} = 30\,\text{meV}$ in case of perfect alignment [156]. I approximate the case of misaligned hBN by taking a Δ_{hBN} in Eq. (3.21) smaller than the value of 30 meV corresponding to perfect alignment.

The results at charge neutrality $\nu = 0$ that are, in reality, representative of the behaviour at all integer fillings are presented in Fig. 3.6. Increasing Δ_{hBN}, the density matrix of the system develops a small C_{2z} symmetry breaking term, characterized by the order parameter $\sigma_3\,\tau_3$. The S-KVB order parameter is slightly diminished by the presence of the substrate, but the band structure and the topological properties of the ground states are unaffected. In the case of a perfectly aligned substrate, i.e. $\Delta_{hBN} = 30\,\text{meV}$, the S-KVB order parameter is vanishingly small, and the system is driven into a valley polarized insulator characterized by $\sigma_3\,\tau_3 \simeq \pm 1$.

Summary of HF results and comparison with experimental evidences

The Hartree-Fock calculations suggest that the introduction of the coupling to moiré phonons radically changes the phase diagram of the system, in accordance with a successive preprint that also considers strain effects [154]. At all integer fillings, when the electron-phonon coupling reaches approximately 0.3 meV, the lowest energy solutions are insulating, exhibit a local Kekulé pattern, and are topological but at charge neutrality. It is important to remark that these results, consistent

with experimental evidence [12, 16, 22, 157–163], depend on the Kekulé coupling overruling the Coulomb exchange [153]. In the opposite case, the K-IVC state would be stable at charge neutrality, and Coulomb exchange would presumably realize conventional Hund's rules, thereby lifting spin degeneracy to create high-spin states. This would lead, for example, to spin $S = 1$ non-topological insulators at $\nu = \pm 2$ [133, 134, 137], in contrast to the $S = 0$ topological ones that I find.

I stress that only the former scenario is consistent with experimental evidence of anomalous quantum Hall effect at $\nu = \pm 2$ [24, 25], and in particular, with recent high-resolution STM measurements on ultra-low-strain samples [28]. According to these measurements, the ground state wavefunction breaks the $U_v(1)$ valley symmetry displaying a Kekulé pattern at the graphene scale, but does not show the circulating currents peculiar to K-IVC, ruling out this state and pointing toward the S-KVB one as the most promising candidate for the actual insulating states realized in TBLG.

I conclude the discussion of the HF results by mentioning, for completeness, that there is actually a third possibility I have not taken into account: that the insulators break moiré translational symmetry [27]. This scenario appears to be realized only under large enough strain, both theoretically [154, 164] and experimentally [28].

3.4 Resonating valence bonds beyond mean field

Hartree-Fock is only able to describe static Kekulé distortions, and predicts tiny atomic displacement because of the large phonon frequency compared to the narrow insulating gaps that are opened. Since the A_1 and B_1 moiré optical phonon dispersions in momentum space are negligible, around four orders of magnitude less than the center-of-mass frequency [27], one can legitimately regard those modes as collective vibrations of almost independent moiré supercells [144] as if they were thousand-atom large molecules. Therefore, also in light of the extremely narrow width of the flat bands, it cannot be excluded that, in reality, Kekulé valence bonds resonate, namely they occurs without spontaneously breaking $U_v(1)$. As earlier mentioned, that would corresponds to the S-KVB distortion, see Fig. 3.1, being replaced by a R-KVB one. If that were the case, the above mean-field insulating phases should be replaced by their dynamical counterparts, i.e., by Jahn-Teller Mott insulators [147] in which the effectively inverted Hund's rules and the Coulomb repulsion conspire to halt electron motion and to freeze each moiré supercell in the state that maximises the local energy gain with a number of electrons equal to the average one. In the present case of magic-angle TBLG, a simple description of a Jahn-Teller Mott insulator runs into several obstacles. First, each supercell contains an unmanageable large number of π-orbitals that prevents dealing with Jahn-Teller effect as one would do in a simple molecule. For that reason, I assume that focusing just on the flat-bands already yields a reasonable physical description, in that akin to dealing just with LUMO and HOMO in a molecule. That raises another issue: the topological obstruction [130, 151, 165] prevents building localised Wannier orbitals for the flat bands. To overcome such obstacle, I note that the Jahn-Teller Mott insulator has built-in pairing correlations [148–150]. With this in mind, I argue that a reasonable description of that state can be gained through a Gutzwiller projected BCS wavefunction [148]

$$|\nu\rangle = P_{\mathrm{G}}(\nu)\,|BCS\rangle\ , \tag{3.22}$$

where $|BCS\rangle$ is the BCS wavefunction for the flat bands, and $P_{\rm G}(\nu)$ the Gutzwiller projector onto the configurations where each supercell is strictly occupied by $4+\nu$ flat-band electrons. Since the goal is just to infer physical features of the resonating counterparts of the S-KVB mean-field insulating states, I shall not attempt to optimise the ansatz wavefunction (3.22), which is anyhow practically impossible, but assume that its properties are simply inherited by the BCS wavefunction [166], hence by the geminal pair-wavefunctions that are favoured by the phonon-mediated attraction and Coulomb repulsion. For that, I am first going to project H_P (3.7) onto the eigenoperators of the flat bands, as previously done for the Coulomb interaction [131,133,137], then I am going to include the effect of the Coulomb repulsion via its pseudopotential.

Phonon mediated electron-electron attraction projected onto the flat bands

Fist, I define the non-interacting flat bands wavefunctions

$$\hat{H}^{(0)}\,|u_{\eta n}(\mathbf{k})\rangle = \epsilon_{\eta n}(\mathbf{k})\,|u_{\eta n}(\mathbf{k})\rangle\ , \tag{3.23}$$

where $n=1$ for the lower and $n=2$ for the upper flat bands at given valley ν, and the gauge for the wave-function introduced in [136] is adopted

$$\begin{aligned} &C_{2z}T\,|u_{\eta n}(\mathbf{k})\rangle = |u_{\eta n}(\mathbf{k})\rangle\ ,\\ &C_{2z}\mathcal{P}\,|u_{\eta n}(\mathbf{k})\rangle = \eta\,(-)^{n+1}\ |u_{-\eta\overline{n}}(\mathbf{k})\rangle\ , \end{aligned} \tag{3.24}$$

where $\overline{1}=2$, $\overline{2}=1$. Moreover, a smooth gauge across the BZ is selected

$$\lim_{\mathbf{q}\to 0}\Big(\langle u_{\eta 1}(\mathbf{k}+\mathbf{q})|u_{\eta 1}(\mathbf{k})\rangle - \langle u_{-\eta 2}(\mathbf{k}+\mathbf{q})|u_{-\eta 2}(\mathbf{k})\rangle\Big) = 0\,. \tag{3.25}$$

The creation operators of the flat bands can be now defined as

$$\Psi^\dagger_{\mathbf{k},\sigma,\eta,n} \equiv \sum_{\mathbf{Q}\alpha} u_{\eta n;\mathbf{Q}\alpha}(\mathbf{k})\,\Psi^\dagger_{\mathbf{k},\mathbf{Q}\alpha,\sigma,\eta} \tag{3.26}$$

where $\alpha = A,B$ refers to the graphene sublattice. Finally, I remark that the phonon mediated attraction

$$H_P = -\frac{g}{2N}\sum_{\mathbf{q}}\left(\,L^\dagger_x(\mathbf{q})\,L_x(\mathbf{q}) + L^\dagger_y(\mathbf{q})\,L_y(\mathbf{q})\,\right), \tag{3.27}$$

is controlled by the pseudo-density operators which couples only two electrons with opposite valleys

$$\begin{aligned} L_{x(y)}(\mathbf{q}) &= \sum_{\mathbf{k}\,\sigma}\sum_{\mathbf{Q}\mathbf{Q}'}\Psi^\dagger_{\mathbf{k},\mathbf{Q},\sigma}\,\tau_{x(y)}\,\hat{L}_{\mathbf{Q}\mathbf{Q}'}\ \Psi_{\mathbf{k}+\mathbf{q},\mathbf{Q}',\sigma}\,,\\ \hat{L}_{\mathbf{Q}\mathbf{Q}'} &= \left(\,\frac{1}{10}\delta_{\mathbf{Q},\mathbf{Q}'}\sigma_0 + \sum_{i=1}^{3}\left(\delta_{\mathbf{Q},\mathbf{Q}'+\mathbf{q}_i}+\delta_{\mathbf{Q},\mathbf{Q}'-\mathbf{q}_i}\right)T_i\left(1,\frac{1}{2.5}\right)\,\right). \end{aligned} \tag{3.28}$$

Considering only the flat bands and restricting to electron pairs with zero total momentum, I obtain

$$\begin{aligned} H_P = -\frac{g}{N}\sum_{\mathbf{k}\mathbf{k}'}\sum_{\sigma\sigma'\eta}\sum_{mnm'n'} &L^{\eta}_{mn}(\mathbf{k},\mathbf{k}')\,L^{-\eta}_{m'n'}(-\mathbf{k},-\mathbf{k}')\times\\ &\times\Psi^\dagger_{\mathbf{k},\sigma,\eta,m}\Psi^\dagger_{-\mathbf{k},\sigma',-\eta,m'}\Psi_{-\mathbf{k}',\sigma',\eta,n'}\Psi_{\mathbf{k}',\sigma,-\eta,n}\,, \end{aligned} \tag{3.29}$$

where the form factors are defined as the valley off diagonal matrix elements of the pseudo-density

$$L^{\eta}_{mn}(\mathbf{k},\mathbf{k}') \equiv \langle u_{\eta m}(\mathbf{k})|\, \hat{L}\, |u_{-\eta n}(\mathbf{k}')\rangle \ . \tag{3.30}$$

I shall analyse the spin-singlet channel first, and then discuss the spin-triplet one. I can already anticipate that, because Jahn-Teller effectively realizes inverted Hund's rules [149, 150, 153], the latter will be higher in energy.
Spin-singlet pair creation operators can be straightforwardly defined as

$$S^{\dagger}_{nm}(\mathbf{k},\eta) \equiv \frac{1}{\sqrt{2}} \left(\Psi^{\dagger}_{\mathbf{k},\uparrow,\eta,n} \Psi^{\dagger}_{-\mathbf{k},\downarrow,-\eta,m} + \Psi^{\dagger}_{-\mathbf{k},\uparrow,-\eta,m} \Psi^{\dagger}_{\mathbf{k},\downarrow,\eta,n} \right) , \tag{3.31}$$

which, by definition,

$$S^{\dagger}_{nm}(\mathbf{k},\eta) = S^{\dagger}_{mn}(-\mathbf{k},-\eta)\,, \tag{3.32}$$

and transforms under C_{2z} and particle-hole $\mathcal{P}$ as [136]

$$\begin{aligned} C_{2z}\, S^{\dagger}_{nm}(\mathbf{k},\eta)\, C^{-1}_{2z} &= S^{\dagger}_{nm}(-\mathbf{k},-\eta)\,, \\ \mathcal{P}\, S^{\dagger}_{nm}(\mathbf{k},\eta)\, \mathcal{P}^{-1} &= (-)^{nm}\, S^{\dagger}_{\overline{n}\,\overline{m}}(-\mathbf{k},\eta)\,. \end{aligned} \tag{3.33}$$

In particular, C_{2z} symmetry entails four invariant channels

C_{2z}	(+)	(+)	(+)	(-)
	$S^{\dagger}_{11}(\mathbf{k},\eta)$	$S^{\dagger}_{22}(\mathbf{k},\eta)$	$S^{\dagger}_{12}(\mathbf{k},\eta) + S^{\dagger}_{21}(\mathbf{k},\eta)$	$S^{\dagger}_{12}(\mathbf{k},\eta) - S^{\dagger}_{21}(\mathbf{k},\eta)$

Using Eq.(3.32), I can write the Hamiltonian in a block diagonal form

$$\begin{aligned} H_P = -\frac{g}{N} \sum_{\mathbf{k}\mathbf{k}'} \sum_{\eta} \sum_{mnm'n'} & L^{\eta}_{mn'}(\mathbf{k},-\mathbf{k}')\, L^{-\eta}_{m'n}(-\mathbf{k},\mathbf{k}') \times \\ & \times S^{\dagger}_{mm'}(\mathbf{k},\eta)\, S_{nn'}(\mathbf{k}',\eta)\,. \end{aligned} \tag{3.34}$$

From the combined C_{2z} symmetry of both the singlet creation operators and the wave-functions, it follows that the two diagonal blocks with opposite η are actually the same object, such that η it is a redundant index. I thus get rid of this redundancy by defining

$$\begin{aligned} \Delta^{\dagger}_{\mathbf{k},nm} &\equiv S^{\dagger}_{nm}(\mathbf{k},+1)\,, \\ V_{nm,n'm'}(\mathbf{k},\mathbf{k}') &\equiv 2\, L^{+1}_{nm'}(\mathbf{k},-\mathbf{k}')\, L^{-1}_{mn'}(-\mathbf{k},\mathbf{k}')\,. \end{aligned} \tag{3.35}$$

The phonon-mediated attraction projected upon the singlet Cooper pairs with zero total momentum finally becomes

$$H_P = -\frac{g}{N} \sum_{\mathbf{k}\mathbf{k}'} \sum_{mnm'n'} V_{nm,n'm'}(\mathbf{k},\mathbf{k}')\, \Delta^{\dagger}_{\mathbf{k},nm}\, \Delta_{\mathbf{k}',n'm'}\,, \tag{3.36}$$

and is diagonalized by the creation operators

$$H_P \to -g \sum_i \lambda_i\, \Delta^{\dagger}_i\, \Delta_i \qquad \Delta^{\dagger}_i = \sum_{\mathbf{k},nm} \psi^{i}_{nm}(\mathbf{k})\, \Delta^{\dagger}_{\mathbf{k},nm}\,. \tag{3.37}$$

The wavefunction $\psi^{i}_{nm}(\mathbf{k})$ inherits the same symmetry properties of the singlet creation operators in Eq. (3.33). Accordingly, if $\psi^{nn}_{i}(\mathbf{k}) \neq 0$, then $\psi^{12}_{i}(\mathbf{k}) = \psi^{21}_{i}(\mathbf{k})$ and the eigenstate is even

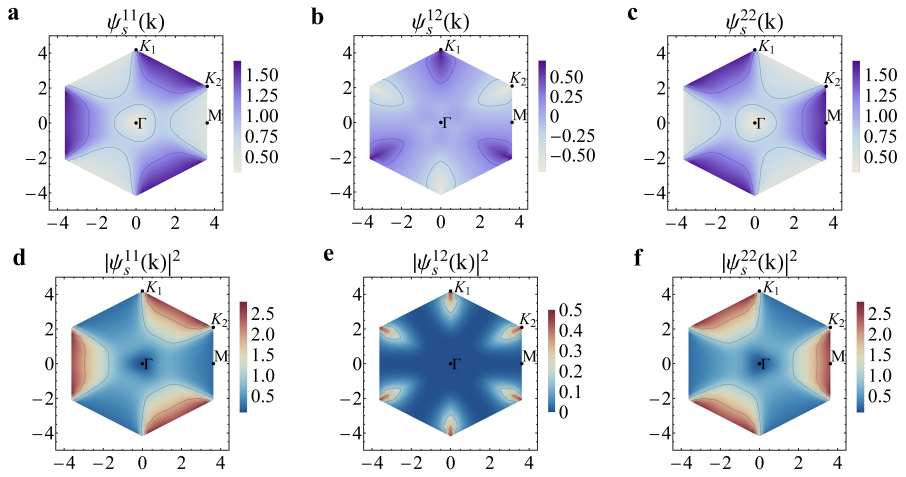

Figure 3.7: ***s*-wave pair wavefunction in momentum space**. Panels **a-c**: intra-band, $\psi_s^{11}(\mathbf{k})$ (**a**) and $\psi_s^{22}(\mathbf{k})$ (**c**), and inter-band, $\psi_s^{12}(\mathbf{k}) = \psi_s^{21}(\mathbf{k})$ (**b**), components of the spin-singlet s-wave pair wavefunctions in momentum space. Panels **d-f**: same as in panels **a-c** but showing the probability distribution in momentum space.

under C_{2z}, while it is odd if $\psi_i^{nn}(\mathbf{k}) = 0$ and $\psi_i^{12}(\mathbf{k}) = -\psi_i^{21}(\mathbf{k})$. Moreover, since particle-hole symmetry $\mathcal{P}$ is nearly satisfied, the eigenstate is (almost) even under $\mathcal{P}$ if $\psi_i^{11}(\mathbf{k}) \simeq \psi^{22}(-\mathbf{k})$ and $\psi_i^{12}(\mathbf{k}) \simeq -\psi_i^{12}(-\mathbf{k})$, and odd otherwise. Similarly, the eigenstate is even under C_{2x} if $\psi_i^{nn}\big(C_{2x}(\mathbf{k})\big) = \psi_i^{nn}(\mathbf{k})$ and $\psi_i^{12}\big(C_{2x}(\mathbf{k})\big) = -\psi_i^{12}(\mathbf{k})$, and odd in the opposite case. Finally, the component of $\psi_i^{nm}(\mathbf{k})$ even under $\mathbf{k} \to -\mathbf{k}$ corresponds to the spin-singlet, valley-triplet with $\tau_3 = 0$, while that odd to the spin- and valley-singlet. Both components have $\tau_3 = 0$ and therefore their mutual coupling is allowed by $U_v(1)$.

By construction, the lowest-energy pair-eigenstate is the one with the largest λ_i. Not surprisingly, I find that the largest eigenvalue $\lambda_s = 2.33$ is non-degenerate and its eigenvector, i.e., the pair wavefunction, transforms like the totally symmetric irreducible representation of D_6, which is alike an s-wave Cooper pair, see Fig. 3.7.

The next largest eigenvalue $\lambda_d = 1.79$ is doubly degenerate, and the corresponding pair wavefunctions transform like the two-dimensional irreducible representation of D_6 even under C_{2z}, alike a d-wave Cooper pair. In the real representation, one eigenstate $\psi_{d_1}^{nm}(\mathbf{k}) \sim x^2 - y^2$, even under C_{2x}, and the other $\psi_{d_2}^{nm}(\mathbf{k}) \sim xy$, odd under C_{2x}, see Fig. 3.8. In reality, since $\psi_{d_i}^{nn}(\mathbf{k}) \neq \psi_{d_i}^{nn}(-\mathbf{k})$, each eigenstate has also a weak p-wave valley-singlet component, p_x and $-p_y$ the eigenstates d_1 and d_2, respectively. Both d_1 and d_2 are (almost) odd under p-h symmetry, as can be noticed in Fig. 3.8, which hints at a non-trivial topological character [136, 167]. Indeed, the combinations $d_\pm = \big(d_1 \pm i\, d_2\big)/\sqrt{2} \sim Y_{2\pm2}$ do have finite Chern number C $= \pm 2$, the same value of the angular momentum, as discussed later in the chapter.

For completeness, I further checked that a spin-triplet Cooper pair is unfavoured. Being $T^\dagger_{\mathbf{k},n_1 n_2,s_z}$ the triplet creation operator with z-spin projection $s_z = 0, \pm 1$, the Hamiltonian pro-

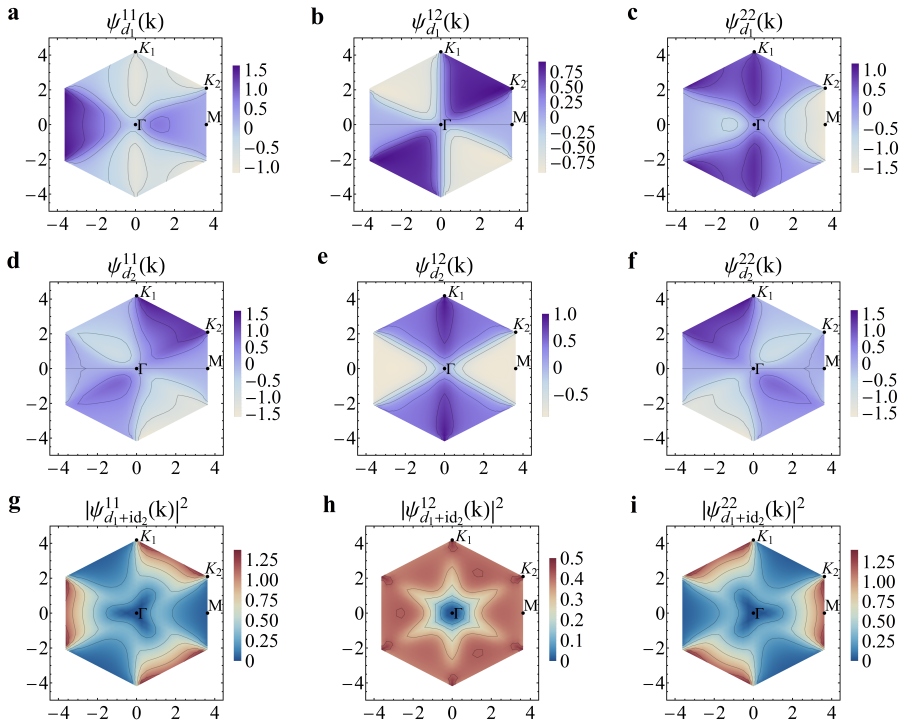

Figure 3.8: **d-wave pair wavefunctions in momentum space**. Panels **a-f**: pair wavefunction components in momentum space of the two d-wave real eigenstates d_1 and d_2, namely, $\psi^{11}_{d_1}(\mathbf{k})$ (**a**), $\psi^{12}_{d_1}(\mathbf{k}) = \psi^{21}_{d_1}(\mathbf{k})$ (**b**), $\psi^{22}_{d_1}(\mathbf{k})$ (**c**), $\psi^{11}_{d_2}(\mathbf{k})$ (**d**), $\psi^{12}_{d_2}(\mathbf{k}) = \psi^{21}_{d_2}(\mathbf{k})$ (**e**), and $\psi^{22}_{d_2}(\mathbf{k})$ (**f**). Panels **g-h**: probability distribution of the complex $d_1 + id_2$ combination, eigenstate of C_{3z} with eigenvalue $\mathrm{e}^{-i2\pi/3}$. The orthogonal combination $d_1 - id_2$, eigenstate of C_{3z} with complex conjugate eigenvalue, has right the same probability distribution.

jected onto the triplet Cooper pairs takes the form

$$H_P = +\frac{g}{N}\sum_{\mathbf{k}\mathbf{k}',s_z}\sum_{n_1n_2n_3n_4} V_{n_1n_2,\,n_3n_4}(\mathbf{k},\mathbf{k}')\,T^{\dagger}_{\mathbf{k},n_1n_2,s_z}\,T_{\mathbf{k}',n_3n_4,s_z}\,, \tag{3.38}$$

with an overall positive sign. Now, I must take the most negative $\lambda \simeq -1.18$ which is smaller in magnitude both of λ_s and $\lambda_{d_1\pm id_2}$, implying my assumption to focus only on the singlet channel was legit.

Coulomb pseudopotential

I have so far just considered the phonon-mediated attraction that, unsurprisingly, favours the s-wave pairing channel. That result may change taking into account also the Coulomb repulsion H_C in Eq. (3.5). The projected interaction yields [136]

$$\begin{aligned} H_C = -\frac{1}{2N\Omega_c}\sum_{\mathbf{k}\mathbf{k}'}\sum_{\mathbf{q}\,\mathbf{G}}\sum_{\sigma\sigma'}\sum_{nmn'm'}\sum_{\eta\eta'} U(\mathbf{q}+\mathbf{G})\,M^{\eta}_{nn'}(\mathbf{k},\mathbf{q}+\mathbf{G})M^{\eta'}_{mm'}(\mathbf{k}',-\mathbf{q}-\mathbf{G})\times \\ \times\,\Psi^{\dagger}_{\mathbf{k}+\mathbf{q},\sigma,\eta,n}\Psi^{\dagger}_{\mathbf{k}'-\mathbf{q},\sigma',\eta',m}\Psi_{\mathbf{k}',\sigma',\eta',m'}\Psi_{\mathbf{k},\sigma,\eta,n'}\,, \end{aligned} \tag{3.39}$$

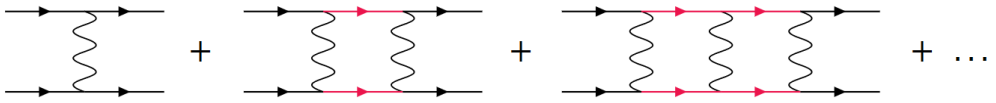

Figure 3.9: Diagrammatic representation of the Coulomb pseudo-potential. The black Green functions correspond to flat bands, the red ones to other bands, while the wavy line is the RPA screened interaction. The values in Eq. (3.46) refers only to the first diagram.

where the form factor for transferred momentum $\mathbf{q}+\mathbf{G}$ is defined as

$$M^{\eta}_{nn'}(\mathbf{k},\mathbf{q}+\mathbf{G}) = \langle u_{\eta n}(\mathbf{k}+\mathbf{q}+\mathbf{G}) \,|\, u_{\eta n'}(\mathbf{k})\rangle \ , \tag{3.40}$$

and, for simplicity, a layer independent interaction is considered

$$U(\mathbf{q}) = \frac{2\pi e^2}{\epsilon_\infty}\,\frac{\tanh(d_s q)}{q}\,. \tag{3.41}$$

A proper treatment of H_C would require including all thousands π-bands, because the Coulomb repulsion projected just onto the flat bands, i.e., without the screening by all other bands, is unphysical. Since this calculation is infeasible, I project the interaction onto the four flat bands and account for the screening of the other bands through random phase approximation (RPA), neglecting retardation effects due to the small energy window of the flat bands

$$U(\mathbf{q}+\mathbf{G}) \ \to\ U_{sc}(\mathbf{q}+\mathbf{G}) = U(\mathbf{q}+\mathbf{G})\left(1+U(\mathbf{q}+\mathbf{G})\,\chi^0(\mathbf{q}+\mathbf{G},\omega=0)\right)^{-1}, \tag{3.42}$$

where the non-interacting density-density particle-hole bubble is summed upon all the bands but the flat ones

$$\chi^0(\mathbf{q}+\mathbf{G},\omega) = \frac{2}{V}\sum_{\mathbf{k},\eta}\sum_{nn'\neq 1,2} |M^{\eta}_{nn'}(\mathbf{k},\mathbf{q}+\mathbf{G})|^2\,\frac{f(\epsilon_{\eta n}(\mathbf{k}+\mathbf{q}))-f(\epsilon_{\eta n'}(\mathbf{k}))}{\omega-\epsilon_{\eta n}(\mathbf{k}+\mathbf{q})+\epsilon_{\eta n'}(\mathbf{k})}\,. \tag{3.43}$$

I estimate the electrostatic energy paid by a single the Cooper pair in perturbation theory, i.e. the Coulomb pseudo-potential μ_*

$$\begin{aligned}\mu^{ij}_* &= \langle 0|\Delta_i\, H_C\, \Delta^\dagger_j|0\rangle \\ &= -\frac{1}{V}\sum_{\mathbf{k}\mathbf{k}'}\sum_{mm'nn'}\left(\psi^i_{nm}(\mathbf{k})\right)^*\, U_{nm,n'm'}(\mathbf{k},\mathbf{k}')\,\psi^j_{n'm'}(\mathbf{k}')\,,\end{aligned} \tag{3.44}$$

where the Coulomb kernel is now defined as

$$\begin{aligned}U_{nm,n'm'}(\mathbf{k},\mathbf{k}') = \sum_{\mathbf{G}} U_{sc}(\mathbf{k}-\mathbf{k}'+\mathbf{G})\, M^{+1}_{nn'}(\mathbf{k}',\mathbf{k}-\mathbf{k}'+\mathbf{G})\times \\ \times\, M^{-1}_{mm'}(-\mathbf{k}',-\mathbf{k}+\mathbf{k}'-\mathbf{G})\,.\end{aligned} \tag{3.45}$$

Due to invariance under the D_6 symmetry of the Coulomb repulsion, the pseudo-potential is diagonal in the $d_{1(2)}$ space and does not couple s and d ones. Specifically,

$$\begin{aligned}\mu^s_* &= 27.48\,\text{meV}\,, \\ \mu^d_* &= 26.97\,\text{meV}\,, \\ \Delta\mu_* &= \mu^s_* - \mu^d_* \simeq 0.49\,\text{meV}\,.\end{aligned} \tag{3.46}$$

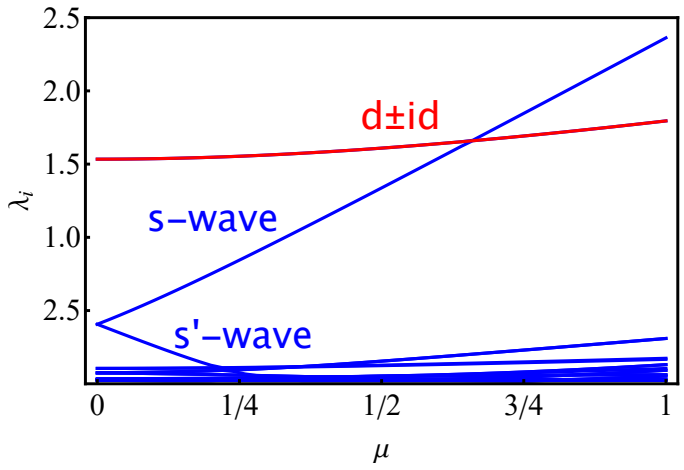

Figure 3.10: Evolutions of the kernel eigenvalues of the tHamiltonian in Eq. (3.53). As in Eq. (3.37), the larger the kernel eigenvalue the smaller the energy eigenvalue. For $\mu = 0$, there are present two degenerate s, s' states with $C = 0$ that splits for $\mu > 0$. The $d_1 \pm id_2$ states, with $C = \pm 2$, remains doubly degenerate for all the evolution of the Hamiltonian.

Reminding that $\lambda_s - \lambda_d = 0.56$, I conclude that the interplay of electron-phonon coupling and Coulomb interaction favours the $d-$wave Cooper pairing [129] for values of the coupling

$$g \lesssim 0.88\,\text{meV}\,, \tag{3.47}$$

due to the nodes of the wave-function that pay less electrostatic energy.
I note that the pseudo-potential μ^i_* is bigger than the pair energy $-g\,\lambda_i$, resulting in a net positive energy for each pair. That is because a faithful estimate of μ^i_* requires summing the ladder diagram in Fig. 3.9 over all bands but the flat ones. Unfortunately, this calculation is infeasible: the non-trivial momentum dependence of the interaction prevents to analytically sum the series. However, I expect that the net result would still favour the d-wave pair with respect to the s-one, as suggested by the non-trivial topology of the HF solutions. Moreover, even if μ^i_* were still larger than $-g\,\lambda_i$, the proximity to the Mott insulator could nonetheless stabilize a R-VBD state, since vertex corrections and wavefunction renormalization strongly supress the Coulomb pseudo-potential whereas have weak effect on the phonon coupling constant [149].

Topology of the d-wave Cooper pair

As previously anticipated, here I analyse the topological character of the $d_\pm$-waves introducing the Chern band creation operators, which creates electrons belonging to the flat bands with definite Chern number $C = e_Y = \pm 1$ [136]

$$\Psi^\dagger_{\mathbf{k},\sigma,\eta,e_Y} \equiv \frac{\Psi^\dagger_{\mathbf{k},\sigma,\eta,2} + i\,e_Y\,\Psi^\dagger_{\mathbf{k},\sigma,\eta,1}}{\sqrt{2}}\,, \tag{3.48}$$

and the Chern number operator as

$$\mathcal{E}_Y = \sum_{\mathbf{k}} \sum_{\sigma\,\eta\,e_Y} e_Y\, \Psi^\dagger_{\mathbf{k},\sigma,\eta,e_Y} \Psi_{\mathbf{k},\sigma,\eta,e_Y}\,. \tag{3.49}$$

A single Cooper pair is described by the wave-function

$$|BCS(\pm)\rangle = \Delta^\dagger_{d_\pm}\,|0\rangle \tag{3.50}$$

and the expectation value of the Chern number operator over such state is

$$\langle \mathcal{E}_Y \rangle_\pm = \pm 1.75\,, \tag{3.51}$$

signature of a nontrivial topology of the pair wavefunction, but below the quantized value $C = \pm 2$. The discrepancy is due to a small mixing of non-interacting flat bands with opposite Chern numbers by the phonon-mediated attraction, such that the one-to-one correspondence between $\mathcal{E}_Y$ and the Chern number of the pair is no longer valid once interactions are introduced. To demonstrate that the Cooper pair is anyway still topological, I divide the Hamiltonian in two parts, one that preserve and one that breaks the chiral symmetry

$$\begin{gathered} H_P = H_P^1 + H_P^2\,, \\ \left[\, H_P^1,\, \mathcal{E}_Y \,\right] = 0 \qquad \left[\, H_P^2,\, \mathcal{E}_Y \,\right] \neq 0\,, \end{gathered} \tag{3.52}$$

and define a new Hamiltonian through

$$H_P(\mu) = H_P^1 + \mu\, H_P^2\,. \tag{3.53}$$

For $\mu = 0$, $\mathcal{E}_Y$ commutes with the Hamiltonian by construction and allows only Cooper pairs with definite Chern number $\mathcal{E}_Y = 0, \pm 2$. The $d_\pm$-states posses a non-zero Chern number $\mathcal{E}_Y = C = \pm 2$ at $\mu = 0$, explicitly signalling a nontrivial topology. Adiabatically increasing μ, they always remain doubly degenerate but for an accidental degeneracy with the s-one at $\mu \simeq 0.7$. The mixing between these states is forbidden by symmetry, such that the nontrivial topological character of the $d_\pm$-ones is left untouched by the crossing. Moreover, the d-states can not even mix between themselves since they are characterized by opposed quantized angular momentum $\ell_z = \pm 2$. This indicates that the $d_\pm$-wave are characterized by $C = \pm 2$ Chern numbers also in the case of $\mu = 1$, corresponding to the actual phonon Hamiltonian.

Resulting physical scenario

Therefore, under all the above assumptions, and neglecting the flat band dispersion since the large $U(4) \times U(4)$ symmetry of the Coulomb repulsion is already lifted by the effective attraction, R-KVB insulators can be stabilised at all integer fillings ν. These are described by the projected BCS wavefunctions, see Eq. (3.22),

$$|\nu\rangle \propto P_{\mathrm{G}}(\nu) \left(\Delta^\dagger_{d_+}\right)^{\frac{N}{2}\, n_+} \left(\Delta^\dagger_{d_-}\right)^{\frac{N}{2}\, n_-} |0\rangle\,, \tag{3.54}$$

where, by definition, the 'vacuum' $|0\rangle$ is the ground state state at $\nu = -4$ with all bands below the flat ones occupied, and $n_\pm \geq 0$ are the numbers of $d_\pm$ pairs per unit cell. The filling factor is

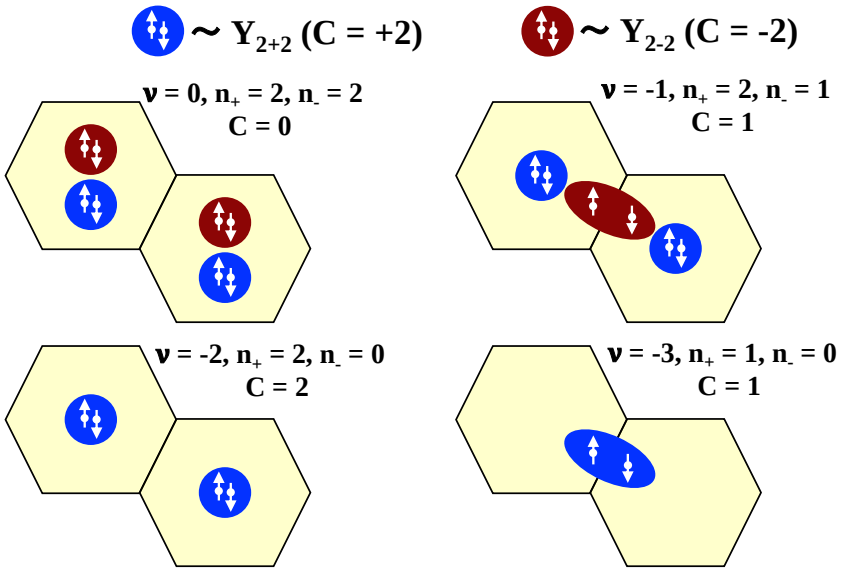

Figure 3.11: **R-KVB insulators at integer $\nu \leq 0$.** The two spin-singlet, $\tau_3 = 0$ geminal operators: $\Delta_+^\dagger \sim Y_{2+2}$ with Chern number $C = +2$ is represented by the blue circle, while $\Delta_-^\dagger \sim Y_{2-2}$ with $C = -2$ by the red one. A pictorial representation of the resonating Kekulé valence bond insulators, dynamical counterparts of the static mean-field ones in Figs. 3.3, 3.4 and 3.5, is displayed for all negative integer fillings. For each case, I draw two nearest neighbour moirè unit cells, each of which, for odd ν, hosts one electron from the shared pair; a very oversimplified picture of spin- and valley-liquid insulators.

simply $\nu = -4 + n_+ + n_-$. Whenever $n_+ \neq n_-$, the projected wavefunction (3.54) breaks time-reversal symmetry, carries Chern number $C(n_+, n_-) = 2(n_+ - n_-)$, and has finite orbital magnetic moment $M = \mu_B\, g_*\, C(n_+, n_-)$ per supercell, with g_* the gyromagnetic ratio. Since the explicit calculation [168] of the gyromagnetic ratio is infeasible in this scheme, I rely on the experimental estimate of $g_* \sim 3$ [24], yielding an orbital magnetic moment per pair of ~ 6 Bohr magnetons.
The dynamical counterparts of the S-KVB mean-field insulators Figs. 3.3, 3.4 and 3.5 correspond to specific values of n_+ and n_-, see Fig. 3.11. However, due to the large value of g_* it is well possible that pairs (n_+, n_-) with Chern number higher in absolute value than the mean-field solutions could become stable in presence of a magnetic field, possibly realising the peculiar Landau fan diagrams that have been observed [22, 157–159, 161–163].
I note that, since at odd integer ν the R-KVB cannot quench spin and valley degrees of freedom, the wavefunction (3.54) describes in that case spin- and valley-liquid topological insulators, whereas Hartree-Fock predicts fully-polarised symmetry breaking ones. Nonetheless, that wavefunction still has finite orbital magnetisation, which, e.g., could be as large as $3\mu_B$ per moirè supercell at $\nu = 3$, not in disagreement with recent observations [160]. Moreover, the sizeable orbital magnetic moment implies the emergence of magnetic domains at any integer filling $\nu \neq 0$ rather than a uniform magnetic polarisation. Since the orbital magnetic moment of each pair is directly proportional to its Chern number, that envisages the existence of domains with different Chern numbers, as indeed observed experimentally [169]. I further remark that R-KVB insulators are prone to turn upon doping into superconductors [149, 150], in the present case nodeless chiral d-wave ones that are still topological [29], whose driving mechanism, I emphasise, is the electron-phonon Kekulé coupling [30].
The former scenario assumes that time reversal breaking operators $\Delta_\pm^\dagger$ are favoured over the real ones $\Delta_1^\dagger$ and $\Delta_2^\dagger$. I cannot exclude that the latter correspond to the $SU(2)$ invariant dynamical counterpart of the earlier discussed quantum spin-Hall insulating HF solution [154]. However, within this RVB scenario, these two states have exactly the same energy.
Therefore, for completeness, I will briefly discuss what would change if $\Delta_1^\dagger$ and $\Delta_2^\dagger$ were instead favoured. In that case, $\left(\Delta_\pm^\dagger, n_\pm\right)$ are simply replaced by $\left(\Delta_{1(2)}^\dagger, n_{1(2)}\right)$ in the wavefunction (3.54), which would thus describe non-topological R-KVB insulators with a weak nematic character due to the small p-wave component. Moreover, the symmetry of the superconducting order parameter stabilised upon doping would be now a real combination of $d_{x^2-y^2}$, plus a small p_x component, and d_{xy}, plus a small $-p_y$ component, implying nodes in the Brillouin zone [31] and weak nematicity [140].
However, I emphasise that this scenario would imply a topologically trivial insulator at $\nu = \pm 2$, at odd with experimental evidence of an anomalous quantum Hall effect [24, 25].

3.5 Summary

The surprisingly rich phase diagram of magic-angle twisted bilayer graphene, which includes topological and non-topological correlated insulators [11,12,16,22,157,158,160–163], sometimes competing with each other [159], and superconducting domes [12, 24–26], is explained by the constructive interplay of the Coulomb repulsion and the effective attraction mediated by a rather peculiar set of moiré optical phonons. The Kekulé-like valence-bond state, only metastable in presence of just the Coulomb repulsion, is stabilized by this interplay and characterized by a distortion localised mostly into the AA regions and along the domain walls separating AB and BA Bernal Stacked regions of twisted bilayer graphene. The resulting physical scenario is in agreement with the experimentally observed insulating states at all integer fillings and, in particular, with the Kekulé distortion measured at half-filling in a recent STM experiment [28, 170]. Moreover, it naturally offers an explanation of the observed superconductivity [30] and its proximity to the insulating phases [149, 150].

CHAPTER 4

GREEN'S FUNCTION ZEROS AND TOPOLOGICAL INVARIANTS

4.1 Introduction

The determinant of the retarded Green's function $G_0(\epsilon, \mathbf{k})$, with ϵ the frequency and $\mathbf{k}$ the momentum, for periodic models of non-interacting electrons have poles whenever ϵ hits the dispersion energy $\epsilon_n(\mathbf{k})$ of a band n, i.e., a single-particle excitation. Similarly, the poles of the determinant of the fully-interacting $G(\epsilon, \mathbf{k})$ can be associated to coherent, i.e., with infinite lifetime, single-particle excitations, which thus have a clear physical meaning. The manifold in the Brillouin zone where these poles are at $\epsilon = 0$ defines the Fermi surface, in which case the system is metallic.
However, the determinant of $G(\epsilon, \mathbf{k})$ in presence of interaction may also develop zeros [1], whose manifold at $\epsilon = 0$ defines the so-called Luttinger surface [175]. For long time, these zeros have not been given any physical significance, despite Volovik [32] early on recognised that a Luttinger surface bears the same non-trivial topological content of a Fermi surface. Only recently, the Green's function zeros started to attract growing physical interest. For instance, it has been shown that a Luttinger surface defined by the simple roots of $\det\big(G(0, \mathbf{k})\big)$ does sustain Landau's quasiparticles [33], even in non-symmetry breaking Mott insulators [34]. Those quasiparticles have the same physical properties as conventional ones at a Fermi surface, with the major difference that they are incompressible [35] and do not contribute to charge transport [34]. Elaborating on Volovik's observation [32], Gurarie [36] and Essin and Gurarie [37] have proposed that, upon increasing electron correlations, topological edge modes, i.e., edge poles of the Green's function, may transform into edges zeros without making the topological insulator a trivial one or closing the single-particle gap. More recently, this intriguing scenario has been further explored in Ref. [38], whose authors show

[1] Equivalently, in the basis that diagonalises $G(\epsilon, \mathbf{k})$ for strictly real ϵ, there may be elements along the diagonal that vanish at certain ϵ and $\mathbf{k}$. That is evidently different from the case in which the Green's function, represented in a basis in which it is not diagonal, has diagonal terms that may cross zero. This circumstance has been discussed in [171]. In particular, the diagonal elements of the non-interacting Green's function have only poles in the diagonal basis, while they may have also zeros in a generic non-diagonal basis, whose role has been analysed, e.g., in [172–174]

that model topological insulators turn, upon rising interaction strength, into Mott insulators with topologically trivial lower and upper Hubbard bands, but with ingap valence and conduction bands of Green's function zeros that are topological and yield Green's function edge zeros. This result suggests that an edge-bulk correspondence exists also for Green's function zeros, thus clarifying the mechanism underlying the transformation of edge poles into edge zeros [36, 37].
All these small pieces of evidence suggest that Green's function zeros, that may arise only in strongly correlated systems, do have a physical meaning as important as that of Green's function poles. This connection has been uncovered when the zeros cross the chemical potential, thus in the presence of a Luttinger surface [32–34]. However, despite the supporting evidences [36–38], the direct role of Green's function zeros in assessing the topological character of an insulator has not been explicitly demonstrated. That is precisely this chapter.

4.2 Topological invariant in two dimensions

The Hall conductance in non-interacting insulators is quantized in units $e^2/2\pi\hbar$, where the integer quantum is a topological invariant known as the first Chern number. This is calculated upon the occupied bands and is robust under any smooth deformation of the Hamiltonian. On the other hand, in the case of interacting electrons, band theory of independent electrons does not hold and yet a quantized topological invariant, which reduces to the Chern number if the interaction is switched off, can be still defined.
However, while the expression of this invariant, the winding number (4.8), could be well anticipated by algebraic topology arguments, the most accepted derivation, see, e.g., Refs. [39, 40], is not formally correct. In particular, it neglects a term which is in principle non-zero when perturbation theory breakdowns and can lead to a mismatch between the winding number and the Hall conductance.
Therefore, I here rederive the Hall conductance by standard quantum many-body theory [176]. consider a periodic model of interacting electrons and use units in which $\hbar = 1$. The off-diagonal component σ_{ij}, $i \neq j$, of the conductivity tensor is related to the current-current response function $\chi_{ij}(\omega)$ through

$$\sigma_{ij} = -\lim_{\omega\to 0} \frac{e^2}{i\omega}\, \chi_{ij}(\omega)\,,$$

where, in the basis of the Hamiltonian eigenstates $|n\rangle$, with eigenvalues E_n,

$$\chi_{ij}(\omega) = \chi_{ji}(-\omega) = \frac{1}{Z} \sum_{nm} \frac{\mathrm{e}^{-\beta E_n} - \mathrm{e}^{-\beta E_m}}{\omega - E_m + E_n} \int d\mathbf{x}\, d\mathbf{y}\ \langle n|\, J_i(\mathbf{x})\, |m\rangle\, \langle m|\, J_j(\mathbf{y})\, |n\rangle\ ,$$

with $J_i(\mathbf{x})$ the i-the component of the current density operator at position $\mathbf{x}$. Therefore, the antisymmetric component of the current-current tensor is, for small ω,

$$\begin{aligned}\frac{\chi_{ij}(\omega) - \chi_{ji}(\omega)}{2} &\simeq -\frac{\omega}{Z} \sum_{nm} \frac{\mathrm{e}^{-\beta E_n} - \mathrm{e}^{-\beta E_m}}{\big(E_m + E_n\big)^2} \int d\mathbf{x}\, d\mathbf{y}\ \langle n|\, J_i(\mathbf{x})\, |m\rangle\, \langle m|\, J_j(\mathbf{y})\, |n\rangle \\ &= \omega\ \frac{\partial \chi_{ij}(\omega)}{\partial\omega}\Big|_{\omega=0}\,,\end{aligned}$$

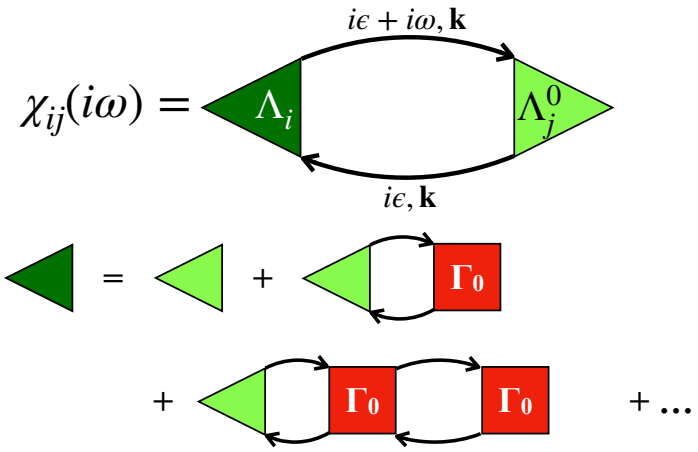

Figure 4.1: Top panel: current-current correlation function $\chi_{ij}(i\omega)$ in skeleton diagrams. Black arrow lines are interacting single-particle Green's functions G, whose Matsubara frequency and momentum are explicitly shown; green triangle represents the non-interacting current vertex Λ_j^0, while dark green triangle the fully interacting one Λ_i. Bottom panel: Bethe-Salpeter equation satisfied by the interacting Λ_i in terms of the interaction vertex Γ_0 irreducible in the particle-hole channel.

which is imaginary, and thus, switching to Matsubara frequencies and for $i \neq j$,

$$\frac{\sigma_{ij} - \sigma_{ji}}{2} = i\, e^2\, \frac{\partial \chi_{ij}(i\omega)}{\partial i\omega}\Big|_{\omega=0},$$

where now

$$\chi_{ij}(i\omega) = -\int_0^\beta d\tau\, \mathrm{e}^{i\omega\tau} \int d\mathbf{x}\, d\mathbf{y}\, \langle\, T_\tau \Big(J_i(\mathbf{x},\tau)\, J_j(\mathbf{y},0) \Big) \,\rangle\,,$$

is the correlation function in the Matsubara formalism, with τ the imaginary time. Fig. 4.1 shows the representation of $\chi_{ij}(i\omega)$ in skeleton diagrams. It is worth noticing that only one of the two current vertices is fully interacting, otherwise interaction effects would be double counted as mistakenly done in Ref. [40].

I am interested in the derivative of $\chi_{ij}(i\omega)$ with respect to $i\omega$ calculated at $\omega = 0$, which, by inspection of Fig. 4.1, can be represented as in Fig. 4.2, where, only because of the derivative, the current vertices are now both fully interacting. Through the Ward-Takahashi identity the fully interacting current vertex at $\omega = 0$ is simply $\Lambda_i = -\partial G^{-1}/\partial k_i$, and, since $\partial G = -G\, \partial G^{-1}\, G$, I can write in 2D and for $T = 0$

$$\begin{aligned} \frac{\sigma_{12} - \sigma_{21}}{2} &= \frac{e^2}{2\pi}\, \nu_{\mathrm{H}} \\ &= \frac{e^2}{2\pi}\, (I_1 + K_L) \end{aligned} \tag{4.1}$$

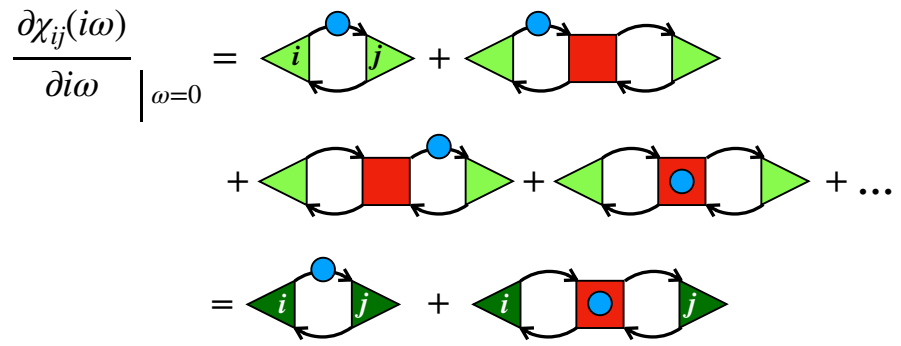

Figure 4.2: Diagrammatic representation of $\partial\chi_{ij}(i\omega)/\partial i\omega$ up to first order in the skeleton expansion. The cyan circle represents $\partial/\partial i\omega$. Note that all diagrams must be evaluated at $\omega = 0$ after taking the derivative. Ultimately, the first diagram leads to the winding number $W(G)$ while the second one to K_L.

where ν_H is the quantised Hall conductance, and I_1 and K_L are the contribution coming respectively from the first and second diagrams in Fig.4.2. The first integral can be recasted as

$$\begin{aligned} I_1 &= \frac{1}{8\pi^2}\int d\epsilon\, d\mathbf{k}\,\mathrm{Tr}\Big(G(i\epsilon,\mathbf{k})\,\partial_{k_1}G(i\epsilon,\mathbf{k})^{-1}\,G(i\epsilon,\mathbf{k})\,\partial_\epsilon G(i\epsilon,\mathbf{k})^{-1}\,G(i\epsilon,\mathbf{k})\,\partial_{k_2}G(i\epsilon,\mathbf{k})^{-1}\Big) \\ &= \frac{1}{24\pi^2}\int d\epsilon\, d\mathbf{k}\,\epsilon_{\mu\nu\rho}\,\mathrm{Tr}\Big(G(i\epsilon,\mathbf{k})\,\partial_\mu G(i\epsilon,\mathbf{k})^{-1}\times \\ &\qquad\qquad \times G(i\epsilon,\mathbf{k})\,\partial_\nu G(i\epsilon,\mathbf{k})^{-1}\,G(i\epsilon,\mathbf{k})\,\partial_\rho G(i\epsilon,\mathbf{k})^{-1}\Big) \\ &= W(G)\,, \end{aligned} \tag{4.2}$$

where $\epsilon_{\mu\nu\rho}$, with indices running from 0 to 2, the antisymmetric tensor, $\partial_0 = \partial_\epsilon$ and $\partial_{1(2)} = \partial_{k_{1(2)}}$, and $W(G)$, see (4.8), is the winding number of the map $(\epsilon,\mathbf{k}) \to G(i\epsilon,\mathbf{k}) \in \mathrm{GL}(n,\mathbb{C})$, assuming that the Green's function $G(i\epsilon,\mathbf{k})$ is an $n\times n$ invertible matrix, with n the dimension of the single-particle wavefunction basis, which is true provided the system is insulating and has no Luttinger surface.

The additional term besides the winding number involves the derivative of the irreducible vertex Γ_0 and reads explicitly

$$K_L = \frac{i\pi}{(2\pi)^6}\sum\int d\epsilon\, d\mathbf{k}\, d\epsilon'\, d\mathbf{k}'\;\epsilon_{ij}\;\partial_i G_{ba}(i\epsilon,\mathbf{k})\;F_{ab;a'b'}\big(i\epsilon,\mathbf{k};i\epsilon',\mathbf{k}'\big)\;\partial_j G_{b'a'}(i\epsilon',\mathbf{k}')\,, \tag{4.3}$$

where

$$\begin{aligned} F_{ab;a'b'}\big(i\epsilon,\mathbf{k};i\epsilon',\mathbf{k}'\big) &= \lim_{\omega\to 0}\frac{1}{2i\omega}\Big\{\Gamma_0\big(i\epsilon+i\omega\,\mathbf{k}\,a, i\epsilon'\,\mathbf{k}'\,a'; i\epsilon'+i\omega\,\mathbf{k}'\,b', i\epsilon\,\mathbf{k}\,b\big) \\ &\qquad - \Gamma_0\big(i\epsilon\,\mathbf{k}\,a, i\epsilon'+i\omega\,\mathbf{k}'\,a'; i\epsilon'\,\mathbf{k}'\,b', i\epsilon+i\omega\,\mathbf{k}\,b\big)\Big\} \\ &= -F_{a'b';ab}\big(i\epsilon',\mathbf{k}';i\epsilon,\mathbf{k}\big)\,, \end{aligned} \tag{4.4}$$

with

$$\begin{aligned}&\Gamma_0\big(i\epsilon + i\omega\,\mathbf{k}\,a, i\epsilon'\,\mathbf{k}'\,a'; i\epsilon' + i\omega\,\mathbf{k}'\,b', i\epsilon\,\mathbf{k}\,b\big)\\&\quad = \Gamma_0\big(i\epsilon'\,\mathbf{k}'\,a', i\epsilon + i\omega\,\mathbf{k}\,a; i\epsilon\,\mathbf{k}\,b, i\epsilon' + i\omega\,\mathbf{k}'\,b'\big)\,,\end{aligned}$$

the irreducible vertex in the particle-hole channel with transferred frequency ω. Since

$$\begin{aligned}&\Gamma_0\big(i\epsilon + i\omega\,\mathbf{k}\,a, i\epsilon'\,\mathbf{k}'\,a'; i\epsilon' + i\omega\,\mathbf{k}'\,b', i\epsilon\,\mathbf{k}\,b\big)^*\\&\quad = \Gamma_0\big(-i\epsilon\,\mathbf{k}\,b, -i\epsilon' - i\omega\,\mathbf{k}'\,b'; -i\epsilon'\,\mathbf{k}'\,a', -i\epsilon - i\omega\,\mathbf{k}\,a\big)\,,\end{aligned}$$

and $G_{ba}(i\epsilon,\mathbf{k})^* = G_{ab}(-i\epsilon,\mathbf{k})$, one can readily show that K_L in (4.3) is indeed real. I observe that F in (4.4) is odd under $(i\epsilon,\mathbf{k},ab) \leftrightarrow (i\epsilon,\mathbf{k}',a'b')$, unlike what claimed in [39,40], which compensates the change of sign of the antisymmetric tensor ϵ_{ij} under $i \leftrightarrow j$. Therefore, K_L may well be finite in principle. Nonetheless, one may still argue that F could vanish. Indeed, the irreducibility in the particle-hole channel suggests that Γ_0 depends on $i\omega$ only through the frequency carried by the particle-particle channel, as can be verified by inspection of few orders in the skeleton expansion. That frequency remains invariant if in the top panel of Fig. 4.1 I change the frequency of the upper Green's function from $i\epsilon + i\omega$ to $i\epsilon$, and that of the lower one from $i\epsilon$ to $i\epsilon + i\omega$, thus $\omega \to -\omega$ in the particle-hole channel. If that is true, Γ_0 is even in ω, and since it must also be smooth, then its derivative at $\omega = 0$ has to vanish, as also argued by Ref. [43] on the basis of the skeleton expansion. I note that, from a physical point of view, it is reasonable that K_L vanishes for weak interaction, i.e. when perturbation theory holds. Adiabatically switching on the interaction would otherwise lead to a possible failure of the TKNN formula in any realistic material, where Coulomb repulsion is small but always present.

However, once perturbation theory breaks down, i.e. the Green's function develops zeros, one cannot exclude that the full series develops odd contributions, and thus that K_L becomes non zero. Further insight in that direction can be gained through the Streda formula [177,178]

$$\frac{\partial\rho}{\partial B}\Big|_{B=0} = \frac{e}{2\pi c}\,\nu_{\rm H}\,, \tag{4.5}$$

where ρ is the electron density. The case of spin-Hall conductance is defined similarly provided ρ is replaced by the spin density [179]. The electron density at $T = 0$ can be calculated through [35]

$$\begin{aligned}\rho &= \frac{n}{2} + \int \frac{d\epsilon\,d\mathbf{k}}{(2\pi)^3}\,\mathrm{Tr}\Big(G(i\epsilon,\mathbf{k})\Big)\\&= \frac{n}{2} - \int \frac{d\epsilon\,d\mathbf{k}}{(2\pi)^3}\,\frac{\partial \ln\det G(i\epsilon,\mathbf{k})}{\partial i\epsilon} + I_L\\&= \frac{n}{2} - \int \frac{d\epsilon\,d\mathbf{k}}{(2\pi)^3}\,\frac{\partial \ln\det G_*(i\epsilon,\mathbf{k})}{\partial i\epsilon} + I_L\\&= \int \frac{d\mathbf{k}}{(2\pi)^2}\,\theta\big(-\epsilon_\alpha(0,\mathbf{k})\big) + I_L\,,\end{aligned} \tag{4.6}$$

where n is the number of bands, including spin, I used the fact that

$$\ln\det G(i\epsilon,\mathbf{k}) = \ln\det G_*(i\epsilon,\mathbf{k}) + \ln\det Z(\epsilon,\mathbf{k})\,,$$

and $\ln\det Z(\epsilon,\mathbf{k})$ gives no contribution to the integral since its derivative is odd, and, finally,

$$\begin{aligned} I_L &= \int \frac{d\epsilon\, d\mathbf{k}}{(2\pi)^3}\ \mathrm{Tr}\Big(G(i\epsilon,\mathbf{k})\ \frac{\partial\Sigma(i\epsilon,\mathbf{k})}{\partial i\epsilon}\Big) \\ &= \frac{1}{\pi}\int \frac{d\mathbf{k}}{(2\pi)^2}\,\Im m\,\mathcal{I}(i0^+,\mathbf{k})\,. \end{aligned}$$

The function $\mathcal{I}(i\epsilon,\mathbf{k}) = \mathcal{I}(-i\epsilon,\mathbf{k})^*$ is defined as [35]

$$\mathcal{I}(i\epsilon,\mathbf{k}) = \Phi(i\epsilon,\mathbf{k}) - \mathrm{Tr}\Big(\Sigma(i\epsilon,\mathbf{k})\,G(i\epsilon,\mathbf{k})\Big)\,,$$

having written the Luttinger-Ward functional, which can be constructed fully unperturbatively [180], as

$$\Phi[G] = T\sum_{\ell}\int \frac{d\mathbf{k}}{(2\pi)^2}\ \mathrm{e}^{i\epsilon_\ell 0^+}\ \Phi(i\epsilon_\ell,\mathbf{k})\,.$$

In the perturbative regime, $\Im m\,\mathcal{I}(i\epsilon,\mathbf{k}) \sim \epsilon$ for small ϵ and thus $I_L = 0$, in which case (4.6) reduces to the well known statement of Luttinger's theorem [181]. However, when perturbation theory breaks down, I_L is generally nonzero [35].
In presence of a magnetic field B, the derivative of the first term in (4.6) with respect to B and calculated at $B = 0$ yields the Streda formula for non-interacting electrons described by the quasiparticle Hamiltonian $H_*(0,\mathbf{k})$, which is just the TKNN expression (4.21). It follows that

$$\frac{\partial I_L}{\partial B}\Big|_{B=0} \equiv \frac{e}{2\pi c}\ K_L\,, \tag{4.7}$$

namely that the winding number (4.8) may not correspond to the quantised Hall conductance when perturbation theory breaks down and $I_L \neq 0$, in accordance, e.g., with the results of [182, 183]. Most recently, another work linked the breakdown of the Luttinger theorem to a mismatch between the winding number and the transverse conductivity via the Stresa formula [184]. It starts, however, from the expression of the Green's function in the magnetic Brillouin zone and thus corroborates this result by a different analytical technique.

4.3 TKNN formula for interacting insulators

The expression of the topological invariant of two dimensional periodic insulators in presence of interaction, which coincides with the zero temperature Hall conductance in units of $e^2/2\pi\hbar$ [39, 40] at least when perturbation theory is valid, reads

$$\begin{aligned} W(G) = \frac{1}{24\pi^2}\int d\epsilon\, d\mathbf{k}\,\epsilon_{\mu\nu\rho}\,\mathrm{Tr}\Big(&G(i\epsilon,\mathbf{k})\ \partial_\mu G(i\epsilon,\mathbf{k})^{-1}\ \times \\ &\times G(i\epsilon,\mathbf{k})\ \partial_\nu G(i\epsilon,\mathbf{k})^{-1}\ G(i\epsilon,\mathbf{k})\ \partial_\rho G(i\epsilon,\mathbf{k})^{-1}\Big)\,, \end{aligned} \tag{4.8}$$

I hereafter assume that $G(i\epsilon,\mathbf{k})$ is invertible, which implies that the system is an insulator without any Luttinger surface. The winding number satisfies

$$W(G_1\,G_2) = W(G_1) + W(G_2)\,,\quad W(G) = 0 \quad \text{if} \quad G^\dagger = G\,. \tag{4.9}$$

Zhong and Zhang have shown [42] that the topological invariant (4.8) reduces to the TKNN expression of the quantised Hall conductance [2] in which the role of the Bloch waves of the occupied bands is played by the eigenstates of the hermitian matrix $-G(0,\mathbf{k})^{-1}$ with negative eigenvalues. The proof is based on the observation that the two maps $(\epsilon,\mathbf{k}) \to G(i\epsilon,\mathbf{k})^{-1}$ and $(\epsilon,\mathbf{k}) \to i\epsilon + G(0,\mathbf{k})^{-1}$ are homotopic, and thus the winding number (4.8) of the former map coincides with that of the latter, which, in turns, reduces to the TKNN formula.
Here, I will prove explicitly the equivalence relation but using a different map $(\epsilon,\mathbf{k}) \to G_*(i\epsilon,\mathbf{k})^{-1}$, which has the more transparent physical meaning of the inverse of the *quasiparticle* Green's function, which I discuss more extensively at the end of the section. Specifically, following [34, 35] I write the interacting Green's function matrix as

$$\begin{aligned} G(i\epsilon,\mathbf{k}) &= \frac{1}{i\epsilon - H_0(\mathbf{k}) - \Sigma(i\epsilon,\mathbf{k})} \\ &= \sqrt{Z(\epsilon,\mathbf{k})}\ \frac{1}{i\epsilon - H_*(\epsilon,\mathbf{k})}\ \sqrt{Z(\epsilon,\mathbf{k})} \\ &\equiv \sqrt{Z(\epsilon,\mathbf{k})}\ G_*(i\epsilon,\mathbf{k})\ \sqrt{Z(\epsilon,\mathbf{k})}\ , \end{aligned} \tag{4.10}$$

where $H_0(\mathbf{k})$ is the non-interacting Hamiltonian represented in the chosen basis of single-particle wavefunctions,

$$\begin{aligned} \Sigma(i\epsilon,\mathbf{k}) &= \Sigma(-i\epsilon,\mathbf{k})^\dagger \equiv \Sigma_1(i\epsilon,\mathbf{k}) + i\,\Sigma_2(i\epsilon,\mathbf{k}) \\ \Sigma_1(i\epsilon,\mathbf{k}) &= \Sigma_1(i\epsilon,\mathbf{k})^\dagger = \Sigma_1(-i\epsilon,\mathbf{k}) \\ &= \frac{\Sigma(i\epsilon,\mathbf{k}) + \Sigma(-i\epsilon,\mathbf{k})}{2} \\ \Sigma_2(i\epsilon,\mathbf{k}) &= \Sigma_2(i\epsilon,\mathbf{k})^\dagger = -\Sigma_2(-i\epsilon,\mathbf{k}) \\ &= \frac{\Sigma(i\epsilon,\mathbf{k}) - \Sigma(-i\epsilon,\mathbf{k})}{2i} \end{aligned}$$

the self-energy matrix in that same basis, which accounts for all interaction effects,

$$Z(\epsilon,\mathbf{k}) = Z(-\epsilon,\mathbf{k}) = \left(1 - \frac{\Sigma_2(i\epsilon,\mathbf{k})}{\epsilon}\right)^{-1}, \tag{4.11}$$

an even in ϵ and positive definite matrix, the latter if the system is insulating without a Luttinger surface, which can be regarded as the *quasiparticle* residue, and

$$H_*(\epsilon,\mathbf{k}) = H_*(-\epsilon,\mathbf{k}) = \sqrt{Z(\epsilon,\mathbf{k})}\,\Big(H_0(\mathbf{k}) + \Sigma_1(i\epsilon,\mathbf{k})\Big)\,\sqrt{Z(\epsilon,\mathbf{k})}\,, \tag{4.12}$$

is the *quasiparticle* Hamiltonian, which is hermitian and even in ϵ. Therefore, if $|\alpha(\epsilon,\mathbf{k})\rangle$ is eigenstate of $H_*(\epsilon,\mathbf{k})$ with eigenvalue $\epsilon_\alpha(\epsilon,\mathbf{k})$, I can always define $|\alpha(-\epsilon,\mathbf{k})\rangle = |\alpha(\epsilon,\mathbf{k})\rangle$ the eigenstate of $H_*(-\epsilon,\mathbf{k})$ with the same eigenvalue $\epsilon_\alpha(\epsilon,\mathbf{k})$. I emphasising that the representation (4.10) of the Green's function in terms of the quasiparticle one,

$$G_*(i\epsilon,\mathbf{k}) = \frac{1}{i\epsilon - H_*(\epsilon,\mathbf{k})}\ ,$$

with hermitian $H_*(\epsilon,\mathbf{k})$ is a rigorous result that remains valid also when $H_*(0,\mathbf{k})$ has zero eigenvalues, i.e., when Fermi and/or Luttinger surfaces are present.

It follows that the winding number (4.8) can be written as

$$\begin{aligned} W\big(G\big) &= W\Big(\sqrt{Z}\; G_*\, \sqrt{Z}\Big) = W\big(G_*\big) + W\big(Z\big) \\ &= W\big(G_*\big)\,, \end{aligned}$$

since the winding number of the positive definite matrix Z vanishes.
A further reason for choosing the map $(\epsilon, \mathbf{k}) \to G_*(i\epsilon, \mathbf{k})^{-1}$ is that, under the analytic continuation on the real axis from above, $i\epsilon \to \epsilon + i0^+$, i.e., for the retarded components of Green's function and self-energy, the poles of $G_*(\epsilon, \mathbf{k})$ correspond to both poles and zeros of $G(\epsilon, \mathbf{k})$, i.e., the vanishing eigenvalues of the quasiparticle residue matrix (4.11) on the real axis, thus making more explicit their deep connection.

In the basis that diagonalises $H_*(\epsilon, \mathbf{k})$, i.e.,

$$H_*(\epsilon, \mathbf{k})\, |\alpha(\epsilon, \mathbf{k})\rangle = \epsilon_\alpha(\epsilon, \mathbf{k})\; |\alpha(\epsilon, \mathbf{k})\rangle\;,$$

and choosing $|\alpha(\epsilon, \mathbf{k})\rangle = |\alpha(-\epsilon, \mathbf{k})\rangle$,

$$\begin{aligned} W\big(G\big) = \frac{1}{24\pi^2} \int d\epsilon\, d\mathbf{k}\, \epsilon_{\mu\nu\rho} \sum_{\alpha\beta\gamma} \frac{1}{i\epsilon - \epsilon_\alpha(\epsilon, \mathbf{k})} \frac{1}{i\epsilon - \epsilon_\beta(\epsilon, \mathbf{k})} \times \\ \times \frac{1}{i\epsilon - \epsilon_\gamma(\epsilon, \mathbf{k})}\, \partial_\mu G_*(i\epsilon, \mathbf{k})^{-1}_{\alpha\beta}\, \partial_\mu G_*(i\epsilon, \mathbf{k})^{-1}_{\beta\gamma}\, \partial_\mu G_*(i\epsilon, \mathbf{k})^{-1}_{\gamma\alpha}\;, \end{aligned} \tag{4.13}$$

having defined

$$\begin{aligned} \partial_\mu G_*(i\epsilon, \mathbf{k})^{-1}_{\alpha\beta} &\equiv \langle \alpha(\epsilon, \mathbf{k})|\, \partial_\mu G_*(i\epsilon, \mathbf{k})^{-1}\, |\beta(\epsilon, \mathbf{k})\rangle \\ &= i\,\delta_{\mu 0}\,\delta_{\alpha\beta} - \langle \alpha(\epsilon, \mathbf{k})|\, \partial_\mu H_*(\epsilon, \mathbf{k})\, |\beta(\epsilon, \mathbf{k})\rangle \\ &\equiv i\,\delta_{\mu 0}\,\delta_{\alpha\beta} - F^\mu_{\alpha\beta}(\epsilon, \mathbf{k})\,. \end{aligned}$$

The term in (4.13) with $\alpha = \beta = \gamma$ vanishes because of the antisymmetric tensor, so that only the cases of either two states equal and different from the third, or of all states different are finite, which I denote as $W^{(1)}(G)$ and $W^{(2)}(G)$, respectively. Specifically,

$$\begin{aligned} W^{(1)}(G) = -\frac{1}{8\pi^2} \int d\epsilon\, d\mathbf{k}\, \epsilon_{\mu\nu\rho} \sum_{\alpha\beta}{}' \frac{1}{i\epsilon - \epsilon_\beta(\epsilon, \mathbf{k})} \times \\ \times\; \partial_\mu \left(\frac{1}{i\epsilon - \epsilon_\alpha(\epsilon, \mathbf{k})} \right) \Big\{ F^\nu_{\alpha\beta}(\epsilon, \mathbf{k})\, F^\rho_{\beta\alpha}(\epsilon, \mathbf{k}) \Big\}\,, \\ W^{(2)}(G) = -\frac{1}{24\pi^2} \int d\epsilon\, d\mathbf{k}\, \epsilon_{\mu\nu\rho} \sum_{\alpha\beta\gamma}{}' \frac{1}{i\epsilon - \epsilon_\alpha(\epsilon, \mathbf{k})} \frac{1}{i\epsilon - \epsilon_\beta(\epsilon, \mathbf{k})} \times \\ \times\; \frac{1}{i\epsilon - \epsilon_\gamma(\epsilon, \mathbf{k})} \Big\{ F^\mu_{\alpha\beta}(\epsilon, \mathbf{k})\, F^\nu_{\beta\gamma}(\epsilon, \mathbf{k})\, F^\rho_{\gamma\alpha}(\epsilon, \mathbf{k}) \Big\}\,, \end{aligned} \tag{4.14}$$

where Σ' means the summation over different indices.
I begin by analysing $W^{(1)}(G)$ in Eq. (4.14). I note that, for $\alpha \neq \beta$,

$$\begin{aligned} F^\nu_{\alpha\beta}(\epsilon, \mathbf{k}) &= \langle \alpha(\epsilon, \mathbf{k})|\, \partial_\nu H_*(\epsilon, \mathbf{k})\, |\beta(\epsilon, \mathbf{k})\rangle \\ &= \Big(\epsilon_\alpha(\epsilon, \mathbf{k}) - \epsilon_\beta(\epsilon, \mathbf{k})\Big)\; \langle \partial_\nu \alpha(\epsilon, \mathbf{k})|\, \beta(\epsilon, \mathbf{k})\rangle \\ &= \Big(\epsilon_\beta(\epsilon, \mathbf{k}) - \epsilon_\alpha(\epsilon, \mathbf{k})\Big)\; \langle \alpha(\epsilon, \mathbf{k})|\, \partial_\nu \beta(\epsilon, \mathbf{k})\rangle\,, \end{aligned} \tag{4.15}$$

so that

$$\begin{aligned} W^{(1)}(G) &= -\frac{1}{8\pi^2}\int d\epsilon\, d\mathbf{k}\,\epsilon_{\mu\nu\rho}\sum_{\alpha\beta}\frac{\big(\epsilon_\alpha(\epsilon,\mathbf{k})-\epsilon_\beta(\epsilon,\mathbf{k})\big)^2}{i\epsilon-\epsilon_\beta(\epsilon,\mathbf{k})}\times \\ &\qquad\times\partial_\mu\left(\frac{1}{i\epsilon-\epsilon_\alpha(\epsilon,\mathbf{k})}\right)\langle\partial_\nu\alpha(\epsilon,\mathbf{k})|\,\beta(\epsilon,\mathbf{k})\rangle\,\langle\beta(\epsilon,\mathbf{k})|\,\partial_\rho\alpha(\epsilon,\mathbf{k})\rangle \\ &= -\frac{1}{16\pi^2}\int d\epsilon\, d\mathbf{k}\,\epsilon_{\mu\nu\rho}\sum_{\alpha\beta}\partial_\mu\, S_{\alpha\beta}(\epsilon,\mathbf{k})\;\langle\partial_\nu\alpha(\epsilon,\mathbf{k})|\,\beta(\epsilon,\mathbf{k})\rangle\,\langle\beta(\epsilon,\mathbf{k})|\,\partial_\rho\alpha(\epsilon,\mathbf{k})\rangle\,, \end{aligned} \tag{4.16}$$

where the constraint $\alpha\neq\beta$ is automatically fulfilled and one can readily demonstrate that

$$S_{\alpha\beta}(\epsilon,\mathbf{k}) = 2\,\ln\frac{i\epsilon-\epsilon_\alpha(\epsilon,\mathbf{k})}{i\epsilon-\epsilon_\beta(\epsilon,\mathbf{k})} - \frac{i\epsilon-\epsilon_\alpha(\epsilon,\mathbf{k})}{i\epsilon-\epsilon_\beta(\epsilon,\mathbf{k})} + \frac{i\epsilon-\epsilon_\beta(\epsilon,\mathbf{k})}{i\epsilon-\epsilon_\alpha(\epsilon,\mathbf{k})}\,,$$

which has a discontinuous imaginary part crossing $\epsilon=0$ if $\epsilon_\alpha(0,\mathbf{k})\,\epsilon_\beta(0,\mathbf{k})<0$. I can write

$$S_{\alpha\beta}(\epsilon,\mathbf{k}) = K_{\alpha\beta}(\epsilon,\mathbf{k}) + 2\pi i\,\mathrm{sign}(\epsilon)\left[\theta\big(\epsilon_\alpha(\epsilon,\mathbf{k})\big)-\theta\big(\epsilon_\beta(\epsilon,\mathbf{k})\big)\right],$$

where $K_{\alpha\beta}(\epsilon,\mathbf{k})$ is now continuous at $\epsilon=0$, so that, since $S_{\alpha\beta}(\epsilon,\mathbf{k})$ is antisymmetric, and $\epsilon_\alpha(\epsilon,\mathbf{k})\neq 0$, $\forall\,\alpha,\epsilon,\mathbf{k}$, then

$$\begin{aligned} W^{(1)}(G) &= \frac{i}{2\pi}\int d\mathbf{k}\,\epsilon_{ij}\sum_\alpha\theta\big(-\epsilon_\alpha(0,\mathbf{k})\big)\,\langle\partial_i\alpha(0,\mathbf{k})|\,\partial_j\alpha(0,\mathbf{k})\rangle + \\ &\quad -\frac{1}{16\pi^2}\int d\epsilon\, d\mathbf{k}\,\epsilon_{\mu\nu\rho}\sum_{\alpha\beta}\partial_\mu\, K_{\alpha\beta}(\epsilon,\mathbf{k})\;\langle\partial_\nu\alpha(\epsilon,\mathbf{k})|\,\beta(\epsilon,\mathbf{k})\rangle\,\langle\beta(\epsilon,\mathbf{k})|\,\partial_\rho\alpha(\epsilon,\mathbf{k})\rangle\,, \end{aligned} \tag{4.17}$$

where $i,j=1,2$. The second term, which I denote as I, is only contributed by $\Im m\, K_{\alpha\beta}(\epsilon,\mathbf{k})$, which is odd in ϵ, vanishes at $\epsilon\to\pm\infty$ and, by definition, is continuous at $\epsilon=0$. That allows partial integration, which, through Eq. (4.15), leads to

$$\begin{aligned} I &= -\frac{1}{8\pi^2}\int d\epsilon\, d\mathbf{k}\,\epsilon_{\mu\nu\rho}\sum_{\alpha\beta}K_{\alpha\beta}(\epsilon,\mathbf{k})\;\langle\partial_\mu\alpha(\epsilon,\mathbf{k})|\,\partial_\nu\beta(\epsilon,\mathbf{k})\rangle\,\langle\beta(\epsilon,\mathbf{k})|\,\partial_\rho\alpha(\epsilon,\mathbf{k})\rangle \\ &= -\frac{1}{8\pi^2}\int d\epsilon\, d\mathbf{k}\,\epsilon_{\mu\nu\rho}\sum_{\alpha\beta\gamma}\frac{K_{\alpha\beta}(\epsilon,\mathbf{k})}{\epsilon_\alpha(\epsilon,\mathbf{k})-\epsilon_\gamma(\epsilon,\mathbf{k})}\,\frac{1}{\epsilon_\beta(\epsilon,\mathbf{k})-\epsilon_\gamma(\epsilon,\mathbf{k})}\times \\ &\qquad\times\frac{1}{\epsilon_\alpha(\epsilon,\mathbf{k})-\epsilon_\beta(\epsilon,\mathbf{k})}\left\{F^\mu_{\alpha\gamma}(\epsilon,\mathbf{k})\,F^\nu_{\gamma\beta}(\epsilon,\mathbf{k})\,F^\rho_{\beta\alpha}(\epsilon,\mathbf{k})\right\}. \end{aligned} \tag{4.18}$$

Since I is real, I can take the complex conjugate, send $\epsilon\to-\epsilon$ and then either exchange β and γ as well as μ and ρ, thus getting

$$\begin{aligned} I &= -\frac{1}{8\pi^2}\int d\epsilon\, d\mathbf{k}\,\epsilon_{\mu\nu\rho}\sum_{\alpha\beta\gamma}\frac{-K_{\alpha\gamma}(\epsilon,\mathbf{k})}{\epsilon_\alpha(\epsilon,\mathbf{k})-\epsilon_\gamma(\epsilon,\mathbf{k})}\,\frac{1}{\epsilon_\beta(\epsilon,\mathbf{k})-\epsilon_\gamma(\epsilon,\mathbf{k})}\times \\ &\qquad\times\frac{1}{\epsilon_\alpha(\epsilon,\mathbf{k})-\epsilon_\beta(\epsilon,\mathbf{k})}\left\{F^\mu_{\alpha\gamma}(\epsilon,\mathbf{k})\,F^\nu_{\gamma\beta}(\epsilon,\mathbf{k})\,F^\rho_{\beta\alpha}(\epsilon,\mathbf{k})\right\}, \end{aligned} \tag{4.19}$$

or, instead, exchange α and γ as well as ν and ρ, in that way obtaining

$$\begin{aligned} I &= -\frac{1}{8\pi^2}\int d\epsilon\, d\mathbf{k}\,\epsilon_{\mu\nu\rho}\sum_{\alpha\beta\gamma}\frac{-K_{\gamma\beta}(\epsilon,\mathbf{k})}{\epsilon_\alpha(\epsilon,\mathbf{k})-\epsilon_\gamma(\epsilon,\mathbf{k})}\,\frac{1}{\epsilon_\beta(\epsilon,\mathbf{k})-\epsilon_\gamma(\epsilon,\mathbf{k})}\times \\ &\qquad\times\frac{1}{\epsilon_\alpha(\epsilon,\mathbf{k})-\epsilon_\beta(\epsilon,\mathbf{k})}\left\{F^\mu_{\alpha\gamma}(\epsilon,\mathbf{k})\,F^\nu_{\gamma\beta}(\epsilon,\mathbf{k})\,F^\rho_{\beta\alpha}(\epsilon,\mathbf{k})\right\}. \end{aligned} \tag{4.20}$$

Therefore, recalling that $K_{\alpha\beta}(\epsilon,\mathbf{k}) = -K_{\beta\alpha}(\epsilon,\mathbf{k})$ is antisymmetric, I can rewrite I as one third of the sum of (4.18), (4.19) and (4.20), thus

$$\begin{aligned} I &= \frac{1}{24\pi^2}\int d\epsilon\, d\mathbf{k}\, \epsilon_{\mu\nu\rho} \sum_{\alpha\beta\gamma} \frac{K_{\alpha\beta}(\epsilon,\mathbf{k}) + K_{\beta\gamma}(\epsilon,\mathbf{k}) + K_{\gamma\alpha}(\epsilon,\mathbf{k})}{\big(\epsilon_\alpha(\epsilon,\mathbf{k}) - \epsilon_\beta(\epsilon,\mathbf{k})\big)\big(\epsilon_\beta(\epsilon,\mathbf{k}) - \epsilon_\gamma(\epsilon,\mathbf{k})\big)\big(\epsilon_\gamma(\epsilon,\mathbf{k}) - \epsilon_\alpha(\epsilon,\mathbf{k})\big)} \\ &\qquad\qquad \times \Big\{ F^{\mu}_{\alpha\gamma}(\epsilon,\mathbf{k})\, F^{\nu}_{\gamma\beta}(\epsilon,\mathbf{k})\, F^{\rho}_{\beta\alpha}(\epsilon,\mathbf{k}) \Big\} \\ &= \frac{1}{24\pi^2}\int d\epsilon\, d\mathbf{k}\, \epsilon_{\mu\nu\rho} \sum_{\alpha\beta\gamma}{}' \frac{1}{i\epsilon - \epsilon_\alpha(\epsilon,\mathbf{k})} \frac{1}{i\epsilon - \epsilon_\beta(\epsilon,\mathbf{k})} \frac{1}{i\epsilon - \epsilon_\gamma(\epsilon,\mathbf{k})} \\ &= -W^{(2)}(G)\,, \end{aligned}$$

where the equivalence between the first and the second equations can be readily worked out.
In conclusion, I have proved that the winding number (4.8) can be written, not unexpectedly, as

$$W(G) = -\frac{1}{16\pi^2}\int d\epsilon\, d\mathbf{k}\, \epsilon_{\mu\nu\rho}\, \partial_\mu \left\{ \sum_{\alpha\beta} S_{\alpha\beta}(\epsilon,\mathbf{k}) \left\langle \partial_\nu \alpha(\epsilon,\mathbf{k}) \right| \beta(\epsilon,\mathbf{k}) \right\rangle \left\langle \beta(\epsilon,\mathbf{k}) \right| \partial_\rho \alpha(\epsilon,\mathbf{k}) \right\rangle \Big\},$$

namely, as the integral of a full derivative of a function that has a discontinuity at $\epsilon = 0$, for which reason the integral does not vanish and yields

$$W(G) = \frac{i}{2\pi}\int d\mathbf{k}\, \epsilon_{ij} \sum_{\alpha} \theta\big(-\epsilon_\alpha(0,\mathbf{k})\big) \left\langle \partial_i \alpha(0,\mathbf{k}) \right| \partial_j \alpha(0,\mathbf{k}) \right\rangle, \tag{4.21}$$

i.e., the TKNN expression [2] for *quasiparticles* described by the non-interacting Hamiltonian $H_*(0,\mathbf{k})$. Since $H_*(\epsilon,\mathbf{k})$ includes by definition both poles and zeros of the retarded Green's function, I argue that both of them contribute on equal footing to the topological invariant $W(G)$.
I emphasise that only through the representation (4.10) of the Green's function $G(i\epsilon,\mathbf{k})$ it has been possible to straightforwardly derive the simple expression of $W(G)$ in Eq. (4.21). Since that same representation is also the key to the proof that Landau's quasiparticles exist at Luttinger as well as Fermi surfaces [33, 34], I suspect this formalism is not just a mathematical trick but hints at a deeper physical meaning. Indeed, it is well possible that the bands of $H_*(0,\mathbf{k})$ lying inside the single-particle gap of a Mott insulator describe *fractionalised* quasiparticles not carrying all electron's quantum numbers, for instance neutral but spinful, even when they do not cross the chemical potential. Moreover, since those fractionalised quasiparticles cannot have any weight in the physical single-particle excitations, it is reasonable to expect that they are associated to the existence of ingap bands of zeros of the physical retarded Green's function.

Finally, I remark that all above results has been obtained in two dimensions (2D). However, the expression of topological invariants in 3D insulators [41–43, 185–187] also involve winding numbers that generalise (4.8) in higher dimensions [42], or describe other invariants like polarisation [43]. In particular, I note that my demonstration relies onto two main building blocks common to any winding number, and thus can be easily generalized to any invariant. First, any winding number that is written in terms of logarithmic derivatives $G\partial G^{-1}$ posses the property of Eq. (4.9), which implies that the quasiparticle residue (4.11) always disappears from the expression, which is therefore only determined by the quasiparticle Green's function $G_*(i\epsilon,\mathbf{k})$, see Eq. (4.10). Moreover,

any winding number can be written as an integral over the Matsubara frequency of a total derivative of a function

$$W \sim \int d\epsilon \, \frac{d}{d\epsilon} \, F(\epsilon)$$

which goes to zero for $\epsilon \to \pm\infty$ and is smooth everywhere but at $\epsilon = 0$, where it has a step discontinuity which makes the integral nonzero. Being the quasiparticle Green's function $G_*(i\epsilon, \mathbf{k})$ only dependent upon the quasiparticle Hamiltonian $H_*(\epsilon, \mathbf{k})$, which is however smooth and even around $\epsilon = 0$. This implies that, eventually, only the quasiparticle Hamiltonian at zero frequency contributes to the actual value of any winding number, both in the perturbative and in the non-perturbative regime.

4.4 A toy example

I now analyse a toy model inspired by Ref. [38]. Specifically, I consider an interacting BHZ model [9], whose inverse Green's function for a fixed spin reads

$$\begin{aligned} \hat{G}(i\epsilon, \mathbf{k})^{-1} &= i\epsilon - \epsilon(\mathbf{k}) \, \hat{\tau}_3 - \lambda \, \sin k_1 \, \hat{\tau}_1 + \lambda \, \sin k_2 \, \hat{\tau}_2 - \hat{\Sigma}(i\epsilon, \mathbf{k}) \\ &= i\epsilon - \hat{H}(\mathbf{k}) - \hat{\Sigma}(i\epsilon, \mathbf{k}) \, , \end{aligned} \tag{4.22}$$

where $\epsilon(\mathbf{k}) = M - \cos k_1 - \cos k_2$, a hat is introduced to distinguish matrices from scalars, and $\hat{\tau}_a$, $a = 1, 2, 3$, are the Pauli matrices in the two-orbital subspace. Without interaction, the model describes a topological insulator if $\epsilon(\mathbf{\Gamma}) \, \epsilon(\mathbf{M}) < \mathbf{0}$, with $\mathbf{M} = (\pi, \pi)$, which occurs if $0 < |M| < 2$. I assume that [38]

$$\hat{\Sigma}(i\epsilon, \mathbf{k}) = \frac{\Delta^2}{i\epsilon + \hat{H}'(\mathbf{k})} \, , \tag{4.23}$$

with $0 < \Delta \sim U$ and where $\hat{H}'(\mathbf{k})$ has the same form as $\hat{H}(\mathbf{k})$ in (4.22) but with renormalised parameters, thus $\epsilon(\mathbf{k}) \to \epsilon'(\mathbf{k}) = M' - t'\big(\cos k_1 + \cos k_2\big)$ and $\lambda \to \lambda'$. It follows that $\hat{H}'(\mathbf{k})$ is topological if $0 < |M'| < 2$, which is taken for granted.

I also assume that the model is deep inside the Mott insulating regime, which implies that Δ is in magnitude much larger than all the other parameters in (4.22). In this case, the poles of the retarded Green's function, $\hat{G}(\epsilon + i0^+, \mathbf{k})$, describes two lower and two upper Hubbard bands, with dispersion, respectively, $\epsilon_{\mathrm{LHB}}(\mathbf{k}) \simeq -\Delta + \delta\epsilon_{1(2)}(\mathbf{k}) \ll 0$ and $\epsilon_{\mathrm{UHB}}(\mathbf{k}) \simeq +\Delta + \delta\epsilon_{1(2)}(\mathbf{k}) \gg 0$, where $\delta\epsilon_{1(2)}(\mathbf{k})$ are the eigenvalues of $\hat{H}(\mathbf{k}) - \hat{H}'(\mathbf{k})$. The occupied lower Hubbard bands have opposite Chern numbers so that, from the point of view of the Green's function poles, the system is a trivial Mott insulator, as noted in [38].

However, besides those poles, the retarded Green's function also has valence and conduction bands of zeros with dispersion the eigenvalues of $-\hat{H}'(\mathbf{k})$ in Eq. (4.23), which are therefore topological [38].

The obvious question is whether the non-trivial topology of the Green's function zeros has any physical significance. For that, I follow the analysis of the previous section. Upon defining $E'(\mathbf{k})^2 = \epsilon'(\mathbf{k})^2 + \lambda'^2 \left(\sin^2 k_1 + \sin^2 k_2\right)$ one readily finds that the quasiparticle residue (4.11) reads in this case

$$\hat{Z}(\epsilon, \mathbf{k}) = \frac{\epsilon^2 + E'(\mathbf{k})^2}{\epsilon^2 + E'(\mathbf{k})^2 + \Delta^2} = Z(\epsilon, \mathbf{k}) \, \hat{I} \, , \tag{4.24}$$

and is proportional to the identity matrix $\hat{I}$, and thus

$$\hat{H}_*(\epsilon,\mathbf{k}) = Z(\epsilon,\mathbf{k})\left(\hat{H}(\mathbf{k}) + \frac{\Delta^2}{\epsilon^2 + E'(\mathbf{k})^2}\,\hat{H}'(\mathbf{k})\right),$$

which has exactly the same form as $\hat{H}$ with frequency dependent parameters $\epsilon_*(\epsilon,\mathbf{k})$ and $\lambda_*(\epsilon,\mathbf{k})$ that can be easily determined. At $\epsilon = 0$ and for large Δ,

$$\hat{H}_*(0,\mathbf{k}) = Z(0,\mathbf{k})\left(\hat{H}(\mathbf{k}) + \frac{\Delta^2}{E'(\mathbf{k})^2}\,\hat{H}'(\mathbf{k})\right) \simeq \hat{H}'(\mathbf{k}),$$

explicitly showing that only the Green's function zeros contribute to the topological invariant (4.21) in this toy example, and with opposite sign respect to the topology of the valence band of zeros that are described by $-\hat{H}'$. I emphasise that the exact correspondence between the ingap quasiparticle bands, eigenvalues of the Hamiltonian $\hat{H}_*(0,\mathbf{k})$, and the inverted bands of zeros of the retarded physical Green's function holds only in the limit of infinite Mott-Hubbard gap.

4.5 Concluding remarks

The winding number $W(G)$ of the physical electron Green's function $G(i\epsilon,\mathbf{k}) \in \mathrm{GL}(n,\mathbb{C})$ can be written as the winding number $W(G_*)$ of a quasiparticle Green's function $G_*(i\epsilon,\mathbf{k}) = 1/\big(i\epsilon - H_*(\epsilon,\mathbf{k})\big)$, see Eq. (4.10), whose poles on the real frequency axis are associated to both poles and zero of $G(\epsilon,\mathbf{k})$. I have shown explicitly that $W(G_*)$ reduces to the famous TKNN formula for free electrons, here the quasiparticles, described by the Hamiltonian $H_*(0,\mathbf{k})$.

This result implies that, against all expectations, the zeros of the real frequency Green's function do have a topological relevance, which is consistent with earlier studies [32–38], and nonetheless striking. Indeed, one would naïvely argue that the position of the ingap zeros could be easily changed from the positive to the negative side of the real frequency axis, or vice versa, by slightly modifying the Hamiltonian parameters, e.g., moving the chemical potential inside the insulating gap. However, if one accepts the viewpoint that ingap bands of zeros, or, more correctly, ingap bands of the quasiparticle Hamiltonian $H_*(0,\mathbf{k})$, may describe genuine excitations that do not carry all electron's quantum numbers, then their response to a shift in chemical potential is expected to differ substantially from that of non-interacting bands.

An enlightening example is, in my opinion, offered by a Hubbard atom with Hamiltonian $U(n-1)^2/2$, the simplest realisation of a Mott insulator. Its Green's function on the real frequency axis,

$$G(\epsilon) = \frac{1}{2}\left(\frac{1}{\epsilon + U/2} + \frac{1}{\epsilon - U/2}\right),$$

has poles at $\epsilon = \pm U/2$ and a zero at $\epsilon = 0$. Through equations (4.10) and (4.11) one finds that, for imaginary frequencies,

$$Z(\epsilon) = \frac{\epsilon^2}{\epsilon^2 + U^2/4}\,, \quad G_*(i\epsilon) = \frac{1}{i\epsilon}\,.$$

It is tempting to associate the zero-frequency pole of the quasiparticle $G_*(i\epsilon)$ and the vanishing

quasiparticle residue $Z(0) = 0$ to the free spin-1/2 of the isolated atom. In contrast, a non-interacting atom, $U = 0$, has

$$G(i\epsilon) = G_*(i\epsilon) = \frac{1}{i\epsilon} \,, \quad Z(\epsilon) = 1 \,,$$

consistently with the fact that the zero frequency excitations are physical single-particle ones, $Z(0) = 1$. I now imagine to couple the atom to a metallic reservoir with which it exchanges electrons, as one would do in statistical mechanics to fix the chemical potential, and assume that the atomic level is at energy ϵ_d with respect to the chemical potential of the reservoir. The atom plus the reservoir thus describe a conventional Anderson impurity model. In the case of the Hubbard atom with $\epsilon_d \ll U$, one expects that the zero-frequency pole of the quasiparticle Green's function is immediately promoted to a Kondo resonance pinned at the bath chemical potential, thus

$$G_*(i\epsilon) = \frac{1}{i\epsilon} \to \frac{1}{i\epsilon + i\, T_K \,\mathrm{sign}(\epsilon)} \,, \quad Z(\epsilon) \to \frac{T_K}{\Gamma} \,,$$

where Γ is the *bare* hybridisation width and T_K the Kondo temperature. In other words, the coupling to the bath allows revealing the hidden physical meaning of the zero, i.e., its being a free spin prompt to Kondo screening. On the contrary, in the case of the non-interacting atom

$$G_*(i\epsilon) = \frac{1}{i\epsilon} \to \frac{1}{i\epsilon - \epsilon_d + i\,\Gamma \,\mathrm{sign}(\epsilon)} \,,$$

which describes a resonant level centred at ϵ_d. It is remarkable that, while the non-interacting atom simply inherits the chemical potential of the bath, the Hubbard atom does not; the Kondo resonance is always pinned at the chemical potential even though the atomic level is offset by ϵ_d. This very simple example not only supports the interpretation that ingap quasiparticle bands in Mott insulators may describe fractionalised excitations, but also suggests that these bands respond very differently from conventional ones to a change in chemical potential induced by the contact with a charge reservoir, in contrast to a recent claim [188].

This analysis also extends the notion of topological transitions and adiabatic transformations for strongly interacting electrons. Indeed, it was already known that some topological invariants are contributed by zero-frequency roots of the Green function [32]. That, however, seems at odds with the expected behaviour of topological invariants under adiabatic transformations, since neither a closure of the charge gap nor any symmetry breaking occurs when Green's function zeros cross the chemical potential. In light of my results, this phenomenon acquires a straightforward physical explanation: Green's function zeros crossing the chemical potential form a Luttinger surface that hosts gapless excitations [33, 34] despite the finite charge gap, thus providing the non-adiabaticity required to change topology.

Finally, my results raise several questions worth being addressed in the future. The correspondence between topological bands and edge modes of Green's function zeros [36–38] suggests that, similarly to the conventional case of edge poles, the edge zeros are may be responsible of the quantised Hall conductance (4.21) if $K_L = 0$, although the surface is charge insulating. In the model quantum spin-Hall insulator of Sec. 4.4, that puzzling prediction can be explained by noticing that, according to Ref. [34], the edge quasiparticles at the Luttinger surface, actually a point, can carry a spin current, thus a quantised spin-Hall conductance. However, that simple explanation would not work for a hypothetical Chern Mott insulator with edge zeros crossing the

chemical potential. Therefore, even though the results of Sec. 4.3 prove that bulk bands of Green's function zeros contributes to the topological invariant (4.8), the actual role of edge zeros remains unclear.

A further question regards fractional Chern insulators. Indeed, if the winding number (4.8) does correspond to the Hall conductance, which may not always be the case if $K_L \neq 0$, one may wonder how it may ever be fractional since the TKNN formula should yield an integer value. In view of the similar issue that arises in the fractional quantum Hall effect [189], I believe that the ground state degeneracy, also expected in a fractional Chern insulator [190], is the key ingredient. Specifically, I suspect that $H_*(0, \mathbf{k})$ calculated over each ground state has valence bands with ill-defined Chern number, because, e.g., they touch the zone boundaries with finite slope. However, assuming, for simplicity, that the ground state is threefold degenerate, the Hall conductance is better defined as [189]

$$\sigma_{\mathrm{H}} = \frac{1}{3}\Big(W(G_1) + W(G_2) + W(G_3)\Big) = \frac{1}{3}\,W\big(G_1\,G_2\,G_3\big)\,,$$

where G_n is the Green's function calculated over the ground state $|n\rangle$, $n = 1, 2, 3$. The sum of the three winding numbers corresponds to the TKNN formula applied to the quasiparticles valence bands of all three ground states. I speculate, see, e.g., Ref. [191], that all these bands as a whole correspond to a well-behaved single band once unfolded into a threefold larger Brillouin zone, whose Chern number is therefore an integer ℓ, thus $\sigma_{\mathrm{H}} = \ell/3$, a fractional value. Incidentally, it is suggestive that the sum of the winding numbers is just the winding number of $G = G_1\,G_2\,G_3$, which is still a complex invertible matrix. The above is just a speculation that worth investigating.

I conclude by emphasising that the winding number (4.8) in two dimensions, although being a topological invariant, not necessarily coincides with the quantised Hall conductance when perturbation theory breaks, where is well possible that $K_L \neq 0$. Similarly, it cannot be excluded that the extensions of the Green's function winding number in three dimensions [41–43, 192] might be unrelated to the physical observables they are supposed to reproduce when there is no adiabatic connection between the interacting system and the non-interacting one. That leaves open the question about the actual physical meaning of those winding numbers [182, 183].

CHAPTER 5

NEUTRAL QUASIPARTICLES IN TOPOLOGICAL KONDO INSULATORS

5.1 Introduction

The Kondo effect serves as a compelling testament to the profound influence of strong correlations in materials, revealing behaviors markedly distinct from their weakly correlated counterparts. When a highly diluted (few parts per millions) concentration of magnetic impurities, typically transition metal or rare earth atoms, is placed into a good metal (copper, silver or gold), the naïve expectation based on band theory is that the partially filled d/f shells of the impurities, which are responsible in isolation of their magnetic behaviour, get either filled up or emptied depending on the position of the d/f levels with respect to the chemical potential of the metal. In either cases, the impurities should lose their magnetic moments that, in turn, implies the same Pauli paramagnetic behavior below the Fermi temperature T_F of the host metal as in absence of impurities. In reality, in most of the cases the physics deviates substantially from the above scenario: the impurities retain well below T_F their magnetic moments, signalled by a Curie-Weiss behavior of the magnetic susceptibility, which get screened only at much lower temperatures. The crossover from the local moment regime to the paramagnetic one occurs around the so-called Kondo temperature $T_K \ll T_F$, and is characterised by a logarithmic in temperature dependence of several physical observables, like, e.g., the resistivity. In the low-temperature screened regime analytic dependence upon T is recovered. Moreover, the d/f electrons get promoted into the conduction band giving rise to resonances in the single-particle spectrum, known as Kondo or Abrikosov-Suhl resonances, of narrow width $\sim T_K$ and which are pinned at the chemical potential irrespective of the specific magnetic impurities and host metals, thus contrasting the band theory expectation. This complex behavior is commonly denoted as Kondo effect and ultimately arises because the impurities oppose against any increase or decrease in the number of electrons that occupy the d/f shell. Such stiffness to valence fluctuations can be incorporated in a model Hamiltonian by adding a Coulomb charging energy within the d/f shell of each impurity plus, eventually, exchange terms that implement the Hund rules. This leads to the celebrated Anderson impurity model [193],

which, for a single-band metal and a single impurity that in isolation has just a half-filled orbital, reads

$$H_{AIM} = \sum_{\mathbf{k}\sigma} \left\{ \epsilon_{\mathbf{k}}\, c^{\dagger}_{\mathbf{k}\sigma}\, c_{\mathbf{k}\sigma} + \left(V_{\mathbf{k}}\, c^{\dagger}_{\mathbf{k}\sigma}\, f_{\sigma} + H.c. \right) \right\} + \epsilon_f\, n_f + \frac{U}{2} \left(n_f - 1 \right)^2 , \tag{5.1}$$

where $V_{\mathbf{k}}$ describes the hybridization between the conduction band and the impurity f-orbital, ϵ_f is the position of the latter with respect to the host-metal chemical potential, and, finally, U parametrizes the charging energy, i.e., the cost of an empty or fully occupied f-orbital.
The physics of the Kondo effect has a bulk counterpart in compounds where one constituent has partially filled f-shells and in which localised f-orbitals coexist with highly dispersive bands, commonly known as heavy-fermion materials. Also in heavy-fermions the local moments residing in the f-shell is eventually screened at low temperature by the conduction bands, and, analogously to the Kondo resonance, the f-electrons acquire coherence throughout the lattice and give rise to a very narrow band crossing the chemical potential. Not unexpectedly, the physics of heavy-fermions is well reproduced by the periodic extension of the Anderson impurity model (PAM) [194]:

$$H_{PAM} = -t \sum_{<ij>\sigma} c^{\dagger}_{i\sigma} c_{j,\sigma} + \sum_i \left[\epsilon_f\, n_{fi} + \frac{U}{2} (n_{fi} - 1)^2 \right] + V \sum_{i\sigma} \left(c^{\dagger}_{i\sigma}\, f_{i\sigma} + h.c. \right) , \tag{5.2}$$

which, in the above simple example, describes a tight-binding model of conduction electrons hybridised on each site i to an f-orbital at energy ϵ_f and charging energy U. The heavy-fermion physics arises in model (5.2) when U is large and the number of electrons per site $n = n_c + n_f \neq 2$. When $n = 2$, the Hamiltonian (5.2) may instead describe a bona fide insulator known as Kondo insulator at large U. In this case, while at high temperature the f-electrons are effectively decoupled from the conduction ones, the former behaving as local moments and the latter responsible of a metallic behavior, the onset of coherence at low-temperature brings about the opening of a hybridisation gap between valence and conduction bands turning the model insulating.

A particularly intriguing subset of Kondo insulators, exemplified by SmB_6 and YbB_{12} as leading candidates, are the topological Kondo insulators (TKI). These materials exhibit f- and d-orbitals with opposite parity and an odd-parity spin-orbit hybridization between them, thus possessing the characteristics to realize Z_2 topological insulators [52, 194].
Remarkably, these materials display a low-temperature resistivity plateau independent of the sample size due to the presence of conducting surface states, see [44–48] for SmB6 and [49–51] for YbB12. These surface states have been interpreted as genuine chiral edge modes arising by the non-trivial bulk topology, although a conclusive experimental confirmation of their topological origin is still lacking.

Strikingly, these compounds also exhibit Fermi liquid properties compatible with a 'neutral' Fermi surface. SmB_6 shows a linear in temperature specific heat [53–55] and thermal conductivity [58], though the latter is still debated [56, 197], whereas YbB_{12} displays unambiguous linearity in both thermal properties [196].
Moreover, SmB_6 exhibits quantum oscillations in magnetization (the de Haas-van Alphen (dHvA) effect) [57–59, 195] and in the specific heat [60], but not in the resistivity (i.e., the Shubnikov-de Haas (SdH) effect). On the other hand, YbB_{12} shows both dHvA [63, 64] and SdH [61, 62, 64] effects. These experimental findings, summarized in Fig. 5.1, represent a well-defined riddle: how

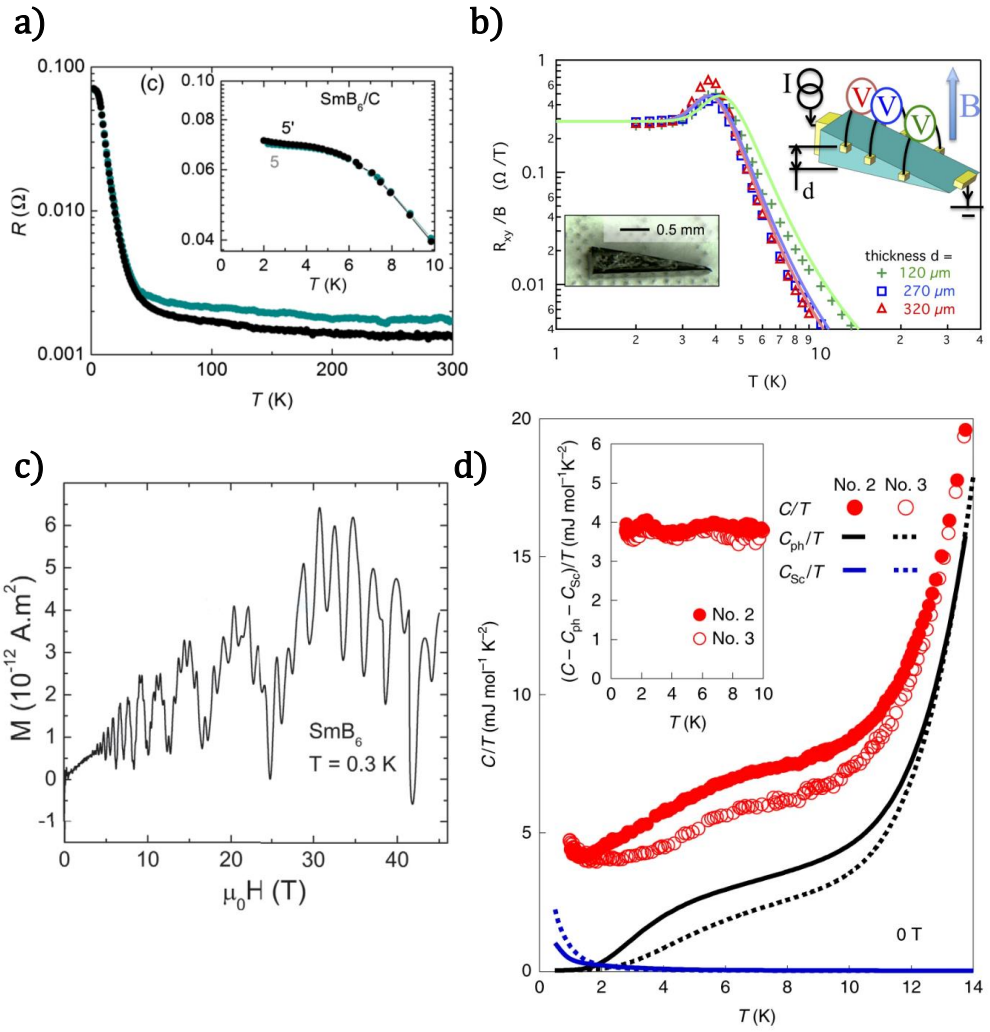

Figure 5.1: **Summary of key experimental evidences for TKI.** Panel a: Low temperature resistivity plateau for SmB_6. In particular, the two dataset corresponds to different thickness but converge the same value of the plateau, indicating a surface origin. Panel b: Hall conductance of SmB_6 at finite magnetic field for different sample thickness. Again, at low temperature it stabilizes to a value independent by the sample thickness. Panel c: quantum oscillation in the magnetization for SmB_6. Panel d: Low temperature specific heat divided by temperature for YbB_{12}. In the inset, the finite quasiparticle contribution is isolated. Figures adapted from Refs. [46, 195, 196].

is it possible to have an insulator with all the textbook Fermi liquid properties of a weakly interacting metal, conduction states aside?
This behaviour contradicts the picture of conventional Kondo insulators. Several theoretical explanations have been proposed, including magneto-excitons [68], the possibility of quantum oscillations in narrow gap insulators [69–71], the enhancement of quantum oscillations in Kondo insulators [72], the interplay between surface states and the Kondo breakdown [73]. However, these theories predict strong deviations from the Lifshitz-Kosevich expression for quantum oscillations, which contradicts experimental observations.

A critical element, in my view, absent from the current understanding is the nature of the itinerant d-electrons. Indeed, in both SmB_6 and YbB_{12}, the d- and the f-orbitals originate from the same rare earth atom, implying that even though the $4f$-orbital is undoubtedly more correlated than the $5d$ one, the interaction between them may be non-negligible.

Expanding upon this insight, I put forward an alternative hypothesis, one that revolves around the presence of a Luttinger surface within the insulating gap. Recent findings [74,75] indicate that, despite the vanishing quasiparticle residue, a Luttinger surface, i.e., the location in the Brillouin zone of the zeros of the single-particle Green's function at zero frequency, can host 'quasiparticles' that exhibit thermal and magnetic behaviour akin to a Fermi liquid but remain hidden in the physical single-particle density of states, typically measured in ARPES experiments. Despite the charge fractionalization due to correlations, these quasiparticles still exhibit a coupling to a magnetic field, potentially leading to observable quantum oscillations [76].

To substantiate this hypothesis, I will present cluster dynamical mean field theory calculations employing the TRIQS package [198] and obtained through the continuous-time quantum Monte Carlo hybridization expansion impurity solver (CTHYB) [199]. To critically address the role of d-correlations, I will explore both the scenario where only the f-orbitals are interacting, and another that incorporates a more realistic interaction that encompasses the d-orbitals as well.

Notably, my results will show that only the latter scenario aligns with the presence of a Luttinger surface within the insulating gap, which could offer a plausible explanation for the ambivalent behaviour of these materials.

5.2 Non-interacting tight binding model for TKI

The low-energy properties of TKI are predominantly governed by the d- and f-bands of the rare earth atoms. Moreover, due to crystal field splitting (CFS) effects, only a fraction of the degenerate d- and f- orbitals resides near the Fermi energy [200]. Therefore in this study, I will consider a minimal model with just one d- and one f-band [52, 201]. Specifically, I assign $J = 5/2$ and $J_z = \pm 5/2$ for the f-orbitals, while $J = 3/2$ and $J_z = \pm 3/2$ for the d-orbitals. Finally, I restrict my analysis to two dimensions.

Introducing the Pauli matrices τ_a and σ_a, $a = 0, 1, 2, 3$, which act on the orbital and pseudo-spin spaces respectively, and defining a four-component spinor as

$$\Psi^\dagger_{\mathbf{k}} = \left(f^\dagger_{\mathbf{k}\uparrow}, f^\dagger_{\mathbf{k}\downarrow}, d^\dagger_{\mathbf{k}\uparrow}, d^\dagger_{\mathbf{k}\downarrow} \right), \tag{5.3}$$

where $\sigma = \uparrow, \downarrow$ refers to $J_z = \pm 5/2$ and $J_z = \pm 3/2$ for f- and d-electrons, respectively, the tight-

binding single-particle Hamiltonian is given by

$$\begin{aligned} H_0 &= \sum_{\mathbf{k}} \Psi^\dagger_{\mathbf{k}} \, \hat{H}_0(\mathbf{k}) \, \Psi_{\mathbf{k}} \,, \\ \hat{H}_0(\mathbf{k}) &= \epsilon_f(\mathbf{k}) \, \frac{\tau_0 + \tau_3}{2} + \epsilon_d(\mathbf{k}) \, \frac{\tau_0 - \tau_3}{2} + V \, \tau_1 \, \mathbf{k}^* \cdot \boldsymbol{\sigma} \,, \end{aligned} \tag{5.4}$$

with $\mathbf{k}^* = 2\big(\sin(k_x), \sin(k_y)\big)$. The dispersions of d- and f- orbitals are described by

$$\begin{aligned} \epsilon_d(\mathbf{k}) &= -2\, t_d \big(\cos(k_x) + \cos(k_y)\big) \,, \\ \epsilon_f(\mathbf{k}) &= D_f + 2\, t_f \big(\cos(k_x) + \cos(k_y)\big) \,, \end{aligned} \tag{5.5}$$

where D_f is the crystal field splitting and t_d, t_f are the hopping amplitudes. Symmetry considerations, particularly the opposite parity under inversion, prevent on-site hybridization between d- and f-orbitals but allow hybridization between nearest neighbours [52], represented by the off-diagonal odd-in-momentum term of strength V. In particular, this hybridization is responsible for the gap opening in the topological regime.

In addition to the $P422$ space group symmetry, the model possesses inversion and time-reversal symmetry, represented by

$$P = \tau_3 \,, \qquad T = i\, \sigma_2 \, K \,. \tag{5.6}$$

Notably, parity plays a pivotal role in defining the Z_2 topological invariant, exactly as in the case of the BHZ model extensively discussed in Chapter 2. At the four high symmetry points, in fact, the hybridization vanishes and the bands have well-defined parity, so that the topology is dictated by the numbers of band inversions in the Brillouin zone, see Fig. 5.2.

Throughout the discussion of this model, I will fix the parameters of the non-interacting Hamiltonian as in Refs. [202, 203]

$$D_f = -6 \,, \quad t_f = -0.2 \,, \quad t_d = 1 \,, \quad V = 0.4 \,. \tag{5.7}$$

5.3 Discussion of the topological periodic Anderson model

5.3.1 The interaction Hamiltonian and the DCA equations

To include correlation effects, I first consider the case where only the f-orbitals are interacting through the simple Hubbard term

$$H_{int} = U \sum_{\mathbf{R}} n_{f\mathbf{R}\uparrow} \, n_{f\mathbf{R}\downarrow} \,, \tag{5.8}$$

where the density operator for spin σ and site $\mathbf{R}$ is simply defined as $n_{f\mathbf{R}\sigma} = f^\dagger_{\mathbf{R}\sigma} \, f_{\mathbf{R}\sigma}$. In this case the model reduces to a topological periodic Anderson model (TPAM), where now the lattice of weakly dispersing f-impurities is coupled via a odd parity hybridization to a bath of conducting and non-interacting d-electrons.

This model has already been analysed by means of single site dynamical mean field theory (DMFT) by Werner and Assad [202, 203], who found that the leading effect of local correlations is an upward renormalization of the crystal field splitting and an increase of the effective f-electron

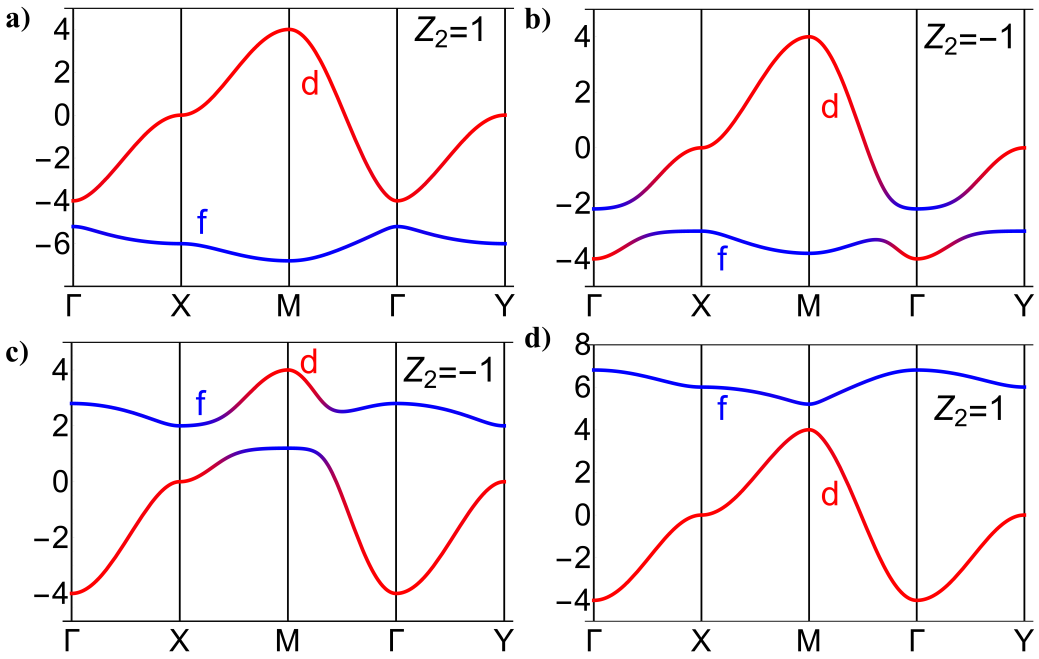

Figure 5.2: **Non-interacting bands of the model for representative values of the crystal field splitting.** For $D_f < 4.8$ (Panel a), the f-band is completely occupied and the d-one completely empty, thus the system is a trivial insulator. For $-4.8 < D_f < 0$ (Panel b), an avoided crossing emerges, when now the valence band has f-character at **X**, **Y** and **Γ** points while a d-character at the **M** point. This band inversion implies that the ground state is a topological insulator with an odd Z_2 invariant. Upon increasing the CFS even more $0 < D_f < 4.8$ (Panel c), the system transition to another topological insulator closing the gap at the **X** and **Y** points, where now the orbital character at the high symmetry points is reversed. Finally, for $D_f > 4.8$ (Panel d), the system is again a trivial insulator with the d-band completely occupied and the f-one completely empty. In general, the transition between a trivial and a topological insulator at $D_f = \pm 4.8$ is characterized by a gap closing at **Γ** while the transition between the two topological insulators at $D_f = 0$ closes the gap at the **X** and **Y** points. I note that all the parameters but the CFS are fixed as in Eq.(5.7).

mass. Approaching $U = 8.9$, the f-band becomes heavier and heavier, with the effective mass rapidly growing. The authors, however, do not explore stronger interactions, mentioning only that the model may develop an orbital selective Mott transition (OSMT). Being interested just in this strongly correlated regime, I will investigate the nature of the paramagnetic ground state by means of DMFT and dynamical cluster approximation (DCA) calculations.

The DCA is performed on a 2x2 site cluster that gives access only to the self-energy at the four momenta $\mathbf{\Gamma}$, $\mathbf{X}$, $\mathbf{Y}$ and $\mathbf{M}$.
Since only the f-electrons are interacting, the DCA equations reduce to those of a simple periodic Anderson model, where a non-self consistent hybridization due to the presence of the d-electrons is added to the auxiliary cluster impurities problem.
Assuming a paramagnetic solution, the cluster quantities are entirely determined by the f-self-energy $\Sigma_f(i\epsilon, \mathbf{K})$, where $\mathbf{K}$ are the four cluster momenta. Each momentum has its own patch within the BZ, which I shall denote as $P(\mathbf{K})$, see Fig. 5.3a, in which the lattice self-energy is constant. Thus, for $\mathbf{k} \in P(\mathbf{K})$, the f-Green's function can be written as

$$G_f(i\epsilon, \mathbf{k}) = \left(i\epsilon + \mu - \epsilon_f(\mathbf{k}) - \Sigma_f(i\epsilon, \mathbf{K}) - 4V^2 \frac{\sin^2(k_x) + \sin^2(k_y)}{i\epsilon + \mu - \epsilon_d(\mathbf{k})} \right)^{-1}, \tag{5.9}$$

which yields the local Green's function

$$G_{loc}(i\epsilon, \mathbf{K}) = \frac{1}{N_{\mathbf{K}}} \sum_{\mathbf{k} \in P(\mathbf{K})} G_f(i\epsilon, \mathbf{k}), \tag{5.10}$$

where $N_{\mathbf{K}}$ is the number of $\mathbf{k}$ point in each patch $P(\mathbf{K})$. Finally, the Weiss fields are obtained trough the Dyson equation

$$\mathcal{G}_0(i\epsilon, \mathbf{K}) = \left(G^{-1}_{loc}(i\epsilon, \mathbf{K}) + \Sigma_f(i\epsilon, \mathbf{K}) \right)^{-1}. \tag{5.11}$$

In the context of DCA the Luttinger-Ward functional and thus the self-energy are calculated summing the Feynman diagrams on all the possible momenta $\mathbf{K}$ allowed by the cluster, see Fig. 5.3b. In particular, being the Hubbard interaction on-site, the cluster interaction Hamiltonian is simply

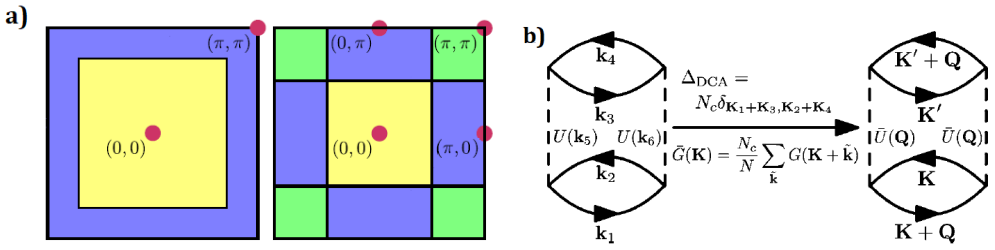

Figure 5.3: **Cluster dynamical approximation.** Panel a: Brillouin zone patches for 2 and 4 site cluster calculations. Panel b: a prototypical diagram contributing to the Luttinger-Ward functional in the DCA approximation. In particular, all the sum over internal momenta are performed only over the one allowed by the cluster. Figures adapted from Refs. [204, 205] respectively.

the Fourier transform over the **K** momenta of Eq.(5.8)

$$H_{DCA} = U \sum_{\mathbf{K}_1,\mathbf{K}_2,\mathbf{K}_3,\mathbf{K}_4} \delta_{\mathbf{K}_1+\mathbf{K}_3,\mathbf{K}_2+\mathbf{K}_4}\, f^\dagger_{\mathbf{K}_1\uparrow} f_{\mathbf{K}_2\uparrow}\, f^\dagger_{\mathbf{K}_3\downarrow} f_{\mathbf{K}_4\downarrow}\,. \tag{5.12}$$

5.3.2 Numerical results and emerging physical scenario

In this section, I present numerical results obtained using both single-site DMFT and DCA over a broad range of interaction strengths, specifically, for $2 \leq U \leq 16$ and all other parameters fixed at the values (5.7). The chemical potential is set at the midpoint of the gap in the case of an insulating state or adjusted to achieve half filling in a metallic state.

I begin by discussing the regime where $U < 9$. Here, the primary consequence of interaction is an upward renormalization of the crystal field splitting (CFS) due to the Hubbard repulsion. To quantify it, I define the effective CFS as:

$$\tilde{D_f} = D_f + \mathrm{Re}\,\Sigma_f(i\omega_1)\,,$$

where Σ_f refers both to DMFT and DCA quantities and $\omega_1 = \pi T$. I stress that in DCA the crystal field splitting calculated at **X** and **Y** is the parameter that controls the topological transition.
Notably, approaching the critical value of $U = 9$ the effective CFS tends to zero, see Fig. 5.4a, implying that the gap starts to close due to the vanishing hybridization at the **X** and **Y** points, as in Figs. 5.5a-c. I note that, due to non-local correlations, this happens earlier in DCA, around $U = 8$. Simultaneously, the quasiparticle residue of the f-electrons, which is the inverse of the mass renormalization in single-site DMFT, defined as

$$Z_f \equiv \left(1 - \frac{\mathrm{Im}\,\Sigma_f(i\omega_1)}{\omega_1}\right)^{-1},$$

rapidly decreases with U, its derivative reaching a maximum (in a semi-logarithmic scale) around $U = 8$, as shown in Fig. 5.4b. Furthermore, the f-band center-of-mass tends to pin at the chemical potential so to achieve half-filling. These observations strongly indicate that the f-electrons are entering a heavy fermion regime, and that some kind of phase transition may be on the verge.

For larger values of U, Werner and Assad [202, 203] proposed that the system would undergo an OSMT. However, a recent study [206] suggests that the OSMT is generally unstable in presence of inter-orbital hybridization at finite temperatures.
My calculations appear to support the latter scenario: the f-orbitals do rapidly lose spectral weight near the chemical potential, except for a small peak that survives at the **X** an **Y** points, see Fig. 5.5. Notably, the height of this peak decreases monotonously with increasing interaction, as seen in Figs. 5.4d, 5.5b-d, at least for interactions up to $U = 16$. It is important to note that the peak appearance in both the DMFT and DCA calculations lends support to its genuine existence. When considering DMFT alone, one might suspect an artefact, since the auxiliary f-impurity naturally seeks to form a singlet state with the d-bath to remove the spin degeneracy. However, the fact that this feature also appears in the DCA calculations, where the spin degeneracy can, in principle, be removed within the cluster itself, further corroborates its existence.

I would like to emphasize that, in this strongly correlated regime, the effective CFS initially increases up to a maximum value, and then starts to diminish, as illustrated in Fig.5.4a. In

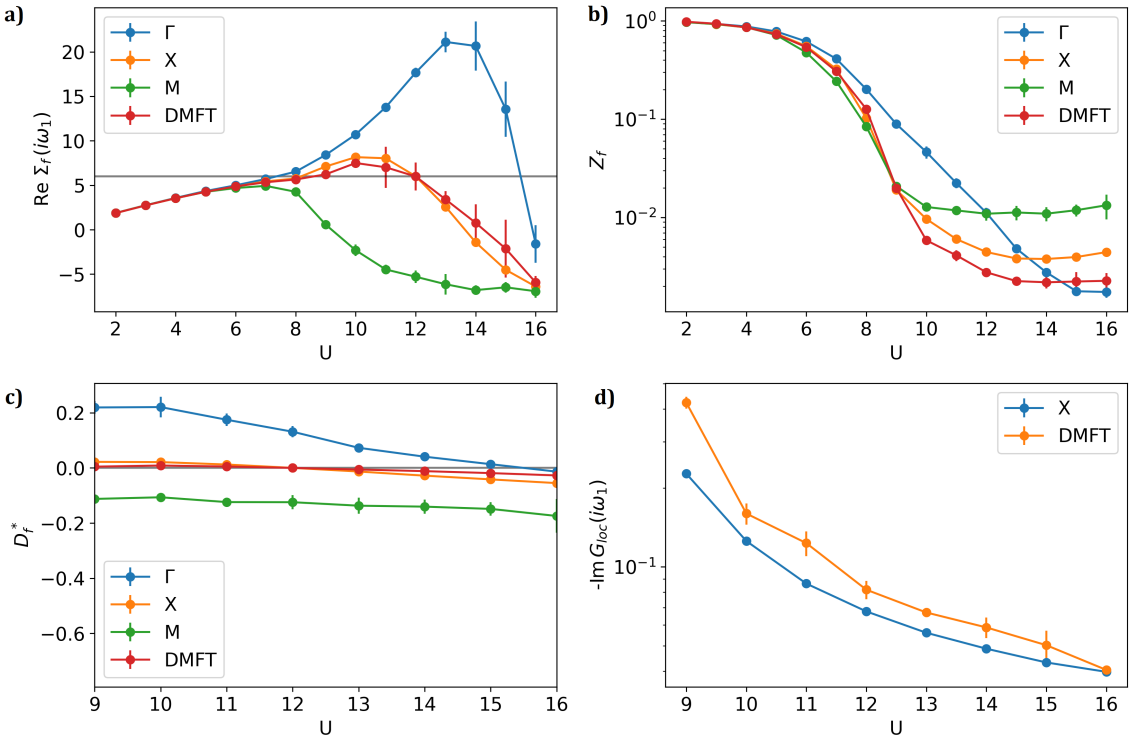

Figure 5.4: **Numerical results in Matsubara frequency for DMFT at β=100 and 2x2 sites DCA calculations at β=50.** In particular, the results are averaged over five iterations, and the (tiny) standard deviation is plotted. Since the **X** and **Y** points are equivalent, only results for the former are presented. Panel a: Real part of the self-energy for the first Matsubara frequency. Panel b: Quasiparticle mass of the f-band m_f^* in logarithmic scale. Panel c: Quasiparticle crystal field splitting D_f^*. Panel d: Minus imaginary part of the local Green's function at the first Matsubara frequency in the quasiparticle-peak regime, which corresponds to the density of states at the chemical potential. In particular, it is possible to see how the height of the quasiparticle peak is renormalized downward increasing the interaction. I note that, due to symmetry reasons, the **X** momenta is representative of the **Y** momenta as well.

particular, it is exactly zero for DMFT and the DCA $\mathbf{X}$ and $\mathbf{Y}$ momenta at $U = 12$, where the model recovers particle-hole symmetry since the bare crystal field splitting exactly counterbalance the Hartree term of the f-orbital, $D_f = -U/2$. In this case the two bands are forced to cross at the $\mathbf{X}$ and $\mathbf{Y}$ momenta where the hybridization vanishes, and the system is a genuine metal without a gap. For different values of the interaction, however, the effective CFS is nonzero. Although the quasiparticle crystal field splitting, $D_f^* = \tilde{D}_f\, Z_f$, is more appropriate to describe the position of the heavy fermion f-band, see Fig. 5.4c, also this quantity is nonzero for $U \neq 12$, though extremely small. This implies that in principle the almost flat f-band crosses the dispersive d-one at momenta slightly different from the $\mathbf{X}$ and $\mathbf{Y}$ ones, where the quasiparticle hybridization $V^* = V\, Z_f$ is tiny but nevertheless finite, implying an equally tiny gap that the calculations are unable to resolve due to finite temperature effects. This eventuality seems confirmed by the single-site DMFT calculations of the quasiparticle bands, see Fig. 5.8 of the Appendix, which predict gaps much smaller than the temperature $T = 0.01$ of the calculations, apart from $U = 12$ where a genuine gap closing appears.

I conclude the discussion of the numerical results by emphasizing that, for this model, the single-site DMFT self-energy is nearly identical to the one calculated in DCA for the $\mathbf{X}$ and $\mathbf{Y}$ points. This similarity is reasonable because at these points the gap closes, suggesting they are pivotal in driving the low energy physics. On the other hand, the $\mathbf{M}$ and $\mathbf{\Gamma}$ points also exhibit a similar behaviour, implying that local correlations primarily govern the physics, with non-local effects playing a smaller quantitative role renormalizing the band dispersion rather than fundamentally altering the qualitative picture.

The numerical results I have presented for the TPAM establish a clear physical scenario. For interaction values $U \lesssim 9$, the system behaves as a correlated topological insulator, exhibiting a non-trivial Z_2 invariant and chiral edge states [203]. However, being this insulator adiabatically connected to a non-interacting one, it is unable to explain the strange Fermi liquid behaviours of TKI. As the interaction strength increases beyond this value, the system remains in the heavy fermion regime without showing an OSMT: the f-band becomes flatter and flatter and remains pinned at the chemical potential, losing progressively spectral weight near zero frequency in favour of the Hubbard bands. In this regime, two different scenarios are plausible: either the system is metallic due to the fact that the band crossing happens exactly at the $\mathbf{X}$ and $\mathbf{Y}$ points where the hybridization vanishes, or it is insulating with a tiny gap due to the fact that the crossing occurs slightly away from those points.
However, to definitely discern between these two scenarios, high accuracy calculations with a temperature much smaller than the gap should be performed, which goes beyond the scope of this work since both scenarios are nonetheless unable to explain the experimental evidence of a sizeable gap insulator that displays Fermi liquid properties.
The general inconsistencies of these results with the experimental evidences has prompted me to reexamine the Coulomb repulsion Hamiltonian for TKI, taking into consideration that both orbitals actually belong to the same atom: a key feature of these materials that has been overlooked in the existing literature.

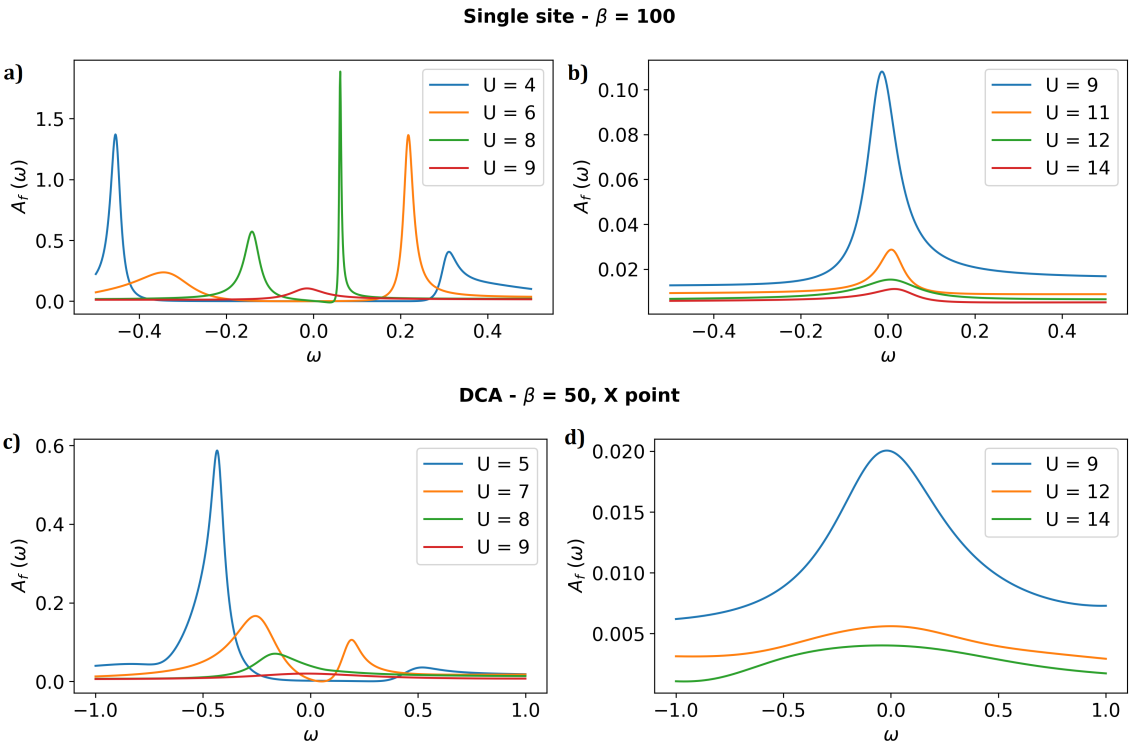

Figure 5.5: **Real frequency f-density of states obtained through Pade approximation.** Panel a,b): DMFT results. For $U < 9$, the system is insulating with a sizable gap. For $U > 9$, only a small Kondo peak survives at the chemical potential. Panel c): DCA results at the **X** point, determinant for the low energy physics. In particular the gap closes at $U = 8$, earlier than in DMFT, an for $U = 9$ the system again displays a small quasiparticle peak.

5.4 A more realistic interaction Hamiltonian

Given the f-orbitals more localized nature, it appears clear way the role of correlations in the d-orbitals has been overlooked in the existing literature. However, as just demonstrated, this oversight may lead to inaccurate theoretical predictions that are inconsistent with experimental evidence.

To address this issue, in the following section I will introduce a new realistic Hamiltonian derived by projecting the local Coulomb repulsion onto the relevant $4f$ and $5d$ atomic orbitals, now considering also d-correlation effects. Subsequently, I will discuss how the DCA equations are modified and the different interpolation that can be used to obtain lattice quantities from the cluster ones. Finally, I will discuss the numerical results of 2-sites DCA calculations and examine the resulting physical scenario.

5.4.1 Local projected Coulomb interaction

As discussed above, in TKI crystal field splitting effects remove the large degeneracy within the d- and f-multiplets. Thus, I will project the local Coulomb repulsion only on the $4f$-atomic orbitals $J = 5/2$, $J_z = \pm 5/2$ and $J = 3/2$, $J_z = \pm 3/2$ $5d$-ones of an isolated Samarium, the same I considered in the tight-binding Hamiltonian but neglecting shape distortions due to crystal field effects. The corresponding atomic wave-functions in spherical coordinates are

$$\begin{aligned}
\phi_{f,5/2}(\Omega, r, \sigma) &= \left(\frac{1}{\sqrt{7}} Y_3^2(\Omega)\, \delta_{\sigma,\uparrow} - \sqrt{\frac{6}{7}} Y_3^3(\Omega)\, \delta_{\sigma,\downarrow} \right) R_{4f}(r)\,, \\
\phi_{f,-5/2}(\Omega, r, \sigma) &= \left(\sqrt{\frac{6}{7}} Y_3^{-3}(\Omega)\, \delta_{\sigma,\uparrow} - \frac{1}{\sqrt{7}} Y_3^{-2}(\Omega)\, \delta_{\sigma,\downarrow} \right) R_{4f}(r)\,, \\
\phi_{d,3/2}(\Omega, r, \sigma) &= \left(\frac{1}{\sqrt{5}} Y_2^1(\Omega)\, \delta_{\sigma,\uparrow} - \frac{2}{\sqrt{5}} Y_2^2(\Omega)\, \delta_{\sigma,\downarrow} \right) R_{5d}(r)\,, \\
\phi_{d,-3/2}(\Omega, r, \sigma) &= \left(\frac{2}{\sqrt{5}} Y_2^{-2}(\Omega)\, \delta_{\sigma,\uparrow} - \frac{1}{\sqrt{5}} Y_2^{-1}(\Omega)\, \delta_{\sigma,\downarrow} \right) R_{5d}(r)\,,
\end{aligned} \tag{5.13}$$

where σ refers to the actual spin of the electrons. Since the two orbitals belong to different shells, to calculate the radial part of the wave-function two different effective charges [207] have to be considered

$$Z_{eff}^{4f} \simeq 23\,, \qquad Z_{eff}^{5d} \simeq 16\,. \tag{5.14}$$

Given the Coulomb interaction expressed generically in terms of the Fermi field

$$\hat{U} = \frac{1}{2} \sum_{\sigma,\sigma'} \int d\mathbf{x}_1\, d\mathbf{x}_2\, \Psi_\sigma^\dagger(\mathbf{x}_1) \Psi_{\sigma'}^\dagger(\mathbf{x}_2)\, \frac{1}{\mathbf{x}_1 - \mathbf{x}_2}\, \Psi_{\sigma'}(\mathbf{x}_2) \Psi_\sigma(\mathbf{x}_1)\,, \tag{5.15}$$

I note that the Coulomb kernel has the following expansion in spherical harmonics

$$\frac{1}{\mathbf{x}_1 - \mathbf{x}_2} = \sum_{l=0}^{\infty} \frac{4\pi}{2l+1} \frac{\min(r_1, r_2)^l}{\max(r_1, r_2)^{l+1}} \sum_{m=-l}^{l} Y_l^m(\Omega_1)\, Y_l^m(\Omega_2)^*\,. \tag{5.16}$$

so that, projecting the Fermi field upon the local orbitals, i.e.

$$\Psi_\sigma^\dagger(\mathbf{x}_1) = \Psi_\sigma^\dagger(\Omega_1, r_1) = \sum_{i=f,d} \sum_{J_z=\pm} \phi_{i,J_z}^*(\Omega_1, r_1, \sigma)\, i_{J_z}^\dagger \tag{5.17}$$

the only non-vanishing Slater integrals originate from the monopole and dipole contributions. The local Hubbard Hamiltonian can thus be written as the sum of a density-density and a dipole-dipole repulsion

$$\begin{aligned} H_{int} &= H_U + H_J \,, \\ H_U &= \sum_{\mathbf{R}} \left[U_f \, n_{f\mathbf{R}\uparrow} \, n_{f\mathbf{R}\downarrow} + U_d \, n_{d\mathbf{R}\uparrow} \, n_{d\mathbf{R}\downarrow} + V \, n_{f\mathbf{R}} \, n_{d\mathbf{R}} \right] , \\ H_J &= \frac{J}{4} \sum_{\mathbf{R}} \left[\left(\Psi^\dagger_{\mathbf{R}} D_x \Psi_{\mathbf{R}} \right)^2 + \left(\Psi^\dagger_{\mathbf{R}} D_y \Psi_{\mathbf{R}} \right)^2 \right] , \end{aligned} \tag{5.18}$$

where now $\uparrow, \downarrow$ denotes the pseudo-spin along the z-direction, with the dipole operators defined as

$$D_x \, = \, S_z \, \tau_x \,, \qquad D_y \, = \, S_0 \, \tau_y, \,. \tag{5.19}$$

I note that, being projected only over a subspace of the $J = 5/2$ and $J = 3/2$ manifold, the Hamiltonian beaks the spin $SU(2)$ symmetry but not the $U(1)$ rotations along the z-axis. In particular, the dipole term enforces Hund's rules, but now favouring high S_z configurations. Moreover, I stress that having used the same orbitals in both the non-interacting Hamiltonian and the projected local Coulomb interaction, they share the same symmetries.
The actual estimate of the coupling constants in units of U_f is

$$U_d = 0.33 \, U_f \,, \quad V = 0.46 \, U_f \,, \quad J = 0.10 \, U_f \,, \tag{5.20}$$

which confirms that, even if U_f is greater in magnitude, as expected, the strength of the other coupling constants is not far smaller, making their role non-negligible.

5.4.2 DCA equations and cumulant periodization

Being also the d-orbital interacting, the DCA equations introduced to describe the TPAM need to be slightly modified. In this case, in fact, one has in principle to take into account the full 4×4 matrix structure of the problem, considering orbital off diagonal elements both in the Green's function and in the self-energy.
However, I note that for DCA calculations up to four sites, the cluster momenta corresponds to the high symmetry points of the Brillouin zone, see Fig. 5.3a, where the inter-orbital hybridization has to vanish by inversion symmetry. For the same reason, both the self-energy and the local Green's functions calculated at these points are diagonal in orbital and spin indexes.
Since I had to consider a two sites cluster to perform feasible calculations, and being interested in the paramagnetic phase, I shall assume a diagonal and spin independent self-energy, resulting in the diagonal terms of the lattice Green's functions, for $\mathbf{k} \in P(\mathbf{K})$

$$\begin{aligned} G_f(i\epsilon, \mathbf{k}) &= \left(i\epsilon + \mu - \epsilon_f(\mathbf{k}) - \Sigma_f(i\epsilon, \mathbf{K}) - 4V^2 \, \frac{\sin^2(k_x) + \sin^2(k_y)}{i\epsilon + \mu - \epsilon_d(\mathbf{k}) - \Sigma_d(i\epsilon, \mathbf{K})} \right)^{-1} , \\ G_d(i\epsilon, \mathbf{k}) &= \left(i\epsilon + \mu - \epsilon_d(\mathbf{k}) - \Sigma_d(i\epsilon, \mathbf{K}) - 4V^2 \, \frac{\sin^2(k_x) + \sin^2(k_y)}{i\epsilon + \mu - \epsilon_f(\mathbf{k}) - \Sigma_f(i\epsilon, \mathbf{K})} \right)^{-1} . \end{aligned} \tag{5.21}$$

From these, the local Green's function and the Weiss field (diagonal itself) can be easily derived. As before, the chemical potential is set at the midpoint of the gap, although otherwise indicated.

DCA is a cluster extension of DMFT introduced directly in reciprocal space and thus is inherently periodical, with the lattice self-energy that is assumed to be a step function in the Brilluoin zone, constant in each patch . However, in order to estimate the shape and position of the Luttinger surface, if any, one has to reconstruct the lattice self-energy: some post-processing interpolation needs to be performed. Therefore I shall briefly discuss the periodic and cumulant interpolations in the case of a two site cluster, where the allowed cluster momenta are $\mathbf{\Gamma}$ and $\mathbf{M}$.
In the weakly correlated regime, the self-energy is almost constant in the Brillouin zone, so that the straightforward periodic interpolation is an accurate approximation of the lattice self-energy. Dropping the orbital indexes for simplicity, this corresponds to find a smooth periodic interpolation between the various cluster momenta

$$\begin{gathered}\Sigma_{per}(i\epsilon,\mathbf{k}) = \alpha_{\mathbf{k}}\,\Sigma(i\epsilon,\mathbf{\Gamma}) + \beta_{\mathbf{k}}\,\Sigma(i\epsilon,\mathbf{M})\,,\\ \alpha_{\mathbf{k}} = \frac{1}{2}\left(1+\frac{1}{2}\big(\cos(k_x)+\cos(k_y)\big)\right)\,, \qquad \beta_{\mathbf{k}} = \frac{1}{2}\left(1-\frac{1}{2}\big(\cos(k_x)+\cos(k_y)\big)\right)\,.\end{gathered} \tag{5.22}$$

I note that, containing the cluster only two sites, the self-energy effectively renormalises the on-site energy and the nearest neighbour hopping.
In the case of a Mott insulator, where strong correlations may yield singular behavior, the expansion near the atomic limit leads to a self-energy displaying poles [38]

$$\Sigma(i\epsilon,\mathbf{k}) = \frac{\Delta^2}{i\epsilon+\mu+\epsilon'(\mathbf{k})} + U_H\,, \tag{5.23}$$

where $\Delta^2 \propto U^2$, U_H is the Hartree potential and $\epsilon'(\mathbf{k})$ is a renormalized dispersion that depends on non-local correlations. It appears clear that is not possible to obtain this behaviour from just a periodic interpolation.
The cumulant interpolation, physically justified by the observation that in this case the inverse of the self-energy is more local than the self-energy itself [208], accounts instead for the interpolation of $\epsilon'(\mathbf{k})$ between the different cluster momenta. First, a smooth interpolation of the cluster cumulant is performed

$$M_{\mathbf{k}} = \frac{\alpha_{\mathbf{k}}}{\Sigma(i\epsilon,\mathbf{\Gamma})-U_H} + \frac{\beta_{\mathbf{k}}}{\Sigma(i\epsilon,\mathbf{M})-U_H}\,, \tag{5.24}$$

and then the self-energy is obtained through

$$\Sigma_{cumu}(i\epsilon,\mathbf{k}) = 1/M_{\mathbf{k}} + U_H\,. \tag{5.25}$$

I note that, in the weakly correlated regime, where the self-energy is dominated by local contributions with the non-local one being just a small correction,

$$\Sigma(i\epsilon,\mathbf{k}) \simeq \Sigma_0(i\epsilon) + \delta\Sigma(i\epsilon,\mathbf{k}) \quad \text{with} \quad \delta\Sigma(i\epsilon,\mathbf{k}) \ll 1\,,$$

the cumulant interpolation reduces to the periodic one. In this sense, one has a little more control on the faithfulness of this interpolation, since it usually predicts poles in the self-energy only in the case when their presence is genuine.

Having introduced the interpolation scheme, I now discuss how the Mott gap opening emerges in the cluster quantities. Assuming a self-energy of the form in Eq.(5.23), it appears clear that the possibility of having a pole exactly at one of the cluster momenta, and thus finding a pole

directly in the cluster self-energy, is accidental and entirely depends on the exact details of the DCA calculation. Consequently, it is well possible that the cluster self-energy is perfectly regular in Matsubara frequencies and yet the system is gapped by the Mott phenomenon. To elucidate how the gap opening may work in DCA, I define the renormalized dispersion

$$r_{\mathbf{k}} = \epsilon(\mathbf{k}) + \mathrm{Re}\,\Sigma(i\omega_1, \mathbf{k}) - \mu\,,$$

whose roots entails the existence of a Fermi surface, and thus metallicity.
In the case of a Mott insulator, one can envisage two different scenarios:

- $r_{\mathbf{k}}$ is positive or negative throughout the whole Brillouin zone, but the orbital is anyway half-filled due to breakdown of Luttinger's theorem.
- $r_{\mathbf{k}}$ changes sign in the Brillouin zone, but the difference between the self-energy at the different patches is high, which suggests that $r_{\mathbf{k}}$ changes sign through a singularity rather than crossing zero.

Both scenarios seem to be realised, see Fig. 5.6a-d. In particular, when $r_{\mathbf{k}}$ is discontinuous, see Fig. 5.6c-d, the interpolation predicts a genuine singularity, Fig. 5.6e-f, which corresponds to the emergence of a Luttinger surface.
I end this discussion mentioning that for two orbitals I just need to introduce two $r_{\mathbf{k}}$ corresponding to the eigenvalues of $\hat{H}_0(\mathbf{k}) + \mathrm{Re}\,\hat{\Sigma}(i\omega_1, \mathbf{k}) - \mu$, noticing that in the Mott case the orbital character is maintained because of the diagonal nature of the self-energy.

5.4.3 Numerical results

In this section, I discuss the DCA results obtained on a 2-sites cluster. For $U \leq 11$ the calculations are performed at $\beta = 50$, while for higher interaction strengths at $\beta = 100$.

The numerical results suggest that, starting from weak interactions and gradually increasing U, two different phases emerge. For $U \leq 10$, the system is a weakly correlated topological insulator adiabatically connected to the non-interacting one. The presence of this topological phase, similar to the one realized in the TPAM, is due to an upward renormalization of the CFS

$$\tilde{D}_f = D_f + \mathrm{Re}\,\Sigma_f(i\omega_1) - \mathrm{Re}\,\Sigma_d(i\omega_1)\,,$$

that falls in the topological interval $-4.8 < \tilde{D}_f < 0$. Moreover, $\Sigma_d(i\omega_1) > 0$ slows down the upward shift of CFS, so that the topological phase resists until $U \sim 10$, rather than $U \sim 8$ as in the TPAM. Approaching this value, the gap starts closing at the **X** and **Y** points and the two orbitals approach half-filling: their centres of mass get closer to the chemical potential and empty/double occupancies get suppressed. I also note that, in the vicinity the gap closure, pronounced non-local correlations start to build up, as can be noted by the strong patch-dependence of the self-energy in Fig.5.6b.
For $U \gtrsim 10$, however, the behavior is rather different from the TPAM one. Since interaction involves both orbitals, it triggers their simultaneous Mott localization, and thus the opening of a sizeable Mott gap.
This Mott phenomenon can be noted in Fig.5.6c-d, where the renormalized dispersion $r_{\mathbf{k}}$ is plotted. In particular, for $U = 11$ and $U = 12$, $r_{\mathbf{k}}$ of the d-electrons changes sign between different patches without crossing the chemical potential, indicating that a d-band of zeros is present inside the

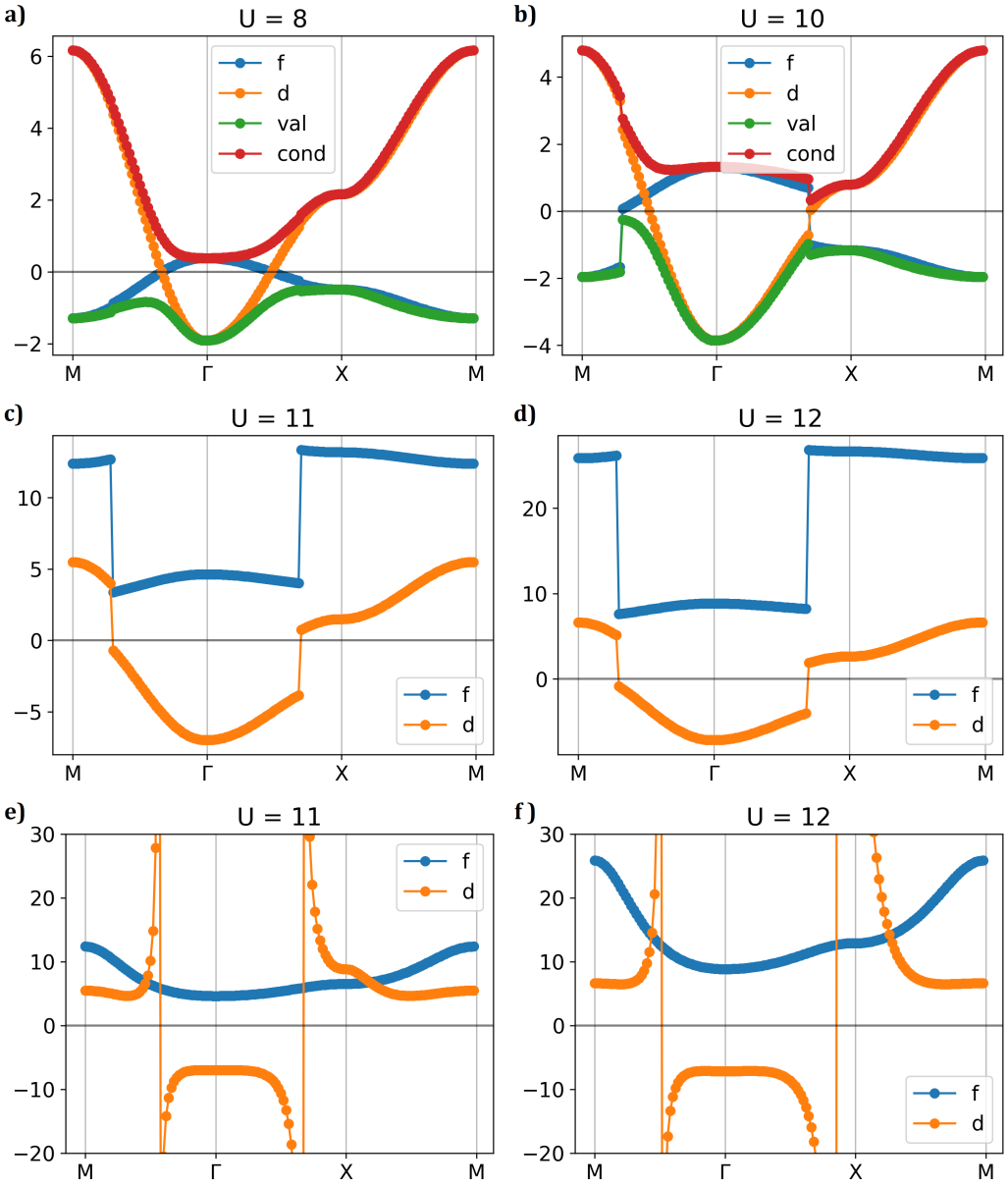

Figure 5.6: **Bands of the renormalized Hamiltonian** $H_0 + \mathbf{Re}\,\Sigma(\omega = 0)$. In panels a) to d), the self-energy is a step function between patches employed in the DCA self-consistency, while in panels e)-f) the cumulant interpolation has been performed. In Panel a)-b), the system is a topological insulator, where the gap opening is due an avoided crossing between the two bands, as can be noted by the plot of the f and d renormalized bands without hybridization. I note that, for $U = 10$, the sizeable discontinuity between different patches implies rising non-local correlations. Panel c)-d): Mott insulating regime, where non-local correlations prohibits the renormalized dispersion of the f- and d-bands from crossing the chemical potential in any point of the Brillouin zone. In this case the dispersion of the f-electrons is always above the chemical potential although they are half filled, a hallmark of the breakdown of Luttinger theorem, while the d-one changes sign without crossing the chemical potential. I clarify that in these calculations the role of the hybridization is negligible, hence I plotted only the orbitals dispersions to improve clarity. Panel e)-f): bands of the renormalized Hamiltonian, now for a cumulant interpolated self-energy. In particular the d-dispersion changes sign not crossing zero energy but rather from $\pm\infty$, sign of a Luttinger surface at the divergences. I note that a direct periodization of the self-energy would lead to a Fermi surface of the d-electrons, and an empty f-one at odd with the half filled insulating Green's function obtained from the cluster quantities.

gap. This leads to divergences of $r_{\mathbf{k}}$ when the cumulant interpolation is applied, see Fig.5.6e-f, thus a d-Luttinger surface. On the other hand, the f-renormalized dispersion is placed above the chemical potential in the whole Brillouin zone. Overall, Luttinger's theorem breaks down.

To comprehensively analyse the nature of the possible Luttinger surfaces in this Mott regime, I performed several DCA calculations changing the chemical potential inside the insulating gap for $\beta = 50$, $U = 12$ and $\beta = 100$, $U = 16$. Then, through the cumulant interpolation of the self-energy, I was able to predict the shape and orbital nature of the Luttinger surfaces.
In the first case, see Fig.5.7b, varying the chemical potential I encompassed only d-Luttinger surfaces, due to the larger Mott gap of the f-electrons. In fact, since the model has no particle-hole symmetry, the f-band of zeros is placed well above the chemical potential. Before reaching this band of zeros, the d-Hubbard bands are first encountered, thus turning the model metallic, see Figs.5.9 and 5.10 in the Appendix for further details. More insights can be gained by studying the quasiparticle Hamiltonian defined in the previous chapter, i.e.,

$$H_*(0,\mathbf{k}) = \sqrt{Z(\hat{\mathbf{k}})}\,\left(\hat{H}_0(\mathbf{k}) - \mu + \mathrm{Re}\hat{\Sigma}(0,\mathbf{k})\right)\,\sqrt{Z(\hat{\mathbf{k}})}\,. \tag{5.26}$$

This Hamiltonian has bands within the Mott gap, see Fig.5.7a, the d-one crossing the chemical potential and thus forming a *quasiparticle Fermi surface* that is just the Luttinger surface. I note that the crossings between d- and f-bands away from high-symmetry points is due to the fact that the patch self-energy has no off-diagonal elements, since the patches are centred at the parity-invariant points $\boldsymbol{\Gamma}$ and $\boldsymbol{M}$. I expect that, should I be able to perform DCA with a number of patches greater than four, the self-energy would acquire off-diagonal elements turning the crossings into avoided ones. I emphasise that for $U = 12$, the values of the chemical potential that keep the model insulating only allow for a d-like Luttinger surface.
On the contrary, for $U = 16$ the larger Mott gap permits also an f-Luttinger surface besides the d-one upon varying the chemical potential inside the Mott gap. Both Luttinger surfaces coexist for $8.5 \leq \mu \leq 9$, and genuine divergences of the cluster self energy are found, see Figs.5.11 and 5.12 in the Appendix. I already mentioned that, being the self-energy calculated at the high symmetry $\boldsymbol{\Gamma}$ and $\boldsymbol{M}$ points of the Brillouin zone, off-diagonal terms are forced to vanish by inversion symmetry. This entails that the bands of zeros, being in direct correspondence with the self-energy poles, have defined orbital character and they cannot hybridize. As earlier discussed, more realistic self energies should develop off-diagonal elements. That would result in avoided crossings between the bands, opening a gap in the quasiparticle Hamiltonian bands in Fig.5.7a-c. In this case, and should the chemical potential between the two bands, they would become topological.
From the above discussion, it emerges very clearly that the precise position of the chemical potential μ inside the Mott gap plays a fundamental role if the in-gap quasiparticle bands correspond to genuine neutral excitations. Unfortunately, it is difficult to locate μ when the model is a Mott insulator. On one side, if one applies conventional thermodynamic arguments, one should fix μ at high temperatures such that the density is half-filled, and try to extrapolate μ to lower, eventually, zero temperature. However, this calculation goes beyond our accuracy being the Mott gap quite large. Moreover, it is not at all guaranteed that thermodynamic arguments are applicable since it is not obvious that the DCA Mott insulator is ergodic. One should better contact the Mott insulator with a metallic bath and exploit the latter to fix the chemical potential, which is a very involved calculation beyond current capabilities.

Therefore, while I can definitely state that in-gap bands of Green's function zeros exist, I cannot conclude whether one of them or both cross the chemical potential, or, rather, that the latter is between them giving rise to topological bands of zeros. All those different possibilities would have specific physical consequences should the quasiparticle bands have physical content, as I discuss next.

5.4.4 Discussion

The numerical results I just presented suggest that for relatively small values of the interaction the system is a weakly correlated topological insulator that, as already discussed in the case of the TPAM, cannot sustain thermal Fermi liquid properties or standard quantum oscillations. For $U \simeq 10.5$, a simultaneous localization of both orbitals drives the system into a Mott insulating state.

Here, I find d- and f-quasiparticle bands, obtained by means of Eq. (5.26) upon filtering out incoherent components, which lie inside the Mott gap, see Fig. 5.7. These two bands cross each other away from the high symmetry points, at least up to $U = 16$, which suggests that a larger, though numerically unaffordable, number of patches giving access to off-diagonal self-energy components might turn the crosses into avoided ones, thus yielding topological quasiparticle valence and conduction bands. If these bands do correspond to genuine neutral excitations, their position with respect to the chemical potential must be fixed, just like a Kondo resonance is always pinned at μ. However, the only way to physically add an in-gap chemical potential in an incompressible Mott insulator and circumvent any issue of ergodicity is by contacting it to a metallic reservoir with which the insulator can exchange particles and thus inherit the bath μ. Unfortunately, this situation is very hard to simulate by DCA. For this reason, here I only examine the possibility that might explain most, but not the whole, experimental evidence.

For that, the first and most important question to address is about the properties of the in-gap quasiparticle bands should they indeed represent neutral excitations. Since they are chargeless, they can only carry magnetic moment and parity, and thus contribute to the magnetic susceptibility and electric polarisability. Since the model lacks spin $SU(2)$, the magnetic susceptibility χ_z to a field along z is contributed by intra-orbital excitations, while the susceptibility $\chi_\perp$ to a field in the x-y plane, associated with $\Delta J_z = \pm 1$, and the electric polarisability Π involve inter-orbital excitations. As earlier mentioned, I expect that off-diagonal components of the self-energy, which must exist though are unaccessible by our DCA calculation with two patches, open a hybridization gap in the quasiparticle bands shown in Fig. 5.7. I argue that either the valence or the conduction quasiparticle band is pinned at the chemical potential, thus forming a Luttinger surface. The latter can explain [76] the observed quantum oscillations, Fermi liquid-like thermal properties and low energy magnetic excitations [209, 210]. However, it cannot rationalise the surface electric conduction and the spectroscopic evidence of metallic surface states, supposedly of topological origin, which would require a calculation with a semi infinite slab geometry similar to that discussed above to simulate the contact with a metallic reservoir, but now with an interface to the topologically trivial vacuum.

5.5 Summary

In this chapter, I developed a novel explanation for the puzzling thermal properties and quantum oscillations of topological Kondo insulators, based on the presence of neutral ingap quasiparticles. In particular, I linked the presence of these quasiparticles to the emergence of bands of Green's function zeros.

To arrive at this result, I first introduced a realistic tight-binding model for these materials, involving itinerant d-orbitals and more localised f-ones. Following the relevant literature on the subject, I discussed an interacting Hamiltonian which, due to its more localised nature, only considers the f-charge density. Starting from the non-interacting case and increasing the interaction, I showed by 4-site DCA calculations that the system initially exhibits a weakly correlated topological insulating phase and, as the correlations are increased, either an extremely narrow gap heavy fermion insulator or a genuine metallic phase is stabilised. In either case, I have shown that this model is unable to account for a sizable gap insulating state with metallic-like Fermi liquid properties throughout the phase diagram.

Therefore, I critically re-analysed the interaction Hamiltonian considering that in topological Kondo insulators both d- and f-orbitals belong to the same rare earth atom. Extending this idea, I derived a more realistic multi-orbital Hubbard Hamiltonian by projecting the Coulomb repulsion onto the relevant atomic wavefunctions. By performing 2-site DCA calculations, I showed that for moderate interaction values the system again becomes a correlated topological insulator, equivalent to that found in the earlier case, but now with d-correlations. However, as the gap closes, the system undergoes a Mott localisation of both orbitals, realising an insulator with a substantial gap. In this Mott phase, a Luttinger surface of either f- or d-character can be realised depending on the Hamiltonian parameters, which could provide a plausible explanation for the Fermi liquid in-gap behaviour of Kondo topological insulators.

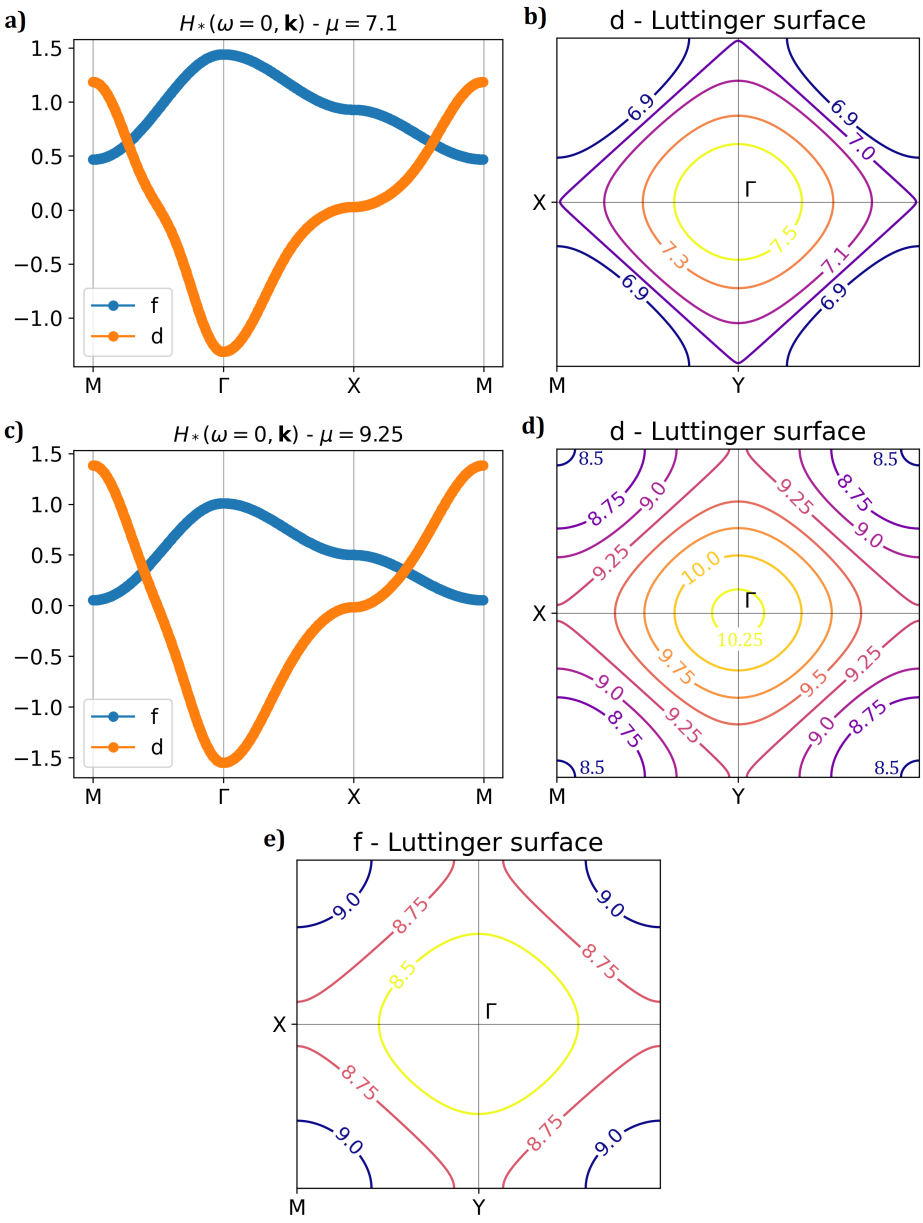

Figure 5.7: **Quasiparticle Hamiltonian and Luttinger surfaces inside the Mott gap.** Panel a) shows the quasiparticle Hamiltonian for $U = 12$ computed with the cumulant interpolation at $\mu = 7.1$. In panel b), the possible d-Luttinger surfaces realized inside the gap are showed. I note that, increasing the chemical potential, the d-Luttinger surface moves toward $\mathbf{\Gamma}$, since the position of the zeros at finite frequencies is described by $-H_*(0, \mathbf{k})$. Panel c)-d), the same for $U = 16$. In this case, due to a large Mott gap, f-Luttinger surfaces are encountered and are presented in panel e). I note that in the case of a realistic calculation, I expect the bands to be gapped implying a nontrivial topology of the quasiparticle Hamiltonian.

APPENDIX: ADDITIONAL DATAPLOTS

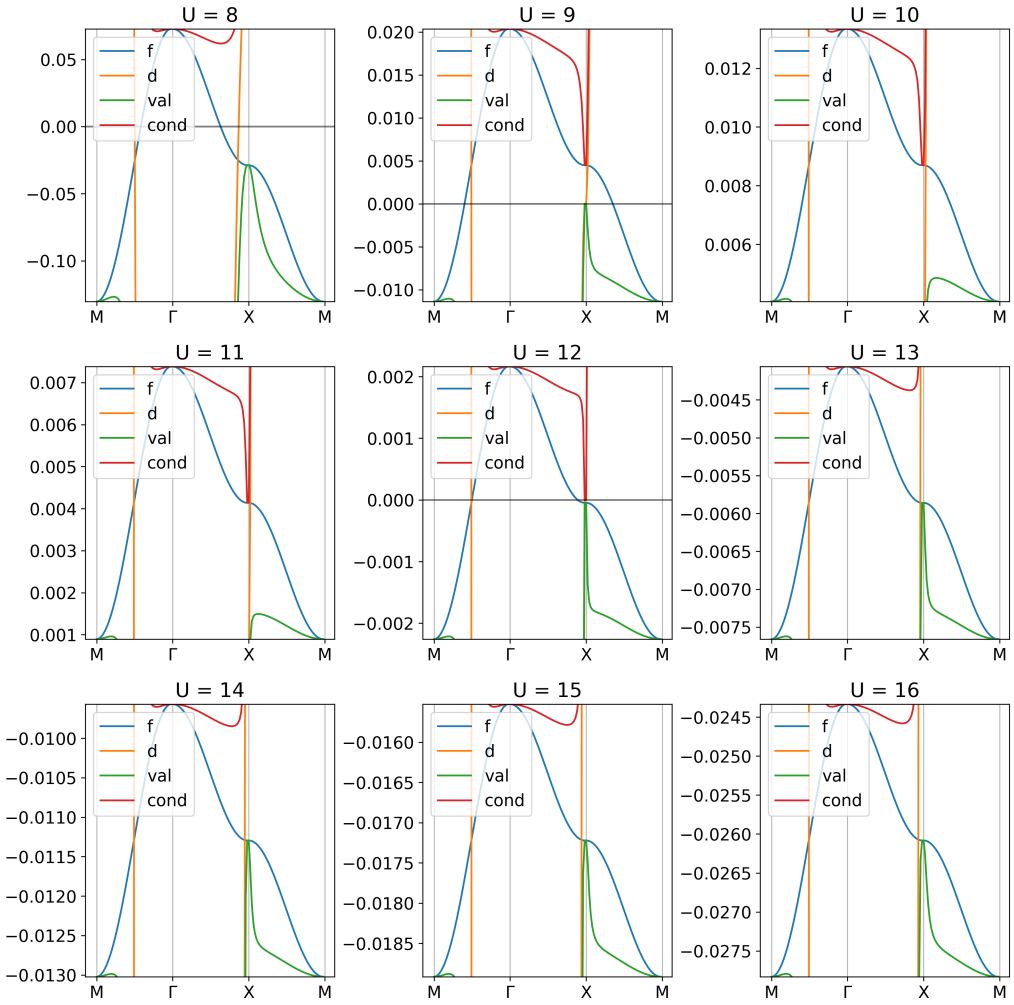

Figure 5.8: **Quasiparticle bands for the TPAM for different interaction strength, calculated within DMFT.** In particular, both the f-, d-bands before hybridization and the valence and conduction ones are plotted. I observe that, already at $U = 9$, the gap is half the temperature $T = 0.01$ and rapidly decreases increasing the interaction. In particular, at $U = 12$ the gap is exactly closed due to an accidental particle-hole symmetry of the model.

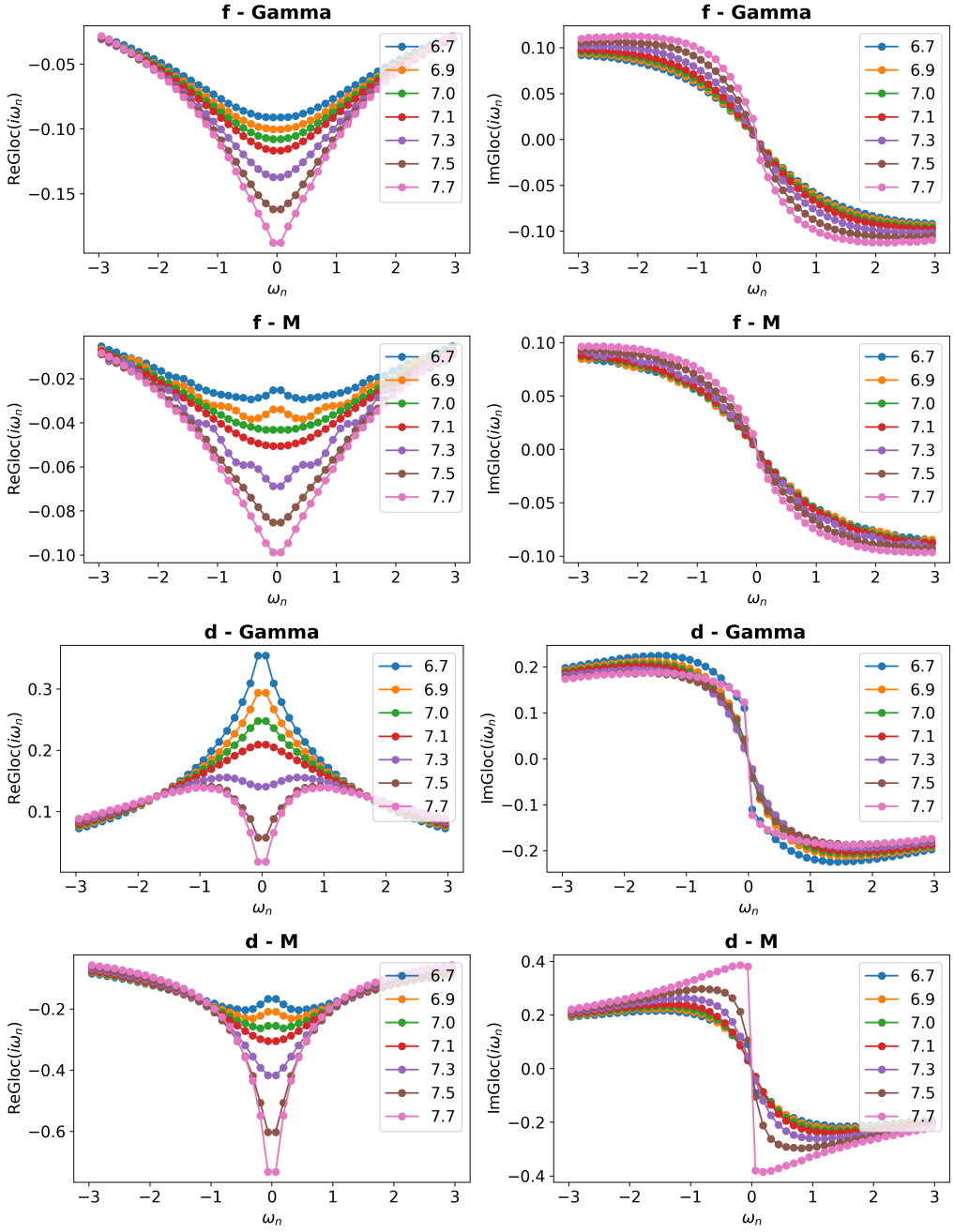

Figure 5.9: **Local Green's functions in Matsubara frequencies for U = 12 and different values of the chemical potential.** In particular, the gap for the d-orbitals is closed at $\mu = 6.7$ and $\mu = 7.7$, while the f-orbitals remain insulating due to the larger Mott gap.

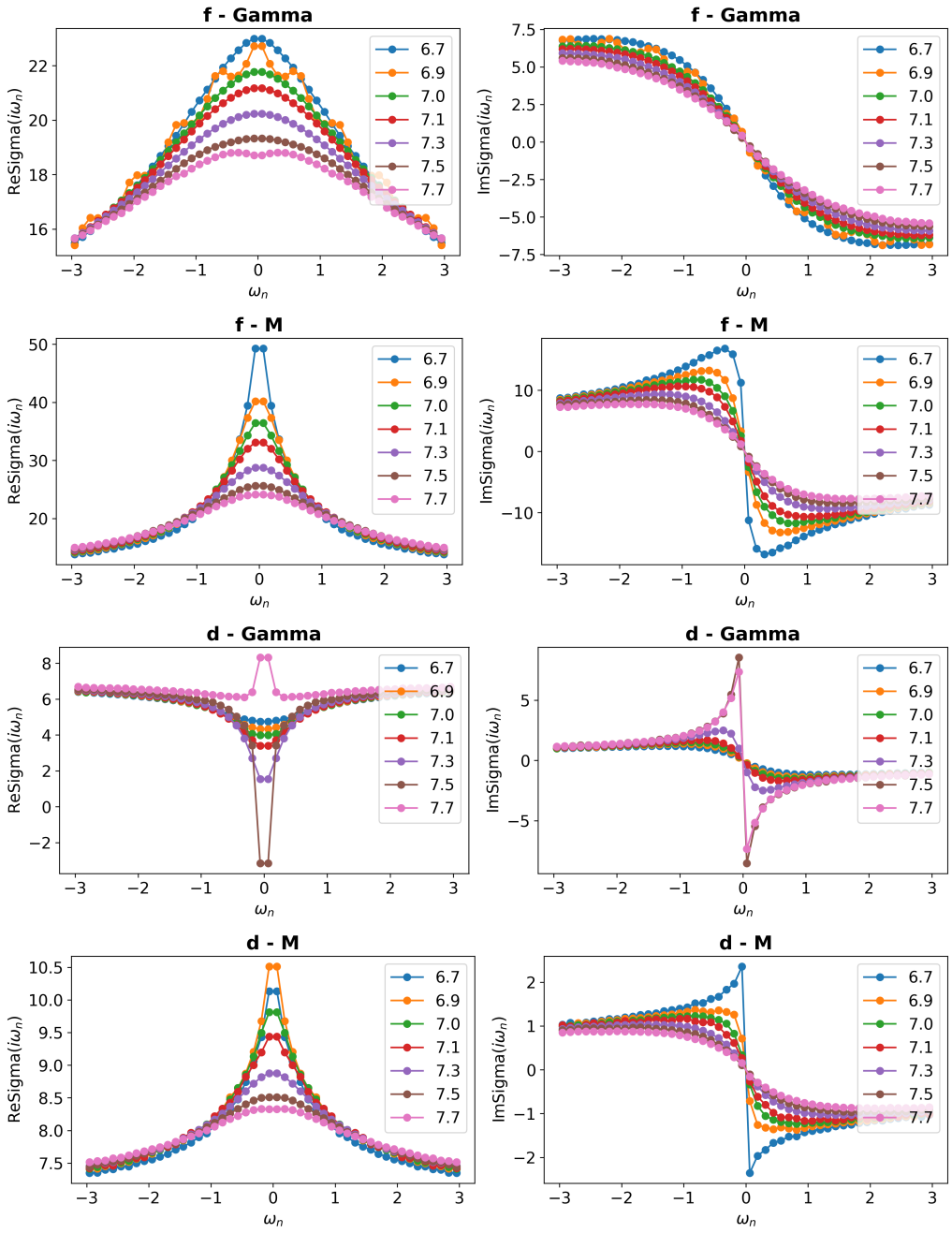

Figure 5.10: **Cluster self energies in Matsubara frequencies for U = 12 and different values of the chemical potential.** Inside the gap, the f- and d- self energy remain smooth, although divergences are encountered at the gap edges, sign that at these points a doped d-pseudo-gapped phase and an f-Mott insulating one could be present.

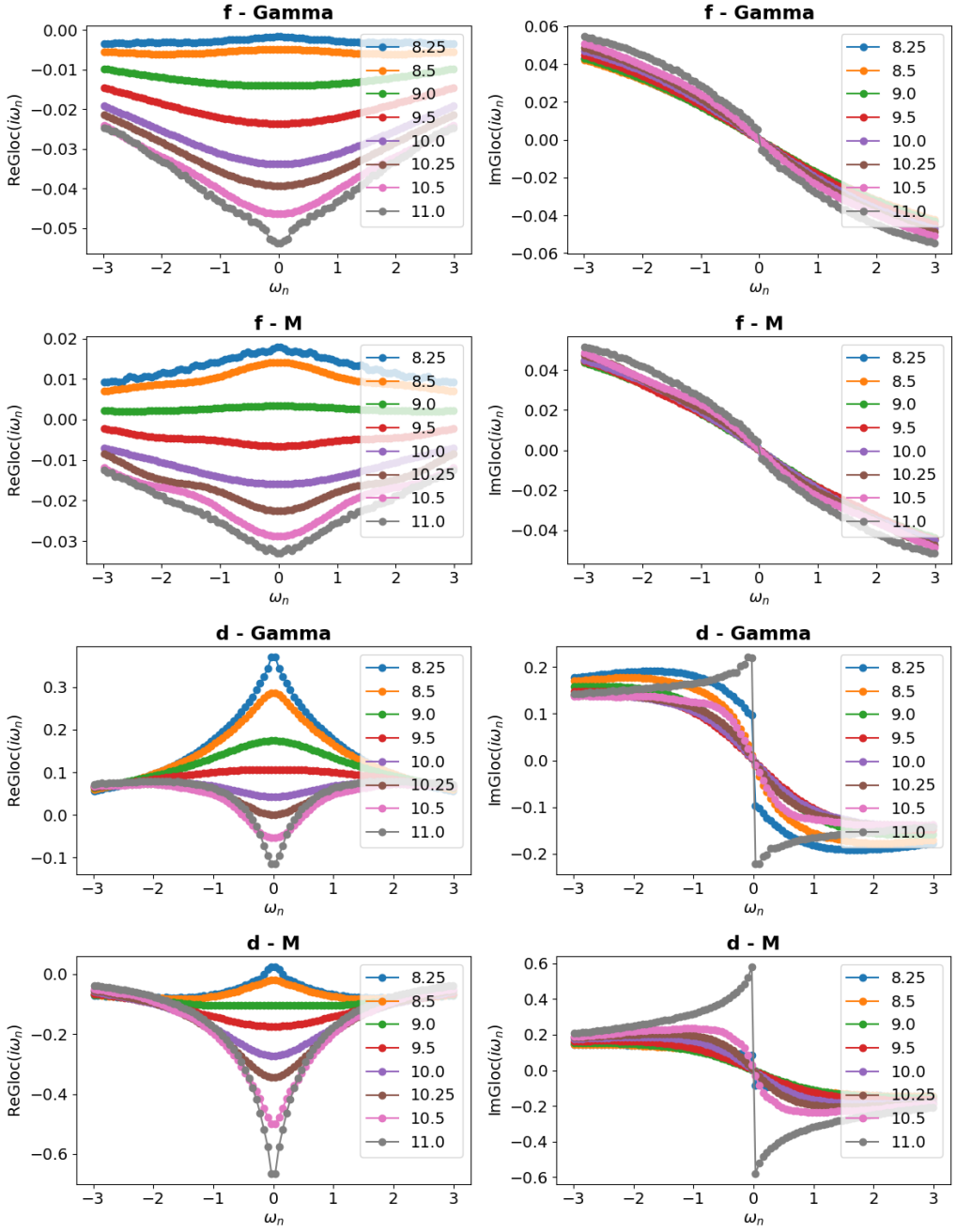

Figure 5.11: **Local Green's functions in Matsubara frequencies for U = 16 and different values of the chemical potential.** In particular, the gap for the d-orbitals is closed at $\mu = 8.25$ and $\mu = 11.0$, while the f-orbitals remain insulating due to the larger Mott gap. I note that a sign change of the real part of the Green's function implies that a zero has been encountered changing the chemical potential.

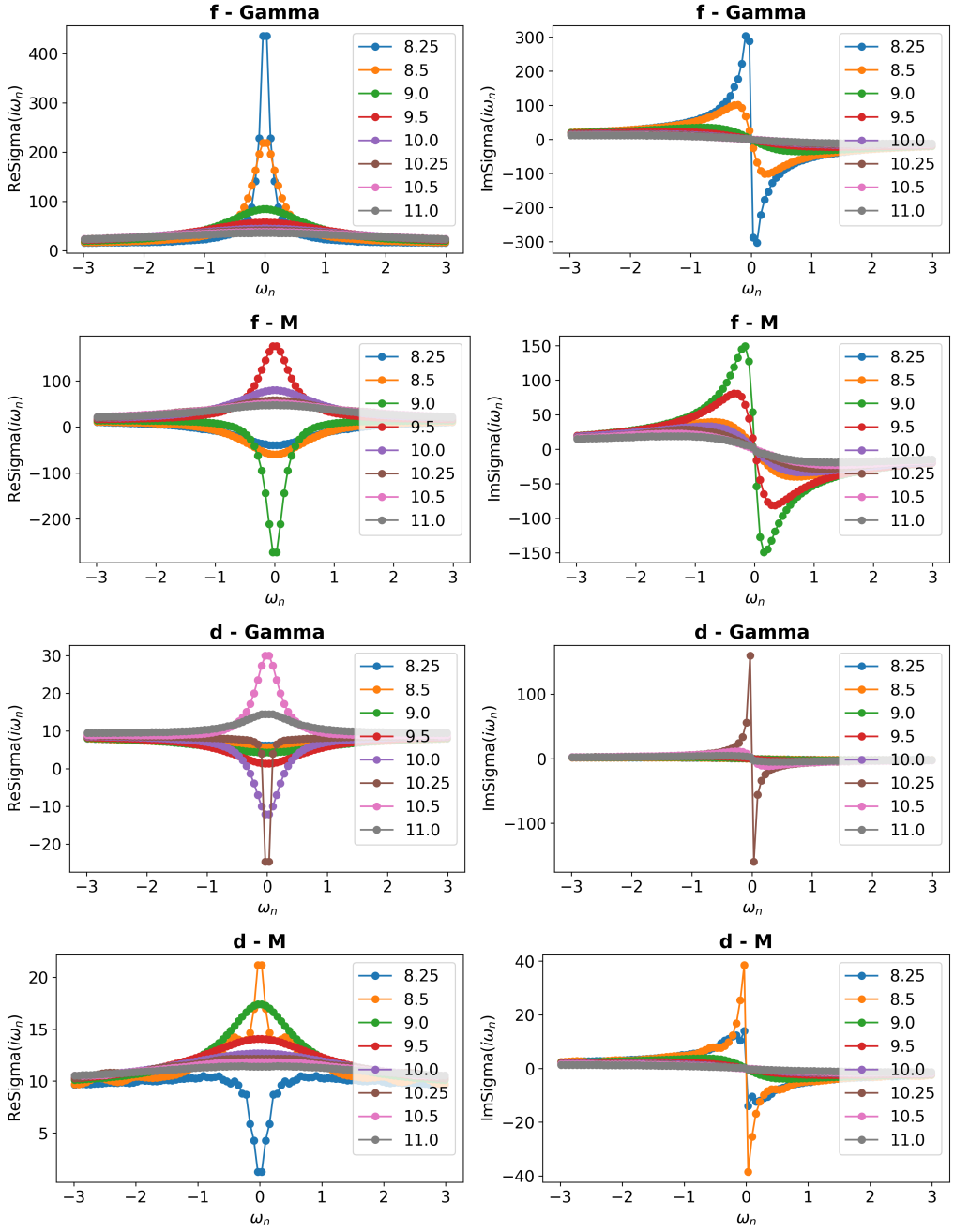

Figure 5.12: **Cluster self energies in Matsubara frequencies for U = 16 and different values of the chemical potential.** I note that in this case genuine poles of the self energy, represented by a sign change in the real part and a divergence in the imaginary one, are encountered of both d- and f-orbitals.

CHAPTER 6

CONCLUSIONS

Throughout this thesis I discussed a variety of theoretical and numerical results, all aiming to expand the current understanding of the interplay between topology and correlations.
In the first part I analysed the excitonic properties of a paradigmatic model for quantum spin Hall insulators. I found that moderate a Coulomb repulsion can stabilise both charge and spin excitons, the latter of which can have a non-trivial Chern number implying the presence of chiral surface spin excitons. By further increasing the interaction strength the bulk spin-exciton can undergo a bosonic condensation, leading to the spontaneous breaking of time reversal, inversion and spin-$SU(2)$ symmetry. The condensate becomes topologically trivial but now exhibits an exotic magneto-electric effect. Interestingly, due to the reduced coordination at the boundary, the condensate may emerge also only at the surface, leading to a topologically non-trivial bulk that however shows a breakdown of the chiral edge states topological protection.

In the second part I considered the effect of a rather special moiré phonon on the phase diagram of twisted bilayer graphene. Integrating the vibrational degrees of freedom to obtain an effective electron-electron attraction, I performed extensive Hartree-Fock calculations including the true Coulomb repulsion. For any integer filling of the flat bands, the inclusion of these phonons stabilises insulators characterised by a static Kekulé distortion of the lattice by breaking the $U_\nu(1)$ valley symmetry, in agreement with recent STM experimental results. In particular, for any integer filling other than charge neutrality, the insulators also exhibit non-trivial Chern numbers. To include dynamical effects, I then introduced a resonating valence bond wavefunction, which assumes that the system fluctuates between Kekulé distortions of different symmetry. In this case, the model predicts topological spin- and valley-liquid ground states for integer fillings, which naturally lead to $d + id$ superconductivity upon doping, in accordance with experimental evidences.

In the third part I extensively discussed the role of the Green's function zeros in topological Mott insulators. In particular, I showed that the different winding numbers for the interacting Green's function can be reduced to the corresponding non-interacting topological invariants calculated upon an effective single particle Hamiltonian, which deep in the Mott phase mimic exactly, apart from a minus sign, the dispersion of the ingap bands of zeros. This result suggests that in the case of a topological Mott insulator, the non-trivial topology of the ground state is entirely carried by

the Green's function zeros rather than by the Hubbard bands, suggesting that a bulk-boundary correspondence may emerge also for the zeros. Finally, I discussed the possible failure of these winding numbers to predict the actual topological response of the system, particularly in relation to the breakdown of the Luttinger theorem.

Finally, in the last part, I gave a new perspective on the strange Fermi liquid behaviour of topological Kondo insulators, motivated by the possible correspondence between Green's function zeros and the presence of ingap fractionalised quasiparticles. In particular I demonstrated, by means of cluster DMFT calculations, that considering only the f-correlations as in the prior literature is unable to resolve the ambivalent insulating-metallic nature of topological Kondo insulators. Introducing a realistic multi-orbital Hubbard Hamiltonian, which now takes into account also d-correlations, I discovered that for strong enough interaction the model may develop a Luttinger surface, which could serve as a plausible explanation of the Fermi liquid properties of topological Kondo insulators.

BIBLIOGRAPHY

[1] K. v. Klitzing, G. Dorda, and M. Pepper, "New method for high-accuracy determination of the fine-structure constant based on quantized hall resistance," *Phys. Rev. Lett.*, vol. 45, pp. 494–497, Aug 1980.

[2] D. J. Thouless, M. Kohmoto, M. P. Nightingale, and M. den Nijs, "Quantized hall conductance in a two-dimensional periodic potential," *Phys. Rev. Lett.*, vol. 49, pp. 405–408, Aug 1982.

[3] A. Abouzaid, J. Dai, S. Feiler, P. Kessler, and C. Waddell, "The integer quantum hall effect," 2018.

[4] X. Liu, K. Watanabe, T. Taniguchi, B. I. Halperin, and P. Kim, "Quantum hall drag of exciton condensate in graphene," *Nature Physics*, vol. 13, no. 8, pp. 746–750, 2017.

[5] Z. Wang, D. A. Rhodes, K. Watanabe, T. Taniguchi, J. C. Hone, J. Shan, and K. F. Mak, "Evidence of high-temperature exciton condensation in two-dimensional atomic double layers," *Nature*, vol. 574, pp. 76–80, Oct 2019.

[6] B. Sun, W. Zhao, T. Palomaki, Z. Fei, E. Runburg, P. Malinowski, X. Huang, J. Cenker, Y.-T. Cui, J.-H. Chu, X. Xu, S. S. Ataei, D. Varsano, M. Palummo, E. Molinari, M. Rontani, and D. H. Cobden, "Evidence for equilibrium exciton condensation in monolayer wte2," *Nature Physics*, vol. 18, pp. 94–99, Jan 2022.

[7] W. K. Park, L. Sun, A. Noddings, D.-J. Kim, Z. Fisk, and L. H. Greene, "Topological surface states interacting with bulk excitations in the kondo insulator smb6 revealed via planar tunneling spectroscopy," *Proceedings of the National Academy of Sciences*, vol. 113, no. 24, pp. 6599–6604, 2016.

[8] A. Arab, A. X. Gray, S. Nemšák, D. V. Evtushinsky, C. M. Schneider, D.-J. Kim, Z. Fisk, P. F. S. Rosa, T. Durakiewicz, and P. S. Riseborough, "Effects of spin excitons on the surface states of smb_6: A photoemission study," *Phys. Rev. B*, vol. 94, p. 235125, Dec 2016.

[9] B. A. Bernevig, T. L. Hughes, and S.-C. Zhang, "Quantum spin hall effect and topological phase transition in hgte quantum wells," *Science*, vol. 314, no. 5806, pp. 1757–1761, 2006.

[10] R. Bistritzer and A. H. MacDonald, "Moiré bands in twisted double-layer graphene," *Proceedings of the National Academy of Sciences*, vol. 108, no. 30, pp. 12233–12237, 2011.

[11] Y. Cao, V. Fatemi, A. Demir, S. Fang, S. L. Tomarken, J. Y. Luo, J. D. Sanchez-Yamagishi, K. Watanabe, T. Taniguchi, E. Kaxiras, R. C. Ashoori, and P. Jarillo-Herrero, "Correlated insulator behaviour at half-filling in magic-angle graphene superlattices," *Nature*, vol. 556, no. 7699, pp. 80–84, 2018.

[12] X. Lu, P. Stepanov, W. Yang, M. Xie, M. A. Aamir, I. Das, C. Urgell, K. Watanabe, T. Taniguchi, G. Zhang, A. Bachtold, A. H. MacDonald, and D. K. Efetov, "Superconductors, orbital magnets and correlated states in magic-angle bilayer graphene," *Nature*, vol. 574, no. 7780, pp. 653–657, 2019.

[13] M. Yankowitz, S. Chen, H. Polshyn, Y. Zhang, K. Watanabe, T. Taniguchi, D. Graf, A. F. Young, and C. R. Dean, "Tuning superconductivity in twisted bilayer graphene," *Science*, vol. 363, no. 6431, pp. 1059–1064, 2019.

[14] Y. Jiang, X. Lai, K. Watanabe, T. Taniguchi, K. Haule, J. Mao, and E. Y. Andrei, "Charge order and broken rotational symmetry in magic-angle twisted bilayer graphene," *Nature*, vol. 573, no. 7772, pp. 91–95, 2019.

[15] E. Codecido, Q. Wang, R. Koester, S. Che, H. Tian, R. Lv, S. Tran, K. Watanabe, T. Taniguchi, F. Zhang, M. Bockrath, and C. N. Lau, "Correlated insulating and superconducting states in twisted bilayer graphene below the magic angle," *Science Advances*, vol. 5, no. 9, 2019.

[16] A. L. Sharpe, E. J. Fox, A. W. Barnard, J. Finney, K. Watanabe, T. Taniguchi, M. A. Kastner, and D. Goldhaber-Gordon, "Emergent ferromagnetism near three-quarters filling in twisted bilayer graphene," *Science*, vol. 365, no. 6453, pp. 605–608, 2019.

[17] Y. Xie, B. Lian, B. Jäck, X. Liu, C.-L. Chiu, K. Watanabe, T. Taniguchi, B. A. Bernevig, and A. Yazdani, "Spectroscopic signatures of many-body correlations in magic-angle twisted bilayer graphene," *Nature*, vol. 572, no. 7767, pp. 101–105, 2019.

[18] A. Kerelsky, L. J. McGilly, D. M. Kennes, L. Xian, M. Yankowitz, S. Chen, K. Watanabe, T. Taniguchi, J. Hone, C. Dean, A. Rubio, and A. N. Pasupathy, "Maximized electron interactions at the magic angle in twisted bilayer graphene," *Nature*, vol. 572, no. 7767, pp. 95–100, 2019.

[19] Y. Saito, J. Ge, K. Watanabe, T. Taniguchi, and A. F. Young, "Independent superconductors and correlated insulators in twisted bilayer graphene," *Nature Physics*, vol. 16, no. 9, pp. 926–930, 2020.

[20] L. Balents, C. R. Dean, D. K. Efetov, and A. F. Young, "Superconductivity and strong correlations in moiréflat bands," *Nature Physics*, vol. 16, no. 7, pp. 725–733, 2020.

[21] M. Serlin, C. L. Tschirhart, H. Polshyn, Y. Zhang, J. Zhu, K. Watanabe, T. Taniguchi, L. Balents, and A. F. Young, "Intrinsic quantized anomalous hall effect in a moiré heterostructure," *Science*, vol. 367, no. 6480, pp. 900–903, 2020.

[22] K. P. Nuckolls, M. Oh, D. Wong, B. Lian, K. Watanabe, T. Taniguchi, B. A. Bernevig, and A. Yazdani, "Strongly correlated chern insulators in magic-angle twisted bilayer graphene," *Nature*, vol. 588, pp. 610–615, Dec 2020.

[23] A. Uri, S. Grover, Y. Cao, J. A. Crosse, K. Bagani, D. Rodan-Legrain, Y. Myasoedov, K. Watanabe, T. Taniguchi, P. Moon, M. Koshino, P. Jarillo-Herrero, and E. Zeldov, "Mapping the twist-angle disorder and landau levels in magic-angle graphene," *Nature*, vol. 581, no. 7806, pp. 47–52, 2020.

[24] J. Díez-Mérida, A. Díez-Carlón, S. Y. Yang, Y. M. Xie, X. J. Gao, J. Senior, K. Watanabe, T. Taniguchi, X. Lu, A. P. Higginbotham, K. T. Law, and D. K. Efetov, "Symmetry-broken josephson junctions and superconducting diodes in magic-angle twisted bilayer graphene," *Nature Communications*, vol. 14, no. 1, p. 2396, 2023.

[25] C.-C. Tseng, X. Ma, Z. Liu, K. Watanabe, T. Taniguchi, J.-H. Chu, and M. Yankowitz, "Anomalous hall effect at half filling in twisted bilayer graphene," *Nature Physics*, 2022.

[26] Y. Cao, V. Fatemi, S. Fang, K. Watanabe, T. Taniguchi, E. Kaxiras, and P. Jarillo-Herrero, "Unconventional superconductivity in magic-angle graphene superlattices," *Nature*, vol. 556, no. 7699, pp. 43–50, 2018.

[27] M. Angeli, E. Tosatti, and M. Fabrizio, "Valley jahn-teller effect in twisted bilayer graphene," *Phys. Rev. X*, vol. 9, p. 041010, Oct 2019.

[28] K. P. Nuckolls, R. L. Lee, M. Oh, D. Wong, T. Soejima, J. P. Hong, D. Călugăru, J. Herzog-Arbeitman, B. A. Bernevig, K. Watanabe, T. Taniguchi, N. Regnault, M. P. Zaletel, and A. Yazdani, "Quantum textures of the many-body wavefunctions in magic-angle graphene," *Nature*, vol. 620, pp. 525–532, Aug 2023.

[29] C.-C. Liu, L.-D. Zhang, W.-Q. Chen, and F. Yang, "Chiral spin density wave and $d + id$ superconductivity in the magic-angle-twisted bilayer graphene," *Phys. Rev. Lett.*, vol. 121, p. 217001, Nov 2018.

[30] X. Liu, Z. Wang, K. Watanabe, T. Taniguchi, O. Vafek, and J. I. A. Li, "Tuning electron correlation in magic-angle twisted bilayer graphene using coulomb screening," *Science*, vol. 371, no. 6535, pp. 1261–1265, 2021.

[31] M. Oh, K. P. Nuckolls, D. Wong, R. L. Lee, X. Liu, K. Watanabe, T. Taniguchi, and A. Yazdani, "Evidence for unconventional superconductivity in twisted bilayer graphene," *Nature*, Oct 2021.

[32] G. Volovik, "A new class of normal Fermi liquids," *Pis'ma Zh. Eksp. Teor. Fiz.*, vol. 53, p. 208, 1991. [JETP Lett. **53**, 222 (1991)].

[33] M. Fabrizio, "Emergent quasiparticles at luttinger surfaces," *Nature Communications*, vol. 13, no. 1, p. 1561, 2022.

[34] M. Fabrizio, "Spin-liquid insulators can be landau's fermi liquids," *Phys. Rev. Lett.*, vol. 130, p. 156702, Apr 2023.

[35] J. Skolimowski and M. Fabrizio, "Luttinger's theorem in the presence of luttinger surfaces," *Phys. Rev. B*, vol. 106, p. 045109, Jul 2022.

[36] V. Gurarie, "Single-particle green's functions and interacting topological insulators," *Phys. Rev. B*, vol. 83, p. 085426, Feb 2011.

[37] A. M. Essin and V. Gurarie, "Bulk-boundary correspondence of topological insulators from their respective green's functions," *Phys. Rev. B*, vol. 84, p. 125132, Sep 2011.

[38] N. Wagner, L. Crippa, A. Amaricci, P. Hansmann, M. Klett, E. König, T. Schäfer, D. Di Sante, J. Cano, A. Millis, A. Georges, and G. Sangiovanni, "Mott insulators with boundary zeros," *arXiv e-prints*, p. arXiv:2301.05588, Jan. 2023.

[39] K. Ishikawa and T. Matsuyama, "Magnetic field induced multi-component qed3 and quantum hall effect," *Zeitschrift für Physik C Particles and Fields*, vol. 33, no. 1, pp. 41–45, 1986.

[40] K. Ishikawa and T. Matsuyama, "A microscopic theory of the quantum hall effect," *Nuclear Physics B*, vol. 280, pp. 523–548, 1987.

[41] Z. Wang, X.-L. Qi, and S.-C. Zhang, "Topological order parameters for interacting topological insulators," *Phys. Rev. Lett.*, vol. 105, p. 256803, Dec 2010.

[42] Z. Wang and S.-C. Zhang, "Simplified topological invariants for interacting insulators," *Phys. Rev. X*, vol. 2, p. 031008, Aug 2012.

[43] R. Nourafkan and G. Kotliar, "Electric polarization in correlated insulators," *Phys. Rev. B*, vol. 88, p. 155121, Oct 2013.

[44] T. Nanba, H. Ohta, M. Motokawa, S. Kimura, S. Kunii, and T. Kasuya, "Gap state of smb6," *Physica B: Condensed Matter*, vol. 186-188, pp. 440–443, 1993.

[45] H. Miyazaki, T. Hajiri, T. Ito, S. Kunii, and S.-i. Kimura, "Momentum-dependent hybridization gap and dispersive in-gap state of the kondo semiconductor smb_6," *Phys. Rev. B*, vol. 86, p. 075105, Aug 2012.

[46] D. J. Kim, S. Thomas, T. Grant, J. Botimer, Z. Fisk, and J. Xia, "Surface hall effect and nonlocal transport in smb6: Evidence for surface conduction," *Scientific Reports*, vol. 3, p. 3150, Nov 2013.

[47] E. Frantzeskakis, N. de Jong, B. Zwartsenberg, Y. K. Huang, Y. Pan, X. Zhang, J. X. Zhang, F. X. Zhang, L. H. Bao, O. Tegus, A. Varykhalov, A. de Visser, and M. S. Golden, "Kondo hybridization and the origin of metallic states at the (001) surface of smb_6," *Phys. Rev. X*, vol. 3, p. 041024, Dec 2013.

[48] Y. Nakajima, P. Syers, X. Wang, R. Wang, and J. Paglione, "One-dimensional edge state transport in a topological kondo insulator," *Nature Physics*, vol. 12, pp. 213–217, Mar 2016.

[49] K. Hagiwara, Y. Ohtsubo, M. Matsunami, S.-i. Ideta, K. Tanaka, H. Miyazaki, J. E. Rault, P. L. Fèvre, F. Bertran, A. Taleb-Ibrahimi, R. Yukawa, M. Kobayashi, K. Horiba, H. Kumigashira, K. Sumida, T. Okuda, F. Iga, and S.-i. Kimura, "Surface kondo effect and non-trivial metallic state of the kondo insulator ybb12," *Nature Communications*, vol. 7, p. 12690, Aug 2016.

[50] Y. Sato, Z. Xiang, Y. Kasahara, S. Kasahara, L. Chen, C. Tinsman, F. Iga, J. Singleton, N. L. Nair, N. Maksimovic, J. G. Analytis, L. Li, and Y. Matsuda, "Topological surface conduction in kondo insulator ybb12," *Journal of Physics D: Applied Physics*, vol. 54, p. 404002, jul 2021.

[51] A. Gupta, A. Weiser, L. Pressley, Y. Luo, C. Lygouras, J. Trowbridge, W. A. Phelan, C. L. Broholm, T. M. McQueen, and W. K. Park, "Topological surface states in the kondo insulator Ybb_{12} revealed via planar tunneling spectroscopy," *Phys. Rev. B*, vol. 107, p. 165132, Apr 2023.

[52] M. Dzero, K. Sun, V. Galitski, and P. Coleman, "Topological kondo insulators," *Phys. Rev. Lett.*, vol. 104, p. 106408, Mar 2010.

[53] M. Orendáč, S. Gabáni, G. Pristáš, E. Gažo, P. Diko, P. Farkašovský, A. Levchenko, N. Shitsevalova, and K. Flachbart, "Isosbestic points in doped Smb_6 as features of universality and property tuning," *Phys. Rev. B*, vol. 96, p. 115101, Sep 2017.

[54] W. A. Phelan, S. M. Koohpayeh, P. Cottingham, J. W. Freeland, J. C. Leiner, C. L. Broholm, and T. M. McQueen, "Correlation between bulk thermodynamic measurements and the low-temperature-resistance plateau in smb_6," *Phys. Rev. X*, vol. 4, p. 031012, Jul 2014.

[55] K. Flachbart, S. Gabáni, K. Neumaier, Y. Paderno, V. Pavlík, E. Schuberth, and N. Shitsevalova, "Specific heat of smb6 at very low temperatures," *Physica B: Condensed Matter*, vol. 378-380, pp. 610–611, 2006. Proceedings of the International Conference on Strongly Correlated Electron Systems.

[56] Y. Xu, S. Cui, J. K. Dong, D. Zhao, T. Wu, X. H. Chen, K. Sun, H. Yao, and S. Y. Li, "Bulk fermi surface of charge-neutral excitations in smb_6 or not: A heat-transport study," *Phys. Rev. Lett.*, vol. 116, p. 246403, Jun 2016.

[57] B. S. Tan, Y.-T. Hsu, B. Zeng, M. C. Hatnean, N. Harrison, Z. Zhu, M. Hartstein, M. Kiourlappou, A. Srivastava, M. D. Johannes, T. P. Murphy, J.-H. Park, L. Balicas, G. G. Lonzarich, G. Balakrishnan, and S. E. Sebastian, "Unconventional fermi surface in an insulating state," *Science*, vol. 349, no. 6245, pp. 287–290, 2015.

[58] M. Hartstein, W. H. Toews, Y.-T. Hsu, B. Zeng, X. Chen, M. C. Hatnean, Q. R. Zhang, S. Nakamura, A. S. Padgett, G. Rodway-Gant, J. Berk, M. K. Kingston, G. H. Zhang, M. K. Chan, S. Yamashita, T. Sakakibara, Y. Takano, J.-H. Park, L. Balicas, N. Harrison, N. Shitsevalova, G. Balakrishnan, G. G. Lonzarich, R. W. Hill, M. Sutherland, and S. E. Sebastian, "Fermi surface in the absence of a fermi liquid in the kondo insulator smb6," *Nature Physics*, vol. 14, pp. 166–172, Feb 2018.

[59] M. Hartstein, H. Liu, Y.-T. Hsu, B. S. Tan, M. Ciomaga Hatnean, G. Balakrishnan, and S. E. Sebastian, "Intrinsic bulk quantum oscillations in a bulk unconventional insulator smb6," *iScience*, vol. 23, no. 11, p. 101632, 2020.

[60] P. G. LaBarre, A. Rydh, J. Palmer-Fortune, J. A. Frothingham, S. T. Hannahs, A. P. Ramirez, and N. A. Fortune, "Magnetoquantum oscillations in the specific heat of a topological kondo insulator," *Journal of Physics: Condensed Matter*, vol. 34, p. 36LT01, jul 2022.

[61] Z. Xiang, Y. Kasahara, T. Asaba, B. Lawson, C. Tinsman, L. Chen, K. Sugimoto, S. Kawaguchi, Y. Sato, G. Li, S. Yao, Y. L. Chen, F. Iga, J. Singleton, Y. Matsuda, and L. Li, "Quantum oscillations of electrical resistivity in an insulator," *Science*, vol. 362, no. 6410, pp. 65–69, 2018.

[62] Z. Xiang, K.-W. Chen, L. Chen, T. Asaba, Y. Sato, N. Zhang, D. Zhang, Y. Kasahara, F. Iga, W. A. Coniglio, Y. Matsuda, J. Singleton, and L. Li, "Hall anomaly, quantum oscillations and possible lifshitz transitions in kondo insulator ybb_{12}: Evidence for unconventional charge transport," *Phys. Rev. X*, vol. 12, p. 021050, Jun 2022.

[63] H. Liu, M. Hartstein, G. J. Wallace, A. J. Davies, M. C. Hatnean, M. D. Johannes, N. Shitsevalova, G. Balakrishnan, and S. E. Sebastian, "Fermi surfaces in kondo insulators," *Journal of Physics: Condensed Matter*, vol. 30, p. 16LT01, mar 2018.

[64] Z. Xiang, L. Chen, K.-W. Chen, C. Tinsman, Y. Sato, T. Asaba, H. Lu, Y. Kasahara, M. Jaime, F. Balakirev, F. Iga, Y. Matsuda, J. Singleton, and L. Li, "Unusual high-field metal in a kondo insulator," *Nature Physics*, vol. 17, pp. 788–793, Jul 2021.

[65] D. Chowdhury, I. Sodemann, and T. Senthil, "Mixed-valence insulators with neutral fermi surfaces," *Nature Communications*, vol. 9, p. 1766, May 2018.

[66] I. Sodemann, D. Chowdhury, and T. Senthil, "Quantum oscillations in insulators with neutral fermi surfaces," *Phys. Rev. B*, vol. 97, p. 045152, Jan 2018.

[67] O. I. Motrunich, "Orbital magnetic field effects in spin liquid with spinon fermi sea: Possible application to $\kappa-(ET)_2cu_2(CN)_3$," *Phys. Rev. B*, vol. 73, p. 155115, Apr 2006.

[68] J. Knolle and N. R. Cooper, "Excitons in topological kondo insulators: Theory of thermodynamic and transport anomalies in smb_6," *Phys. Rev. Lett.*, vol. 118, p. 096604, Mar 2017.

[69] J. Knolle and N. R. Cooper, "Quantum oscillations without a fermi surface and the anomalous de haas–van alphen effect," *Phys. Rev. Lett.*, vol. 115, p. 146401, Sep 2015.

[70] L. Zhang, X.-Y. Song, and F. Wang, "Quantum oscillation in narrow-gap topological insulators," *Phys. Rev. Lett.*, vol. 116, p. 046404, Jan 2016.

[71] A. Panda, S. Banerjee, and M. Randeria, "Quantum oscillations in the magnetization and density of states of insulators," *Proceedings of the National Academy of Sciences*, vol. 119, no. 42, p. e2208373119, 2022.

[72] Y.-W. Lu, P.-H. Chou, C.-H. Chung, T.-K. Lee, and C.-Y. Mou, "Enhanced quantum oscillations in kondo insulators," *Phys. Rev. B*, vol. 101, p. 115102, Mar 2020.

[73] O. Erten, P. Ghaemi, and P. Coleman, "Kondo breakdown and quantum oscillations in smb_6," *Phys. Rev. Lett.*, vol. 116, p. 046403, Jan 2016.

[74] M. Fabrizio, "Landau-fermi liquids without quasiparticles," *Phys. Rev. B*, vol. 102, p. 155122, Oct 2020.

[75] M. Fabrizio, "Emergent quasiparticles at luttinger surfaces," *Nature Communications*, vol. 13, p. 1561, Mar 2022.

[76] M. Fabrizio, "Spin-liquid insulators can be landau's fermi liquids," *Phys. Rev. Lett.*, vol. 130, p. 156702, Apr 2023.

[77] B. Seradjeh, J. E. Moore, and M. Franz, "Exciton condensation and charge fractionalization in a topological insulator film," *Phys. Rev. Lett.*, vol. 103, p. 066402, Aug 2009.

[78] D. I. Pikulin and T. Hyart, "Interplay of exciton condensation and the quantum spin hall effect in InAs/GaSb bilayers," *Phys. Rev. Lett.*, vol. 112, p. 176403, Apr 2014.

[79] J. C. Budich, B. Trauzettel, and P. Michetti, "Time reversal symmetric topological exciton condensate in bilayer hgte quantum wells," *Phys. Rev. Lett.*, vol. 112, p. 146405, Apr 2014.

[80] W. T. Fuhrman, J. Leiner, P. Nikolić, G. E. Granroth, M. B. Stone, M. D. Lumsden, L. DeBeer-Schmitt, P. A. Alekseev, J.-M. Mignot, S. M. Koohpayeh, P. Cottingham, W. A. Phelan, L. Schoop, T. M. McQueen, and C. Broholm, "Interaction driven subgap spin exciton in the kondo insulator smb_6," *Phys. Rev. Lett.*, vol. 114, p. 036401, Jan 2015.

[81] J. Knolle and N. R. Cooper, "Excitons in topological kondo insulators: Theory of thermodynamic and transport anomalies in smb_6," *Phys. Rev. Lett.*, vol. 118, p. 096604, Mar 2017.

[82] L. Du, X. Li, W. Lou, G. Sullivan, K. Chang, J. Kono, and R.-R. Du, "Evidence for a topological excitonic insulator in inas/gasb bilayers," *Nature Communications*, vol. 8, no. 1, p. 1971, 2017.

[83] S. Kung, A. Goyal, D. Maslov, X. Wang, A. Lee, A. Kemper, S.-W. Cheong, and G. Blumberg, "Observation of chiral surface excitons in a topological insulator bi 2 se 3," *Proceedings of the National Academy of Sciences*, vol. 116, p. 201813514, 02 2019.

[84] D. Varsano, M. Palummo, E. Molinari, and M. Rontani, "A monolayer transition-metal dichalcogenide as a topological excitonic insulator," *Nature Nanotechnology*, vol. 15, no. 5, pp. 367–372, 2020.

[85] X. Qian, J. Liu, L. Fu, and J. Li, "Quantum spin hall effect in two-dimensional transition metal dichalcogenides," *Science*, vol. 346, no. 6215, pp. 1344–1347, 2014.

[86] S. Tang, C. Zhang, D. Wong, Z. Pedramrazi, H.-Z. Tsai, C. Jia, B. Moritz, M. Claassen, H. Ryu, S. Kahn, J. Jiang, H. Yan, M. Hashimoto, D. Lu, R. G. Moore, C.-C. Hwang, C. Hwang, Z. Hussain, Y. Chen, M. M. Ugeda, Z. Liu, X. Xie, T. P. Devereaux, M. F. Crommie, S.-K. Mo, and Z.-X. Shen, "Quantum spin hall state in monolayer 1t'-wte2," *Nature Physics*, vol. 13, no. 7, pp. 683–687, 2017.

[87] L. Peng, Y. Yuan, G. Li, X. Yang, J.-J. Xian, C.-J. Yi, Y.-G. Shi, and Y.-S. Fu, "Observation of topological states residing at step edges of wte2," *Nature Communications*, vol. 8, no. 1, p. 659, 2017.

[88] D. K. Efimkin, Y. E. Lozovik, and A. A. Sokolik, "Electron-hole pairing in a topological insulator thin film," *Phys. Rev. B*, vol. 86, p. 115436, Sep 2012.

[89] D. J. J. Marchand and M. Franz, "Lattice model for the surface states of a topological insulator with applications to magnetic and exciton instabilities," *Phys. Rev. B*, vol. 86, p. 155146, Oct 2012.

[90] M. P. Mink, H. T. C. Stoof, R. A. Duine, M. Polini, and G. Vignale, "Probing the topological exciton condensate via coulomb drag," *Phys. Rev. Lett.*, vol. 108, p. 186402, May 2012.

[91] Y. E. Lozovik and A. A. Sokolik, "Electron-hole pair condensation in a graphene bilayer," *JETP Letters*, vol. 87, no. 1, pp. 55–59, 2008.

[92] H. Min, R. Bistritzer, J.-J. Su, and A. H. MacDonald, "Room-temperature superfluidity in graphene bilayers," *Phys. Rev. B*, vol. 78, p. 121401(R), Sep 2008.

[93] N. J. Laurita, C. M. Morris, S. M. Koohpayeh, P. F. S. Rosa, W. A. Phelan, Z. Fisk, T. M. McQueen, and N. P. Armitage, "Anomalous three-dimensional bulk ac conduction within the kondo gap of smb_6 single crystals," *Phys. Rev. B*, vol. 94, p. 165154, Oct 2016.

[94] J. Stankiewicz, M. Evangelisti, P. F. S. Rosa, P. Schlottmann, and Z. Fisk, "Physical properties of sm_xb_6 single crystals," *Phys. Rev. B*, vol. 99, p. 045138, Jan 2019.

[95] M. Hartstein, W. H. Toews, Y. T. Hsu, B. Zeng, X. Chen, M. C. Hatnean, Q. R. Zhang, S. Nakamura, A. S. Padgett, G. Rodway-Gant, J. Berk, M. K. Kingston, G. H. Zhang, M. K. Chan, S. Yamashita, T. Sakakibara, Y. Takano, J. H. Park, L. Balicas, N. Harrison, N. Shitsevalova, G. Balakrishnan, G. G. Lonzarich, R. W. Hill, M. Sutherland, and S. E. Sebastian, "Fermi surface in the absence of a fermi liquid in the kondo insulator smb6," *Nature Physics*, vol. 14, no. 2, pp. 166–172, 2018.

[96] G. A. Kapilevich, P. S. Riseborough, A. X. Gray, M. Gulacsi, T. Durakiewicz, and J. L. Smith, "Incomplete protection of the surface weyl cones of the kondo insulator smb_6: Spin exciton scattering," *Phys. Rev. B*, vol. 92, p. 085133, Aug 2015.

[97] K. Akintola, A. Pal, S. R. Dunsiger, A. C. Y. Fang, M. Potma, S. R. Saha, X. Wang, J. Paglione, and J. E. Sonier, "Freezing out of a low-energy bulk spin exciton in smb6," *npj Quantum Materials*, vol. 3, 12 2018.

[98] I. Garate and M. Franz, "Excitons and optical absorption on the surface of a strong topological insulator with a magnetic energy gap," *Phys. Rev. B*, vol. 84, p. 045403, Jul 2011.

[99] K. Chen and R. Shindou, "Chiral topological excitons in a chern band insulator," *Phys. Rev. B*, vol. 96, p. 161101(R), Oct 2017.

[100] A. A. Allocca, D. K. Efimkin, and V. M. Galitski, "Fingerprints of berry phases in the bulk exciton spectrum of a topological insulator," *Phys. Rev. B*, vol. 98, p. 045430, Jul 2018.

[101] M. Altmeyer, D. Guterding, P. J. Hirschfeld, T. A. Maier, R. Valentí, and D. J. Scalapino, "Role of vertex corrections in the matrix formulation of the random phase approximation for the multiorbital hubbard model," *Phys. Rev. B*, vol. 94, p. 214515, Dec 2016.

[102] T. L. Hughes, E. Prodan, and B. A. Bernevig, "Inversion-symmetric topological insulators," *Phys. Rev. B*, vol. 83, p. 245132, Jun 2011.

[103] M. Ezawa, Y. Tanaka, and N. Nagaosa, "Topological phase transition without gap closing," *Scientific Reports*, vol. 3, no. 1, p. 2790, 2013.

[104] F. Xue and A. H. MacDonald, "Time-reversal symmetry-breaking nematic insulators near quantum spin hall phase transitions," *Phys. Rev. Lett.*, vol. 120, p. 186802, May 2018.

[105] A. Shitade, H. Katsura, J. Kuneš, X.-L. Qi, S.-C. Zhang, and N. Nagaosa, "Quantum spin hall effect in a transition metal oxide na_2iro_3," *Phys. Rev. Lett.*, vol. 102, p. 256403, Jun 2009.

[106] A. Medhi, V. B. Shenoy, and H. R. Krishnamurthy, "Synchronous and asynchronous mott transitions in topological insulator ribbons," *Phys. Rev. B*, vol. 85, p. 235449, Jun 2012.

[107] A. Amaricci, L. Privitera, F. Petocchi, M. Capone, G. Sangiovanni, and B. Trauzettel, "Edge state reconstruction from strong correlations in quantum spin hall insulators," *Phys. Rev. B*, vol. 95, p. 205120, May 2017.

[108] D. G. Rothe, R. W. Reinthaler, C.-X. Liu, L. W. Molenkamp, S.-C. Zhang, and E. M. Hankiewicz, "Fingerprint of different spin–orbit terms for spin transport in HgTe quantum wells," *New Journal of Physics*, vol. 12, p. 065012, jun 2010.

[109] C. L. Kane and E. J. Mele, "Quantum spin hall effect in graphene," *Phys. Rev. Lett.*, vol. 95, p. 226801, Nov 2005.

[110] R. S. K. Mong and V. Shivamoggi, "Edge states and the bulk-boundary correspondence in dirac hamiltonians," *Phys. Rev. B*, vol. 83, p. 125109, Mar 2011.

[111] A. Amaricci, A. Valli, G. Sangiovanni, B. Trauzettel, and M. Capone, "Coexistence of metallic edge states and antiferromagnetic ordering in correlated topological insulators," *Phys. Rev. B*, vol. 98, p. 045133, Jul 2018.

[112] G. Borghi, M. Fabrizio, and E. Tosatti, "Surface dead layer for quasiparticles near a mott transition," *Phys. Rev. Lett.*, vol. 102, p. 066806, Feb 2009.

[113] J. P. Rivera, "A short review of the magnetoelectric effect and relatedexperimental techniques on single phase (multi-) ferroics," *The European Physical Journal B*, vol. 71, no. 3, p. 299, 2009.

[114] A. Amaricci, J. C. Budich, M. Capone, B. Trauzettel, and G. Sangiovanni, "First-order character and observable signatures of topological quantum phase transitions," *Phys. Rev. Lett.*, vol. 114, p. 185701, May 2015.

[115] A. Amaricci, J. C. Budich, M. Capone, B. Trauzettel, and G. Sangiovanni, "Strong correlation effects on topological quantum phase transitions in three dimensions," *Phys. Rev. B*, vol. 93, p. 235112, Jun 2016.

[116] N. N. T. Nam and M. Koshino, "Lattice relaxation and energy band modulation in twisted bilayer graphene," *Phys. Rev. B*, vol. 96, p. 075311, Aug 2017.

[117] M. Angeli, D. Mandelli, A. Valli, A. Amaricci, M. Capone, E. Tosatti, and M. Fabrizio, "Emergent D_6 symmetry in fully relaxed magic-angle twisted bilayer graphene," *Phys. Rev. B*, vol. 98, p. 235137, Dec 2018.

[118] P. Lucignano, D. Alfè, V. Cataudella, D. Ninno, and G. Cantele, "Crucial role of atomic corrugation on the flat bands and energy gaps of twisted bilayer graphene at the magic angle $\theta \sim 1.08^\circ$," *Phys. Rev. B*, vol. 99, p. 195419, May 2019.

[119] F. Guinea and N. R. Walet, "Continuum models for twisted bilayer graphene: Effect of lattice deformation and hopping parameters," *Phys. Rev. B*, vol. 99, p. 205134, May 2019.

[120] S. Carr, S. Fang, Z. Zhu, and E. Kaxiras, "Exact continuum model for low-energy electronic states of twisted bilayer graphene," *Phys. Rev. Research*, vol. 1, p. 013001, Aug 2019.

[121] G. Cantele, D. Alfè, F. Conte, V. Cataudella, D. Ninno, and P. Lucignano, "Structural relaxation and low-energy properties of twisted bilayer graphene," *Phys. Rev. Research*, vol. 2, p. 043127, Oct 2020.

[122] F. Wu, E. Hwang, and S. Das Sarma, "Phonon-induced giant linear-in-t resistivity in magic angle twisted bilayer graphene: Ordinary strangeness and exotic superconductivity," *Phys. Rev. B*, vol. 99, p. 165112, Apr 2019.

[123] I. Yudhistira, N. Chakraborty, G. Sharma, D. Y. H. Ho, E. Laksono, O. P. Sushkov, G. Vignale, and S. Adam, "Gauge-phonon dominated resistivity in twisted bilayer graphene near magic angle," *Phys. Rev. B*, vol. 99, p. 140302, Apr 2019.

[124] H. Polshyn, M. Yankowitz, S. Chen, Y. Zhang, K. Watanabe, T. Taniguchi, C. R. Dean, and A. F. Young, "Large linear-in-temperature resistivity in twisted bilayer graphene," *Nature Physics*, vol. 15, no. 10, pp. 1011–1016, 2019.

[125] B. Lian, Z. Wang, and B. A. Bernevig, "Twisted bilayer graphene: A phonon-driven superconductor," *Phys. Rev. Lett.*, vol. 122, p. 257002, Jun 2019.

[126] S. Das Sarma and F. Wu, "Electron–phonon and electron–electron interaction effects in twisted bilayer graphene," *Annals of Physics*, vol. 417, p. 168193, 2020. Eliashberg theory at 60: Strong-coupling superconductivity and beyond.

[127] C. Lewandowski, D. Chowdhury, and J. Ruhman, "Pairing in magic-angle twisted bilayer graphene: Role of phonon and plasmon umklapp," *Phys. Rev. B*, vol. 103, p. 235401, Jun 2021.

[128] T. Cea and F. Guinea, "Coulomb interaction, phonons, and superconductivity in twisted bilayer graphene," *Proceedings of the National Academy of Sciences*, vol. 118, no. 32, p. e2107874118, 2021.

[129] F. Wu, A. H. MacDonald, and I. Martin, "Theory of phonon-mediated superconductivity in twisted bilayer graphene," *Phys. Rev. Lett.*, vol. 121, p. 257001, Dec 2018.

[130] H. C. Po, L. Zou, A. Vishwanath, and T. Senthil, "Origin of mott insulating behavior and superconductivity in twisted bilayer graphene," *Phys. Rev. X*, vol. 8, p. 031089, Sep 2018.

[131] J. Kang and O. Vafek, "Strong coupling phases of partially filled twisted bilayer graphene narrow bands," *Phys. Rev. Lett.*, vol. 122, p. 246401, Jun 2019.

[132] M. Xie and A. H. MacDonald, "Nature of the correlated insulator states in twisted bilayer graphene," *Phys. Rev. Lett.*, vol. 124, p. 097601, Mar 2020.

[133] N. Bultinck, E. Khalaf, S. Liu, S. Chatterjee, A. Vishwanath, and M. P. Zaletel, "Ground state and hidden symmetry of magic-angle graphene at even integer filling," *Phys. Rev. X*, vol. 10, p. 031034, Aug 2020.

[134] Y. Zhang, K. Jiang, Z. Wang, and F. Zhang, "Correlated insulating phases of twisted bilayer graphene at commensurate filling fractions: A hartree-fock study," *Phys. Rev. B*, vol. 102, p. 035136, Jul 2020.

[135] J. Liu and X. Dai, "Theories for the correlated insulating states and quantum anomalous hall effect phenomena in twisted bilayer graphene," *Phys. Rev. B*, vol. 103, p. 035427, Jan 2021.

[136] B. A. Bernevig, Z.-D. Song, N. Regnault, and B. Lian, "Twisted bilayer graphene. iii. interacting hamiltonian and exact symmetries," *Phys. Rev. B*, vol. 103, p. 205413, May 2021.

[137] B. Lian, Z.-D. Song, N. Regnault, D. K. Efetov, A. Yazdani, and B. A. Bernevig, "Twisted bilayer graphene. iv. exact insulator ground states and phase diagram," *Phys. Rev. B*, vol. 103, p. 205414, May 2021.

[138] Y. D. Liao, J. Kang, C. N. Breiø, X. Y. Xu, H.-Q. Wu, B. M. Andersen, R. M. Fernandes, and Z. Y. Meng, "Correlation-induced insulating topological phases at charge neutrality in twisted bilayer graphene," *Phys. Rev. X*, vol. 11, p. 011014, Jan 2021.

[139] K. Seo, V. N. Kotov, and B. Uchoa, "Ferromagnetic mott state in twisted graphene bilayers at the magic angle," *Phys. Rev. Lett.*, vol. 122, p. 246402, Jun 2019.

[140] Y.-Z. You and A. Vishwanath, "Superconductivity from valley fluctuations and approximate so(4) symmetry in a weak coupling theory of twisted bilayer graphene," *npj Quantum Materials*, vol. 4, no. 1, p. 16, 2019.

[141] B. A. Bernevig, B. Lian, A. Cowsik, F. Xie, N. Regnault, and Z.-D. Song, "Twisted bilayer graphene. v. exact analytic many-body excitations in coulomb hamiltonians: Charge gap, goldstone modes, and absence of cooper pairing," *Phys. Rev. B*, vol. 103, p. 205415, May 2021.

[142] E. Khalaf, S. Chatterjee, N. Bultinck, M. P. Zaletel, and A. Vishwanath, "Charged skyrmions and topological origin of superconductivity in magic-angle graphene," *Science Advances*, vol. 7, no. 19, p. eabf5299, 2021.

[143] X. Y. Xu, K. T. Law, and P. A. Lee, "Kekulé valence bond order in an extended hubbard model on the honeycomb lattice with possible applications to twisted bilayer graphene," *Phys. Rev. B*, vol. 98, p. 121406(R), Sep 2018.

[144] A. C. Gadelha, D. A. A. Ohlberg, C. Rabelo, E. G. S. Neto, T. L. Vasconcelos, J. L. Campos, J. S. Lemos, V. Ornelas, D. Miranda, R. Nadas, F. C. Santana, K. Watanabe, T. Taniguchi, B. van Troeye, M. Lamparski, V. Meunier, V.-H. Nguyen, D. Paszko, J.-C. Charlier, L. C. Campos, L. G. Cançado, G. Medeiros-Ribeiro, and A. Jorio, "Localization of lattice dynamics in low-angle twisted bilayer graphene," *Nature*, vol. 590, no. 7846, pp. 405–409, 2021.

[145] T. O. Wehling, E. Şaşıoğlu, C. Friedrich, A. I. Lichtenstein, M. I. Katsnelson, and S. Blügel, "Strength of effective coulomb interactions in graphene and graphite," *Phys. Rev. Lett.*, vol. 106, p. 236805, Jun 2011.

[146] S. Sorella, K. Seki, O. O. Brovko, T. Shirakawa, S. Miyakoshi, S. Yunoki, and E. Tosatti, "Correlation-driven dimerization and topological gap opening in isotropically strained graphene," *Phys. Rev. Lett.*, vol. 121, p. 066402, Aug 2018.

[147] M. Fabrizio and E. Tosatti, "Nonmagnetic molecular jahn-teller mott insulators," *Phys. Rev. B*, vol. 55, pp. 13465–13472, May 1997.

[148] P. W. Anderson, "The resonating valence bond state in la_2cuo_4 and superconductivity," *Science*, vol. 235, no. 4793, pp. 1196–1198, 1987.

[149] M. Capone, M. Fabrizio, C. Castellani, and E. Tosatti, "Strongly correlated superconductivity and pseudogap phase near a multiband mott insulator," *Phys. Rev. Lett.*, vol. 93, p. 047001, Jul 2004.

[150] M. Capone, M. Fabrizio, C. Castellani, and E. Tosatti, "Colloquium: Modeling the unconventional superconducting properties of expanded A_3c_{60} fullerides," *Rev. Mod. Phys.*, vol. 81, pp. 943–958, Jun 2009.

[151] Z. Song, Z. Wang, W. Shi, G. Li, C. Fang, and B. A. Bernevig, "All magic angles in twisted bilayer graphene are topological," *Phys. Rev. Lett.*, vol. 123, p. 036401, Jul 2019.

[152] M. Angeli and M. Fabrizio, "Jahn–teller coupling to moiréphonons in the continuum model formalism for small-angle twisted bilayer graphene," *The European Physical Journal Plus*, vol. 135, no. 8, p. 630, 2020.

[153] J. F. Dodaro, S. A. Kivelson, Y. Schattner, X. Q. Sun, and C. Wang, "Phases of a phenomenological model of twisted bilayer graphene," *Phys. Rev. B*, vol. 98, p. 075154, Aug 2018.

[154] Y. H. Kwan, G. Wagner, N. Bultinck, S. H. Simon, E. Berg, and S. A. Parameswaran, "Electron-phonon coupling and competing kekulé orders in twisted bilayer graphene," 2023.

[155] X. Sun, S. Zhang, Z. Liu, H. Zhu, J. Huang, K. Yuan, Z. Wang, K. Watanabe, T. Taniguchi, X. Li, M. Zhu, J. Mao, T. Yang, J. Kang, J. Liu, Y. Ye, Z. V. Han, and Z. Zhang, "Correlated states in doubly-aligned hbn/graphene/hbn heterostructures," *Nature Communications*, vol. 12, p. 7196, Dec 2021.

[156] M. Long, P. A. Pantaleón, Z. Zhan, F. Guinea, J. Á. Silva-Guillén, and S. Yuan, "An atomistic approach for the structural and electronic properties of twisted bilayer graphene-boron nitride heterostructures," *npj Computational Materials*, vol. 8, no. 1, p. 73, 2022.

[157] I. Das, X. Lu, J. Herzog-Arbeitman, Z.-D. Song, K. Watanabe, T. Taniguchi, B. A. Bernevig, and D. K. Efetov, "Symmetry-broken chern insulators and rashba-like landau-level crossings in magic-angle bilayer graphene," *Nature Physics*, vol. 17, no. 6, pp. 710–714, 2021.

[158] A. T. Pierce, Y. Xie, J. M. Park, E. Khalaf, S. H. Lee, Y. Cao, D. E. Parker, P. R. Forrester, S. Chen, K. Watanabe, T. Taniguchi, A. Vishwanath, P. Jarillo-Herrero, and A. Yacoby, "Unconventional sequence of correlated chern insulators in magic-angle twisted bilayer graphene," *Nature Physics*, vol. 17, no. 11, pp. 1210–1215, 2021.

[159] P. Stepanov, M. Xie, T. Taniguchi, K. Watanabe, X. Lu, A. H. MacDonald, B. A. Bernevig, and D. K. Efetov, "Competing zero-field chern insulators in superconducting twisted bilayer graphene," *Phys. Rev. Lett.*, vol. 127, p. 197701, Nov 2021.

[160] C. L. Tschirhart, M. Serlin, H. Polshyn, A. Shragai, Z. Xia, J. Zhu, Y. Zhang, K. Watanabe, T. Taniguchi, M. E. Huber, and A. F. Young, "Imaging orbital ferromagnetism in a moiré chern insulator," *Science*, vol. 372, no. 6548, pp. 1323–1327, 2021.

[161] Y. Choi, H. Kim, Y. Peng, A. Thomson, C. Lewandowski, R. Polski, Y. Zhang, H. S. Arora, K. Watanabe, T. Taniguchi, J. Alicea, and S. Nadj-Perge, "Correlation-driven topological phases in magic-angle twisted bilayer graphene," *Nature*, vol. 589, no. 7843, pp. 536–541, 2021.

[162] Y. Saito, J. Ge, L. Rademaker, K. Watanabe, T. Taniguchi, D. A. Abanin, and A. F. Young, "Hofstadter subband ferromagnetism and symmetry-broken chern insulators in twisted bilayer graphene," *Nature Physics*, vol. 17, no. 4, pp. 478–481, 2021.

[163] S. Wu, Z. Zhang, K. Watanabe, T. Taniguchi, and E. Y. Andrei, "Chern insulators, van hove singularities and topological flat bands in magic-angle twisted bilayer graphene," *Nature Materials*, vol. 20, no. 4, pp. 488–494, 2021.

[164] Y. H. Kwan, G. Wagner, T. Soejima, M. P. Zaletel, S. H. Simon, S. A. Parameswaran, and N. Bultinck, "Kekulé spiral order at all nonzero integer fillings in twisted bilayer graphene," *Phys. Rev. X*, vol. 11, p. 041063, Dec 2021.

[165] H. C. Po, H. Watanabe, and A. Vishwanath, "Fragile topology and wannier obstructions," *Phys. Rev. Lett.*, vol. 121, p. 126402, Sep 2018.

[166] Y. Zhang and A. Vishwanath, "Establishing non-abelian topological order in gutzwiller-projected chern insulators via entanglement entropy and modular $\mathcal{S}$-matrix," *Phys. Rev. B*, vol. 87, p. 161113(R), Apr 2013.

[167] Z.-D. Song, B. Lian, N. Regnault, and B. A. Bernevig, "Twisted bilayer graphene. ii. stable symmetry anomaly," *Phys. Rev. B*, vol. 103, p. 205412, May 2021.

[168] R. Resta, "Geometry and topology in many-body physics," 2020.

[169] S. Grover, M. Bocarsly, A. Uri, P. Stepanov, G. Di Battista, I. Roy, J. Xiao, A. Y. Meltzer, Y. Myasoedov, K. Pareek, K. Watanabe, T. Taniguchi, B. Yan, A. Stern, E. Berg, D. K. Efetov, and E. Zeldov, "Chern mosaic and berry-curvature magnetism in magic-angle graphene," *Nature Physics*, vol. 18, no. 8, pp. 885–892, 2022.

[170] D. Călugăru, N. Regnault, M. Oh, K. P. Nuckolls, D. Wong, R. L. Lee, A. Yazdani, O. Vafek, and B. A. Bernevig, "Spectroscopy of twisted bilayer graphene correlated insulators," *Phys. Rev. Lett.*, vol. 129, p. 117602, Sep 2022.

[171] M.-T. Tran, D.-B. Nguyen, H.-S. Nguyen, and T.-M. T. Tran, "Topological green function of interacting systems," *Phys. Rev. B*, vol. 105, p. 155112, Apr 2022.

[172] R.-J. Slager, L. Rademaker, J. Zaanen, and L. Balents, "Impurity-bound states and green's function zeros as local signatures of topology," *Phys. Rev. B*, vol. 92, p. 085126, Aug 2015.

[173] T. Misawa and Y. Yamaji, "Zeros of green functions in topological insulators," *Phys. Rev. Res.*, vol. 4, p. 023177, Jun 2022.

[174] O. E. Obakpolor and P. Hosur, "Surface luttinger arcs in weyl semimetals," *Phys. Rev. B*, vol. 106, p. L081112, Aug 2022.

[175] I. Dzyaloshinskii, "Some consequences of the luttinger theorem: The luttinger surfaces in non-fermi liquids and mott insulators," *Phys. Rev. B*, vol. 68, p. 085113, Aug 2003.

[176] M. Fabrizio, *A Course in Quantum Many-Body Theory*. Springer Cham, 2022.

[177] P. Streda, "Theory of quantised hall conductivity in two dimensions," *Journal of Physics C: Solid State Physics*, vol. 15, p. L717, aug 1982.

[178] P. Streda and L. Smrcka, "Thermodynamic derivation of the hall current and the thermopower in quantising magnetic field," *Journal of Physics C: Solid State Physics*, vol. 16, p. L895, aug 1983.

[179] M.-F. Yang and M.-C. Chang, "Středa-like formula in the spin hall effect," *Phys. Rev. B*, vol. 73, p. 073304, Feb 2006.

[180] M. Potthoff, "Non-perturbative construction of the Luttinger-Ward functional," *Condens. Mat. Phys.*, vol. 9, p. 557, 2006.

[181] J. M. Luttinger, "Fermi surface and some simple equilibrium properties of a system of interacting fermions," *Phys. Rev.*, vol. 119, pp. 1153–1163, Aug 1960.

[182] K. Slagle, Y.-Z. You, and C. Xu, "Exotic quantum phase transitions of strongly interacting topological insulators," *Phys. Rev. B*, vol. 91, p. 115121, Mar 2015.

[183] Y.-Y. He, H.-Q. Wu, Z. Y. Meng, and Z.-Y. Lu, "Topological invariants for interacting topological insulators. ii. breakdown of single-particle green's function formalism," *Phys. Rev. B*, vol. 93, p. 195164, May 2016.

[184] L. P. Gavensky, S. Sachdev, and N. Goldman, "Connecting the many-body chern number to luttinger's theorem through středa's formula," 2023.

[185] A. M. Essin, A. M. Turner, J. E. Moore, and D. Vanderbilt, "Orbital magnetoelectric coupling in band insulators," *Phys. Rev. B*, vol. 81, p. 205104, May 2010.

[186] M. Z. Hasan and J. E. Moore, "Three-dimensional topological insulators," *Annual Review of Condensed Matter Physics*, vol. 2, no. 1, pp. 55–78, 2011.

[187] R. Resta, "Geometry and topology in many-body physics," 2020.

[188] J. Zhao, P. Mai, B. Bradlyn, and P. Phillips, "Failure of topological invariants in strongly correlated matter," 2023.

[189] Q. Niu, D. J. Thouless, and Y.-S. Wu, "Quantized hall conductance as a topological invariant," *Phys. Rev. B*, vol. 31, pp. 3372–3377, Mar 1985.

[190] N. Regnault and B. A. Bernevig, "Fractional chern insulator," *Phys. Rev. X*, vol. 1, p. 021014, Dec 2011.

[191] X. Wu and M. A. Zubkov, "Anomalous fractional quantum hall effect and multi-valued hamiltonians," *Journal of Physics: Condensed Matter*, vol. 33, p. 355601, jul 2021.

[192] Z. Wang, X.-L. Qi, and S.-C. Zhang, "Topological invariants for interacting topological insulators with inversion symmetry," *Phys. Rev. B*, vol. 85, p. 165126, Apr 2012.

[193] P. W. Anderson, "Localized magnetic states in metals," *Phys. Rev.*, vol. 124, pp. 41–53, Oct 1961.

[194] M. Dzero, J. Xia, V. Galitski, and P. Coleman, "Topological kondo insulators," *Annual Review of Condensed Matter Physics*, vol. 7, no. 1, pp. 249–280, 2016.

[195] G. Li, Z. Xiang, F. Yu, T. Asaba, B. Lawson, P. Cai, C. Tinsman, A. Berkley, S. Wolgast, Y. S. Eo, D.-J. Kim, C. Kurdak, J. W. Allen, K. Sun, X. H. Chen, Y. Y. Wang, Z. Fisk, and L. Li, "Two-dimensional fermi surfaces in kondo insulator smb¡sub¿6¡/sub¿," *Science*, vol. 346, no. 6214, pp. 1208–1212, 2014.

[196] Y. Sato, Z. Xiang, Y. Kasahara, T. Taniguchi, S. Kasahara, L. Chen, T. Asaba, C. Tinsman, H. Murayama, O. Tanaka, Y. Mizukami, T. Shibauchi, F. Iga, J. Singleton, L. Li, and Y. Matsuda, "Unconventional thermal metallic state of charge-neutral fermions in an insulator," *Nature Physics*, vol. 15, pp. 954–959, Sep 2019.

[197] M.-E. Boulanger, F. Laliberté, M. Dion, S. Badoux, N. Doiron-Leyraud, W. A. Phelan, S. M. Koohpayeh, W. T. Fuhrman, J. R. Chamorro, T. M. McQueen, X. F. Wang, Y. Nakajima, T. Metz, J. Paglione, and L. Taillefer, "Field-dependent heat transport in the kondo insulator smb_6: Phonons scattered by magnetic impurities," *Phys. Rev. B*, vol. 97, p. 245141, Jun 2018.

[198] O. Parcollet, M. Ferrero, T. Ayral, H. Hafermann, I. Krivenko, L. Messio, and P. Seth, "Triqs: A toolbox for research on interacting quantum systems," *Computer Physics Communications*, vol. 196, pp. 398–415, 2015.

[199] P. Seth, I. Krivenko, M. Ferrero, and O. Parcollet, "Triqs/cthyb: A continuous-time quantum monte carlo hybridisation expansion solver for quantum impurity problems," *Computer Physics Communications*, vol. 200, pp. 274–284, 2016.

[200] B. Roy, J. D. Sau, M. Dzero, and V. Galitski, "Surface theory of a family of topological kondo insulators," *Phys. Rev. B*, vol. 90, p. 155314, Oct 2014.

[201] V. Alexandrov, P. Coleman, and O. Erten, "Kondo breakdown in topological kondo insulators," *Phys. Rev. Lett.*, vol. 114, p. 177202, Apr 2015.

[202] J. Werner and F. F. Assaad, "Interaction-driven transition between topological states in a kondo insulator," *Phys. Rev. B*, vol. 88, p. 035113, Jul 2013.

[203] J. Werner and F. F. Assaad, "Dynamically generated edge states in topological kondo insulators," *Phys. Rev. B*, vol. 89, p. 245119, Jun 2014.

[204] E. Gull, M. Ferrero, O. Parcollet, A. Georges, and A. J. Millis, "Momentum-space anisotropy and pseudogaps: A comparative cluster dynamical mean-field analysis of the doping-driven metal-insulator transition in the two-dimensional hubbard model," *Phys. Rev. B*, vol. 82, p. 155101, Oct 2010.

[205] T. Maier, M. Jarrell, T. Pruschke, and M. H. Hettler, "Quantum cluster theories," *Rev. Mod. Phys.*, vol. 77, pp. 1027–1080, Oct 2005.

[206] F. B. Kugler and G. Kotliar, "Is the orbital-selective mott phase stable against interorbital hopping?," *Phys. Rev. Lett.*, vol. 129, p. 096403, Aug 2022.

[207] E. Clementi, D. L. Raimondi, and W. P. Reinhardt, "Atomic Screening Constants from SCF Functions. II. Atoms with 37 to 86 Electrons," *The Journal of Chemical Physics*, vol. 47, pp. 1300–1307, 05 2004.

[208] T. D. Stanescu, M. Civelli, K. Haule, and G. Kotliar, "A cellular dynamical mean field theory approach to mottness," *Annals of Physics*, vol. 321, no. 7, pp. 1682–1715, 2006. July 2006 Special Issue.

[209] K. Akintola, A. Pal, S. R. Dunsiger, A. C. Y. Fang, M. Potma, S. R. Saha, X. Wang, J. Paglione, and J. E. Sonier, "Freezing out of a low-energy bulk spin exciton in smb6," *npj Quantum Materials*, vol. 3, no. 1, p. 36, 2018.

[210] S. Gheidi, K. Akintola, K. S. Akella, A. M. Côté, S. R. Dunsiger, C. Broholm, W. T. Fuhrman, S. R. Saha, J. Paglione, and J. E. Sonier, "Intrinsic low-temperature magnetism in smb_6," *Phys. Rev. Lett.*, vol. 123, p. 197203, Nov 2019.